



Small-Scale Tensile, Charpy V-Notch, and Fracture Toughness Tests

Final Report 277-T-05

for Project

Weld Design, Testing, and Assessment Procedures for High Strength Pipelines

Prepared for the

Design, Materials, and Construction Technical Committee of
Pipeline Research Council International, Inc.

Project MATH-1 Catalog No. L5XXXX

and

U.S. Department of Transportation

Pipeline and Hazardous Materials Safety Administration

Office of Pipeline Safety

DOT Project BAA DTHP56-07-0001

Prepared by

J.A. Gianetto, W.R. Tyson, D.Y. Park, and G. Shen
CANMET Materials Technology Laboratory

E. Lucon and T.S. Weeks

*National Institute of Standards and Technology

M.A Quintana and V.B Rajan
Lincoln Electric Company

Y.-Y. Wang

Center for Reliable Energy Systems

September 2011

This research was funded in part under the Department of Transportation, Pipeline and Hazardous Materials Safety Administration's Pipeline Safety Research and Development Program. The views and conclusions contained in this document are those of the authors and should not be interpreted as representing the official policies, either expressed or implied, of the Pipeline and Hazardous Materials Safety Administration, or the U.S. Government.

Contribution of an agency of the U.S. government, not subject to copyright

CANMET Materials Technology Laboratory

Small-Scale Tensile, Charpy V-Notch, and Fracture Toughness Tests

J.A. Gianetto, W.R. Tyson, D.Y. Park, and G. Shen

CANMET Materials Technology Laboratory
Minerals and Metals Sector, Natural Resources Canada
183 Longwood Road South, Hamilton, ON, Canada, L8P 0A5

E. Lucon and T.S. Weeks

*National Institute of Standards and Technology

M.A Quintana and V.B Rajan
Lincoln Electric Company

Y.-Y. Wang
Center for Reliable Energy Systems

CANMET Report No. 2011-07(TR)

September 2011

DISCLAIMER

Natural Resources Canada makes no representations or warranties respecting the contents of this report, either expressed or implied, arising by law or otherwise, including but not limited to implied warranties or conditions of merchantability or fitness for a particular purpose.



Catalog No. L5XXXX

Small-Scale Tensile, Charpy V-Notch, and Fracture Toughness Tests

Final Report 277-T-05

for Project

Weld Design, Testing, and Assessment Procedures for High Strength Pipelines

Prepared for the

Design, Materials, and Construction Technical Committee of Pipeline Research Council International, Inc.

Project MATH-1 Catalog No. L5XXXX

and

U.S. Department of Transportation

Pipeline and Hazardous Materials Safety Administration

Office of Pipeline Safety

DOT Project BAA DTHP56-07-0001

Prepared by

J.A. Gianetto, W.R. Tyson, D.Y. Park, and G. Shen
CANMET Materials Technology Laboratory

E. Lucon and T.S. Weeks

*National Institute of Standards and Technology

M.A Quintana and V.B Rajan
Lincoln Electric Company

Y.-Y. Wang

Center for Reliable Energy Systems

(Internal Use Only or Public Access)

Version	Date of Last Revision	Date of Uploading	Comments
Draft	March 2011	March 2011	
Final	Jan 2012	Jan 2012	

This report is furnished to Pipeline Research Council International, Inc. (PRCI) under the terms of PRCI contract [277-PR-348-074512], between PRCI and the MATH-1 contractors:

- Electricore (prime contractor),
- Center for Reliable Energy Systems, CANMET, NIST, and The Lincoln Electric Company (sub-contractors).

The contents of this report are published as received from the MATH-1 contractor and subcontractors. The opinions, findings, and conclusions expressed in the report are those of the authors and not necessarily those of PRCI, its member companies, or their representatives. Publication and dissemination of this report by PRCI should not be considered an endorsement by PRCI of the MATH-1 contractor and subcontractors, or the accuracy or validity of any opinions, findings, or conclusions expressed herein.

In publishing this report, PRCI and the MATH-1 contractors make no warranty or representation, expressed or implied, with respect to the accuracy, completeness, usefulness, or fitness for purpose of the information contained herein, or that the use of any information, method, process, or apparatus disclosed in this report may not infringe on privately owned rights. PRCI and the MATH-1 contractors assume no liability with respect to the use of, or for damages resulting from the use of, any information, method, process, or apparatus disclosed in this report. By accepting the report and utilizing it, you agree to waive any and all claims you may have, resulting from your voluntary use of the report, against PRCI and the MATH-1 contractors.

Pipeline Research Council International Catalog No. L5XXXX

PRCI Reports are Published by Technical Toolboxes, Inc.

3801 Kirby Drive, Suite 520
Houston, Texas 77098
Tel: 713-630-0505
Fax: 713-630-0560
Email: info@ttoolboxes.com

PROJECT PARTICIPANTS

PROJECT TEAM MEMBER	COMPANY AFFILIATION	PROJECT TEAM MEMBER	COMPANY AFFILIATION
Arti Bhatia	Alliance	Jim Costain	GE
Jennifer Klementis	Alliance	Gilmar Batista	Petrobras
Roger Haycraft	Boardwalk	Marcy Saturno de Menezes	Petrobras
David Horsley	BP	Dave Aguiar	PG&E
Mark Hudson	BP	Ken Lorang	PRCI
Ron Shockley	Chevron	Maslat Al-Waranbi	Saudi Aramco
Sam Mishael	Chevron	Paul Lee	SoCalGas
David Wilson	ConocoPhillips	Alan Lambeth	Spectra
Satish Kulkarni	El Paso	Robert Turner	Stupp
Art Meyer	Enbridge	Gilles Richard	TAMSA
Bill Forbes	Enbridge	Noe Mota Solis	TAMSA
Scott Ironside	Enbridge	Philippe Darcis	TAMSA
Sean Keane	Enbridge	Dave Taylor	TransCanada
Laurie Collins	Evraz	Joe Zhou	TransCanada
David de Miranda	Gassco	Jason Skow	TransGas
Adriaan den Herder	Gasunie	Ernesto Cisneros	Tuberia Laguna
Jeff Stetson	GE	Vivek Kashyap	Welsun
		Chris Brown	Williams

CORE RESEARCH TEAM	
RESEARCHER	COMPANY AFFILIATION
Yaoshan Chen	Center for Reliable Energy Systems
Yong-Yi Wang	Center for Reliable Energy Systems
Ming Liu	Center for Reliable Energy Systems
Dave Fink	Lincoln Electric Company
Marie Quintana	Lincoln Electric Company
Vaidyanath Rajan	Lincoln Electric Company
Joe Daniel	Lincoln Electric Company
Radhika Panday	Lincoln Electric Company
James Gianetto	CANMET Materials Technology Laboratory
John Bowker	CANMET Materials Technology Laboratory
Bill Tyson	CANMET Materials Technology Laboratory
Guowu Shen	CANMET Materials Technology Laboratory
Dong Park	CANMET Materials Technology Laboratory
Timothy Weeks	National Institute of Standards and Technology
Mark Richards	National Institute of Standards and Technology
Dave McColskey	National Institute of Standards and Technology
Enrico Lucon	National Institute of Standards and Technology
John Hammond	Consultant Metallurgist & Welding Engineer

FINAL REPORT STRUCTURE

Focus Area 1 - Update of Weld Design, Testing, and Assessment Procedures for High Strength Pipelines		
Report #	Description	Lead Authors
277-T-01	Background of Linepipe Specifications	CRES/CANMET
277-T-02	Background of All-Weld Metal Tensile Test Protocol	CANMET/Lincoln
277-T-03	Development of Procedure for Low-Constraint Toughness Testing Using a Single-Specimen Technique	CANMET/CRES
277-T-04	Summary of Publications: Single-Edge Notched Tension SE(T) Tests	CANMET
277-T-05	Small Scale Tensile, Charpy V-Notch, and Fracture Toughness Tests	CANMET/NIST
277-T-06	Small Scale Low Constraint Fracture Toughness Test Results	CANMET/NIST
277-T-07	Small Scale Low Constraint Fracture Toughness Test Discussion and Analysis	CANMET/NIST
277-T-08	Summary of Mechanical Properties	CANMET
277-T-09	Curved Wide Plate Tests	NIST/CRES
277-T-10	Weld Strength Mismatch Requirements	CRES/CANMET
277-T-11	Curved Wide Plate Test Results and Transferability of Test Specimens	CRES/CANMET
277-S-01	Summary Report 277 Weld Design, Testing, and Assessment Procedures for High Strength Pipelines	CRES

Focus Area 2 - Development of Optimized Welding Solutions for X100 Linepipe Steel		
Report #	Description	Lead Authors
278-T-01	State of The Art Review	Lincoln
278-T-02	Material Selection, Welding and Weld Monitoring	Lincoln/CANMET
278-T-03	Microstructure and Hardness Characterization of Girth Welds	CANMET/Lincoln
278-T-04	Microstructure and Properties of Simulated Weld Metals	CANMET/Lincoln
278-T-05	Microstructure and Properties of Simulated Heat Affected Zones	CANMET/Lincoln
278-T-06	Essential Welding Variables	Lincoln/CANMET
278-T-07	Thermal Model for Welding Simulations	CRES/CANMET
278-T-08	Microstructure Model for Welding Simulations	CRES/CANMET
278-T-09	Application to Other Processes	Lincoln/CANMET
278-S-01	Summary Report 278 Development of Optimized Welding Solutions for X100 Line Pipe Steel	Lincoln

This Page Intentionally Left Blank

EXECUTIVE SUMMARY

This is the fourth of seven reports dealing with small-scale mechanical testing; an outline of the reporting flow is given in the Introduction to the Summary of Mechanical Properties report 277-T-08. This report presents the results of tensile tests and conventional toughness tests, both notch toughness (Charpy) and fracture toughness (through-thickness-notched specimens), and discusses correlation with microstructure.

Reliability and safety of proposed large-diameter, high-pressure pipelines from remote regions in North America are continually being improved through development of modern high-strength steel pipe, advanced welding technologies, and strain-based design (SBD) methodologies. SBD for pipeline projects requires overmatching the strength of the weld metal relative to the parent pipe to avoid strain localization in the weldment during service. Achieving the required strength overmatch, ductility and low temperature toughness in weld metal becomes a challenge as the strength of the pipe increases. The introduction of higher productivity, advanced pulsed-gas-metal-arc-welding (GMAW-P) processes adds further complications from the more complex cooling conditions of the weldment. An improved understanding of weld metal systems required for the successful large scale production of high strength pipeline field girth welds is needed for new and demanding pipeline construction projects.

In this study, the mechanical properties achieved in single- and dual-torch GMAW-P X100 pipe welds were characterized with conventional small-scale testing methods. The main objectives were to further develop an all-weld-metal tensile testing protocol and to assess toughness to provide baseline data for understanding the factors that control both weld metal (WM) and heat affected zone (HAZ) microstructure and properties in pipeline girth welds. In this investigation, two series of rolled (1G) girth welds were made in X100 pipe of 914 mm (36 in) diameter and 19.1 mm (0.75 in) wall thickness with two GMAW-P process variants: single- and dual-torch. A third series of 5G validation girth welds was made with X100 pipes of 1067 mm (42 in) diameter and 14.3 mm (0.563 in) wall thickness from two sources. The small-scale testing program included evaluations of all-weld-metal tensile strength, Charpy impact and standard fracture toughness measured by single-edge bend (SE(B)) tests. The results are discussed in the context of microhardness and microstructure assessments of both WM and HAZ regions.

All-weld-metal (AWM) tensile tests with round and strip tensile specimens showed that strength properties were quite consistent for the full circumference of single- and dual-torch rolled pipe welds. Full stress-strain curves were generated, and 0.2 % offset yield strength, flow stress, ultimate tensile strength, and uniform strain were measured and compared with pipe properties by the use of calculated weld strength mismatch factors based on these properties.

Charpy V-notch (CVN) transition curves were generated for both WM and HAZ (notched within 0.5 mm of the fusion line). Fracture toughness of both WM and HAZ regions of single- and dual-torch welds was assessed using standard SE(B) testing procedures with specimens notched through-thickness at the weld centerline and in the HAZ (within 0.5 mm of the fusion line). For the third series of welds, fracture toughness was also measured at -20 °C on the base metal of one of the pipes.

Some of the observations and conclusions that can be drawn from this evaluation include:

1. AWM tensile properties of single-torch rolled welds exhibited high yield and ultimate strengths and revealed consistent trends: inside-diameter (ID) biased round bars exhibited higher strength compared with outside-diameter (OD) biased specimens. AWM strip tensile specimens provided an average measure of WM strength. WM strength variation was attributed to variations in proportions of as-deposited (AD) and reheated (RH) microstructures in the WM. This was confirmed by microhardness maps that showed more high-hardness (AD) regions near the hot pass (ID side), whereas there were more low-hardness (RH) regions of the WM on the OD side. The same trend was observed for the single-torch 5G weld, although the overall strength of the 5G weld was marginally higher than that of the rolled welds. For the dual-torch rolled welds, the tensile properties were generally very consistent for all test specimens, and it was possible to achieve yield strengths in excess of the targeted value of 810 MPa. In contrast, results were more variable for the 5G dual-torch weld and the yield strengths (~788 MPa, based on AWM strip tensile tests) were marginally below the targeted value. Validation 5G welds made with tight control of welding variables provided AWM strengths (as measured by AWM strip tensile specimens) that were consistent around the pipe and consistently overmatched the corresponding pipe strengths. In this work, the yield strength has been taken as the 0.2 % offset value to conform with common practice. However, for high-strength steels this is often in a region of the stress-strain curve where the rate of work hardening is still high, and so the yield stress is sensitive to small variations in the stress-strain curve and in particular on the choice of elastic slope. A value further up the stress-strain curve, e.g. the 1 % flow stress, is more reproducible.
2. The WM CVN impact energy results (at -60 °C and -20 °C) for the complete series of single-torch welds showed some variation, with the first-produced weld exhibiting slightly higher toughness than the remaining five welds. The three dual-torch welds had very good and reasonably consistent notch toughness. In terms of transition behaviour, the properties were deemed to be good; there was a range of high upper shelf energies and nearly identical transition temperatures close to -70 °C. There was one exception: the HAZ region of the dual-torch weld exhibited a transition temperature of -35 °C, although with a high upper-shelf energy (250 J). The WM CVN impact energy results in the validation welds showed some variation around the pipe, but still showed mostly ductile behaviour at -20 °C.
3. The WM J-integral/crack-tip opening displacement ($J/CTOD(\delta)$) results were very consistent, with fully ductile J_m/δ_m^1 values of about 250 kJ/m² to 300 kJ/m² (0.15 mm to 0.2 mm) at all temperatures. In contrast, most of the HAZ results from the first and second series of welds exhibited brittle cleavage $J_{u/c}/\delta_{u/c}^2$, although only one very low value occurred in the single-torch weld HAZ. However, for the third series of welds, only one HAZ specimen out of five exhibited unstable fracture at -20 °C, and three of the four remaining tests provided J_m/δ_m values in excess of 550 kJ/m² (~0.36 mm).

¹ The subscript “m” designates ductile maximum-load performance.

² Subscripts “u” and “c” designate brittle (cleavage) fracture after and before ductile crack growth of 0.2 mm, respectively.

4. The complex WM microstructures formed in the single-torch pipe welds consisted of mixed bainite/martensite, with higher hardness in AD compared to RH regions. Through-thickness hardness profiles reflect the reheating and tempering of the WM deposited sequentially. In the dual-torch pipe welds, high hardness of the leading-wire deposit is significantly altered by deposition of the trailing wire.
5. Three HAZ structures/regions formed in the multipass pipe welds: grain-coarsened HAZ (GHAZ), supercritically reheated (SCR-GHAZ), and intercritically-reheated (ICR-GHAZ). The microstructures are consistent with the through-thickness variation in hardness.
6. Microhardness maps give a good visual indication of the hardness distribution, especially in the WM region where reheated zones are difficult to distinguish by conventional metallographic examination.
7. Through-thickness microhardness maps provide a good indication of the relative changes in hardness as a function of local thermal cycle and allow specific regions such as the GHAZ to be better quantified. For example, the lower average through-thickness hardness of the HAZ compared to that of the WM provides a good indication of the relative tensile properties of these regions.

TABLE OF CONTENTS

EXECUTIVE SUMMARY	viii
TABLE OF CONTENTS	xi
LIST OF FIGURES	xii
LIST OF TABLES	xiii
1 INTRODUCTION	1
2 EXPERIMENTAL PROCEDURES	1
2.1 X100 PIPE	1
2.2 SINGLE- AND DUAL-TORCH X100 ROLLED WELD PROCEDURES	2
2.3 SINGLE- AND DUAL-TORCH X100 5G WELD PROCEDURES	3
3 ALL-WELD-METAL (AWM) TENSILE TESTING	3
3.1 CHARPY IMPACT TOUGHNESS TESTING	4
3.2 FRACTURE TOUGHNESS TESTING	4
3.3 METALLOGRAPHY AND MICROHARDNESS TESTING	5
4 EXPERIMENTAL RESULTS	5
4.1 PIPE STEEL AND WELD METALS	5
4.2 WELD METAL TENSILE PROPERTIES	6
4.3 WELD METAL AND HAZ CHARPY IMPACT PROPERTIES	9
4.4 WELD METAL AND HAZ FRACTURE TOUGHNESS	9
4.5 METALLOGRAPHIC ANALYSIS AND MICROHARDNESS SURVEYS	10
5 DISCUSSION	12
5.1 AWM TENSILE PROPERTIES	13
5.2 CVN TRANSITION CURVES	14
5.3 FRACTURE TOUGHNESS OF WM AND HAZ	14
6 CONCLUSIONS	15
7 ACKNOWLEDGMENTS	17
8 REFERENCES	17

LIST OF FIGURES

Figure 1: (a) Single- and (b) dual-torch roll welding.....	31
Figure 2: Narrow gap joint design for single- and dual-torch X100 rolled welds (dimensions in mm).....	32
Figure 3: Pass sequences for (a) single- and (b) dual-torch X100 rolled welds.....	32
Figure 4: Details of round bar tensile specimens from weld in 19 mm thick pipe (dimensions in mm).....	33
Figure 5: Details of strip tensile specimen from weld in 19 mm thick pipe (dimensions in mm).....	34
Figure 6: Details of strip tensile specimen from weld in 14.3 mm thick pipe (dimensions in mm).....	35
Figure 7: Orientation and position of WMC and HAZ CVN specimens (dimensions in mm)....	36
Figure 8: Optical micrograph of the X100 pipe steel near mid-wall. Etched with 2 % Nital. ...	36
Figure 9: Stress-strain curves for round bar tensile specimens from X100 pipe as a function of clock position.....	37
Figure 10: Stress-strain curves for strap tensile specimens from X100 pipe as a function of clock position.....	38
Figure 11: Stress-strain curves for strap tensile specimens from X100 Pipe B as a function of clock position (12:00, 3:00 and 6:00).....	39
Figure 12: Stress-strain curves for strap tensile specimens from X100 Pipe A as a function of clock position (12:00, 3:00 and 6:00).....	40
Figure 13: Stress-strain curves for single- and dual-torch welds versus X100 pipe data (Strap).....	41
Figure 14: Stress-strain curves for 5G single-torch weld, 883G.....	42
Figure 15: Stress-strain curves for 5G dual-torch weld, 883-H.....	43
Figure 16: Yield (0.2 % offset) and ultimate tensile strengths versus clock position for the 5G single-torch weld.....	44
Figure 17: Yield (0.2 % offset) and ultimate tensile strengths versus clock position for the 5G dual-torch weld.....	45
Figure 18: Stress-strain curves for 5G single- and dual-torch validation welds.....	46
Figure 19: Yield (0.2% offset), flow stress and ultimate tensile strengths versus clock position for the validation 5G single-torch welds.....	47
Figure 20: Yield (0.2% offset), flow stress and ultimate tensile strengths versus clock position for the validation 5G dual-torch welds.....	48
Figure 21: CVN transition curves for single- and dual-torch welds.....	49
Figure 22: CVN impact energies at -60 and -20°C.....	50
Figure 23: CVN impact energies at -20°C of the validation 5G single-torch welds.....	51
Figure 24: CVN impact energies at -20°C of the validation 5G dual-torch welds.....	52
Figure 25: Load vs. CMOD curves for single-torch WM- and HAZ-notched B x 2B <i>J/CTOD</i> specimens.....	53
Figure 26: Macrographs of X100 rolled welds: (a) single-torch, 807-J and (b) dual-torch, 883-D.....	54
Figure 27: Weld metal microstructure of single-torch weld.....	55
Figure 28: Weld metal microstructure of dual-torch weld.....	56
Figure 29: HAZ microstructures of single-torch weld.....	57
Figure 30: HAZ microstructures of dual-torch weld.....	58

Figure 31: Microhardness maps for single-torch pipe welds. (Units of VHN 300 g)	59
Figure 32: Microhardness maps for dual-torch pipe welds. (Units of VHN 300 g)	60
Figure 33: Weld 3 microhardness maps and stress-strain curves (single-torch). (Units of VHN 300 g)	61
Figure 34: Through-thickness microhardness line map for single-torch pipe weld, 807-J.....	62
Figure 35: Through-thickness microhardness line map for single-torch pipe weld, 883-D.	62
Figure 36: Comparison of through-thickness WMC microhardness line map.	63
Figure 37: Comparison of through-thickness HAZ microhardness line map.	63

LIST OF TABLES

Table 1: Welding parameters for Rolled 1G Welds.....	20
Table 2: Welding parameters for validation 5G welds.....	21
Table 3: Chemical composition of weld metals and pipe steels from 1G rolled welds	22
Table 4: Chemical composition of weld metal and pipe from validation 5G welds	23
Table 5: AWM tensile properties of single-torch 1G rolled welds	22
Table 6: AWM tensile properties of dual-torch welds	23
Table 7: AWM strip tensile properties of validation 5G welds	24
Table 8: CVN results for X100 pipe steel and single-torch welds (807F).....	25
Table 9: CVN results for X100 pipe steel and dual-torch weld (883D)	26
Table 10: Comparison of WM CVN results for tests conducted at -60 and -20 °C	27
Table 11: CVN results of WM and HAZ for validation 5G welds	28
Table 12: J-CTOD SE(B) results for Bx2B specimens from single and dual-torch rolled welds (Series 1 & 2).....	29
Table 13: J-CTOD SE(B) results at -20 °C for B x 2B specimens from single torch 5G pipe welds (952-D and 952-F, Series 3) and Pipe A	30

1 INTRODUCTION

This is the fourth of seven reports dealing with small-scale mechanical testing; an outline of the reporting flow is given in the Introduction to the Summary of Mechanical Properties report 277-T-08. This report presents the results of tensile tests and conventional toughness tests, both notch toughness (Charpy) and fracture toughness (through-thickness-notched specimens), and discusses correlation with microstructure.

Reliability and safety of proposed large diameter, high pressure pipelines from remote regions in North America are continually being improved through development of modern high strength steel pipe, advanced welding technologies, and strain based design (SBD) methodologies [1-10]. The girth welds must meet very demanding weld strength overmatching and low temperature fracture toughness requirements to ensure that an acceptable level of reliability and safety is achieved for the complete pipeline life-cycle, *i.e.* design, construction, operation, and maintenance.

This report provides details of the characterization of experimental girth welds produced for a major consolidated program of research with two primary areas of focus related to the welding of high strength steel pipelines. The first area aims to update weld design, testing, and assessment procedures [11]. The second aims to optimize welding solutions for joining high strength steel X100 (grade 690) pipes by examining the welding process and material variables that lead to variation in weld properties [12]. Characterizing and understanding the mechanical properties achieved in these high strength steel welds is a key element in the overall investigation to reduce variation in weld properties through better control of the welding process. The consistency among the two series of rolled welds produced with single- and dual-torch procedures was assessed by all-weld-metal (AWM) tensile tests, weld metal (WM) Charpy V-notch (CVN) impact tests and microhardness maps. More detailed evaluations of AWM tensile properties to determine strength mismatch, CVN impact transition toughness behavior, and fracture toughness (measured by through-thickness (deeply-notched) single-edge bend SE(B) tests) was also carried out to establish differences between the two process variants. Some of the factors controlling the mechanical properties were established via detailed microstructural characterizations of both weld metal and HAZ regions for the series of single- and dual-torch pipeline girth welds produced for this investigation. The fracture toughness test results from other test specimen types, including surface-notched and shallow-cracked single-edge bend SE(B) and single-edge tension SE(T) tests, are presented in the subsequent series of topical and summary reports [13,14,15].

2 EXPERIMENTAL PROCEDURES

2.1 X100 PIPE

Pipes of X100 (grade 690), 36 in (914 mm) diameter by 0.75 in (19.1 mm) wall thickness, were supplied for the project in the aged condition, *i.e.*, after being subjected to an induction heat-treatment coating cycle at a temperature of ~240 °C. The longitudinal tensile properties of a complete ring section of pipe were determined with large diameter (12.8 mm) round bar and full-thickness (19.1 mm x 19.1 mm) strap tensile specimens. The samples were cut from specific clock positions around the circumference of the pipe. CVN impact transition curves were also

generated from specimens cut parallel to the longitudinal pipe axis, at the mid-wall position and notched through-thickness. The tests were conducted over a wide range of test temperatures from -120 °C to room temperature. The through-thickness chemical composition and microstructure of the pipe were also established. The purpose was to fully characterize the pipe properties as a basis for subsequent work [11].

Additionally, two sets of X100 (grade 690) pipes, 1067 mm (42 in) in diameter and 14.3 mm. (0.563 in) in thickness from two different manufacturers were employed to make validation welds. These pipes were available in lengths varying from 46 in to 74 in. They were cut in two sections such that two single- and two dual-torch 5G welds each could be made at two different welding contractors. The longitudinal tensile properties of the pipes were determined using full-thickness (7.9 mm x 4.8 mm) strap tensile specimens. The samples were cut from nominally the 12:00, 3:00 and 6:00 clock positions corresponding to the 5G girth welding clock orientation. The pipes themselves were also characterized in terms of fracture toughness.

2.2 SINGLE- AND DUAL-TORCH X100 ROLLED WELD PROCEDURES

A series of baseline welds were produced in a well controlled and highly monitored manner, while maintaining essential features of mechanized mainline welding for large diameter pipe. The primary objective was to produce enough weld metal of consistent properties to facilitate the development of weld testing and assessment procedures [11]. During welding, the thermal cycles and welding process variables were carefully monitored in order that these welds would also serve as a valid baseline for the development of more effective welding process control methods [12,16,17,18].

Two series of experimental baseline welds, consisting of six single-torch and three dual-torch rolled welds, were produced in X100 pipes. The welds were produced under contract at CRC Evans, Houston, TX. Pipe strings were produced with two 762 mm (30 in) long pipe sections welded to a central 1524 mm (60 in) long section. This provided two welded pipe sections, approximately 1524 mm (60 in) long with a weld at the centre, for the comprehensive small-scale and curved-wide-plate (CWP) test programs. For single-torch rolled welding trials, the torch was maintained at a position near 1:00 with the pipe rotated to simulate vertical down welding. This allowed nearly identical welding parameters to be achieved for the full circumference of the pipe. Similarly, for the dual-torch rolled welds, the leading torch was positioned normal to the pipe near 12:30, while the trailing torch used a lead angle of several degrees and was positioned closer to 12:00, as shown in Figure 1. The spacing between the torches was fixed at 121 mm (4.75 in). All X100 pipe sections were prepared with a standard mechanized girth weld joint design, Figure 2, consisting of a single-vee bevel for the inside root bead and a narrow-gap compound bevel joint preparation for the hot and fill passes. Figure 3 shows the pass sequences used for the respective welds.

For both series of welds, a standard fixed-position (5G) root pass procedure was completed with a C-Mn (ER48S-6) electrode wire. The single-torch welds were completed with a hot pass followed by five fill passes and a cap pass with pulsed-gas-metal-arc-welding (GMAW-P). The dual-torch welds also employed GMAW-P; the hot pass was followed by two dual-torch runs [denoted D1-2 to D3-4 in Figure 3(b)], a fifth fill single-torch strip pass (F5) and two final split cap passes. For both series a C-Mn-Si-Ni-Mo-Ti electrode wire of ER62S-G classification was

used for the fill and cap passes. Representative welding parameters for the single- and dual-torch welds are listed in Table 1. Minimum preheat temperature of 100 °C and maximum interpass temperature of 125 °C were closely monitored and maintained throughout welding. The welding parameters were monitored through the welding system as well as by an external data acquisition system [16]. The weld thermal cycles were also acquired with a large number of thermocouples, both *in-situ* (predrilled to target the HAZ close to the fusion line) and plunged into the weld pool of selected fill passes.

2.3 SINGLE- AND DUAL-TORCH X100 5G WELD PROCEDURES

To establish the degree of tensile property variation for 5G pipeline girth welds, two additional single- and dual-torch welds were made using the same nominal welding procedures as described above. These were used to characterize the tensile properties as a function of clock position and to determine where specimens should be located to quantify WM strength for field pipe welds.

This approach was utilized in a series of validation girth welds in the 5G position. These welds were made to implement and validate the recommendations for methodology to control the welding variables by two welding contractors A and B, details of which are presented elsewhere [16,19,20]. Briefly, the control methodology involved setting limits on preheat and interpass temperature ranges, true heat input ranges, Wire feed speed/travel speed ratio, contact–tip-to-work-distance (CTWD) variation and groove-offset-distance tolerance. In the validation welds, a C-Mn-Si-Ni-Mo-Cr-Ti electrode (PT-1) of ER76S-G classification was used for single-torch and a C-Mn-Si-Ni-Mo-Cr-Ti electrode (PT-2) of ER83S-G classification was used for dual torch welding. Preheat and interpass temperatures with contractor A were in the same range as in the rolled 1G welds (100 °C to 125 °C), but the heat input was higher (0.6 kJ/mm to 0.8 kJ/mm). With contractor B, the preheat and interpass temperatures were higher, 100 °C to 145 °C for single-torch, and 120 °C to 155 °C for dual-torch, but heat input in the fill passes was comparable to that employed in the 1G rolled welds and in the range of 0.4 kJ/mm to 0.6 kJ/mm. Correspondingly, more passes were needed to fill the joint in welds made by contractor B compared to that of contractor A. In addition, contractor A utilized 85 % Ar:15 % CO₂ shielding gas and a pulse waveform whereas contractor B utilized 50 % Ar:50 % CO₂ shielding gas and a constant voltage. In dual-torch welding, contractor A used a 121 mm (4.75 in) torch spacing whereas contractor B used a 51 mm (2 in) torch spacing. The welding parameters are summarized in Table 2. Mechanical properties were obtained as a function of clock position from these welds, details of which are presented elsewhere [19,20]. Small-scale specimen fracture toughness measurements of the base, weld and HAZ materials from these welds were also completed. Tensile properties were measured using strip tensile specimens which are described in the following section.

3 ALL-WELD-METAL (AWM) TENSILE TESTING

For both series of single- and dual-torch welds, 5 mm diameter round bar tensile specimens biased towards the outside diameter (OD) and inside diameter (ID), along with several modified strip tensile specimens, were accurately cut and machined from various clock positions around the circumference of the pipe. Figure 4, Figure 5, and Figure 6 provide schematic drawings of the AWM tensile specimens. Details of the methods used to cut and profile the specimens are available elsewhere [21,22]. Tensile testing was conducted at room temperature. Full stress-strain curves were generated and tensile properties were measured: 0.2 % offset yield strength,

ultimate tensile strength (UTS), uniform strain (uEL), percent elongation and percent reduction of area. For the series of 5G welds, round and strip tensile specimens were machined in the same manner from 11:30 to 12:00, 9:00 to 9:30 and 6:00 to 6:30 clock positions for testing at room temperature. For the validation 5G welds, strip tensile specimens as depicted in Figure 6 were machined from the 12:00 to 12:30, 2:30 to 3:00 and 5:30 to 6:00 clock positions to nominally represent the 12:00, 3:00 and 6:00 clock positions, details of which are presented elsewhere [16,19,20].

3.1 CHARPY IMPACT TOUGHNESS TESTING

The WM and HAZ notch toughness was evaluated with standard CVN impact specimens (10 mm x 10 mm x 55 mm) cut transverse to the weld and notched through-thickness at the weld metal centerline (WMC) or in the HAZ adjacent to the fusion line. Two sets consisting of eighteen specimens each were cut, biased towards the OD (fill passes) Figure 7(a) from the first weld in each series. Full CVN transition curves were generated by testing triplicate specimens at temperatures between -120 °C and -5 °C. In addition, a partial transition curve was also obtained for through-thickness WMC specimens that were cut towards the hot/root pass region, as indicated in Figure 7(b). The transition curves were fit with a hyperbolic tangent function; lower and upper shelf energies as well as the transition temperature were adjusted to give an optimum least-squares fit to all the data. To determine the consistency within a given series of welds (six single-torch and three dual-torch), additional sets of six WM CVN specimens from each weld were tested in triplicate at -60 °C and -20 °C. In the validation 5G welds, Charpy specimens from the mid-section of the weld were selected from the 12:30 to 1:00, 5:30 to 6:00 and 8:30 to 9:00 clock positions to nominally represent the 12:00, 6:00 and 9:00 clock positions, details of which are presented elsewhere [19,20].

3.2 FRACTURE TOUGHNESS TESTING

3.2.1 J-CTOD SE(B) Testing

A large number of standard *J-CTOD* SE(B) specimens were machined from the single- and dual-torch welds of series 1 and 2. The specimens were the preferred geometry defined as $B \times 2B$, where B is the thickness of the specimen which was as close as practicable to the pipe thickness. These tests were carried out to provide values of WM and HAZ fracture toughness following standard procedures of ASTM E1290 [23] or E1820 [24] and BSI 7448 Part 2 [25]. According to E1290, only a single value of *CTOD* (from J) is measured, either at load for cleavage initiation (c or u) or at end-of-test (eot) for ductile tearing. In this work, the maximum load rather than at end-of-test load is reported for ductile tearing, following common practice in the pipeline industry. In those tests where cleavage occurred, the J -integral and *CTOD* at fracture are reported, whether the fracture event occurred before or after maximum load.³ For selected tests, the full J -integral resistance curve was measured in accordance with ASTM E1820 [24]. These specimens were cut transverse to the girth weld. Each specimen was etched in a 3 % nital solution to reveal the weld

³ It should be noted that test standards are silent on the conditions that should determine the end of test. It would be normal practice to stop the test after maximum load has been established, but cleavage fracture could occur after variable amounts of subsequent growth. The defining condition for δ_u is that cleavage should occur after at least 0.2 mm of ductile crack growth, but there is no requirement that this should be before maximum load. This leads to a certain ambiguity over whether δ_m or δ_u performance is appropriate in cases where cleavage is observed after maximum load.

metal and HAZ region for accurate scribing and through-thickness notching at the WMC or adjacent to the fusion line in the HAZ. Specimens were fatigue precracked to a targeted crack depth to specimen width ratio $a/W=0.5$ where $W = 2B$ for the specimens discussed. After fatigue precracking of a through-thickness-notched sacrificial B x 2B specimen, it was apparent that local compression would be necessary to achieve straight-fronted fatigue cracks. Specimens were tested plane-sided without side grooves. After mechanical testing, specimens were heat tinted at approximately 300 °C for 30 min and broken apart to allow optical measurements of the fatigue precracks to be made in accordance with BSI 7448 Part 2, which contains procedures specifically for welds. The calculated *CTOD* values were further qualified by examination of the fracture surfaces to quantify the extent of ductile tearing and establish whether they met requirements for δ_c , δ_u or δ_m .

3.3 METALLOGRAPHY AND MICROHARDNESS TESTING

Full cross sections from selected single- and dual-torch X100 rolled welds were cut, ground, mounted and polished with standard metallographic techniques [17]. Specimens were etched in a 2 % nital solution to reveal details of the base metal, HAZ and weld metal regions. The respective regions were characterized with optical microscopy and a series of through-thickness microhardness maps that included the WMC and the HAZ adjacent to the fusion line. Microhardness maps were also produced for the series of rolled welds as outlined in the companion technical report [17].

4 EXPERIMENTAL RESULTS

4.1 PIPE STEEL AND WELD METALS

Table 3 and Table 4 provide a list of representative chemical compositions of X100 pipes and selected weld metals. Calculated carbon equivalents along with bainite and martensite start temperatures are shown to enable comparison of relative hardenabilities. The pipe chemistry is based on low carbon and high manganese with Ni, Mo, Cu, Nb and Ti alloy additions. The compositions of weld metal for each series of single- and dual-torch welds (from analysis of samples sectioned along the through-thickness weld centerline) are quite similar. In the validation 5G welds, the pipes A and B have higher Mn and Si contents with lower Ni. In addition, pipe B has higher Cr, lower Mo and higher Cu compared to the other pipes used in this study. Based on composition, Pipe A has a Pcm carbon equivalent similar to the pipe used in the rolled 1G welds, whereas pipe B has a slightly higher Pcm carbon equivalent.

Figure 8 shows a typical microstructure of the X100 pipe steel, consisting predominantly of bainite and martensite, the latter constituent increasing near the central mid-wall region owing to alloy segregation.

Figure 9 and Figure 10 show the range of stress-strain curves obtained for the series of round and strap tensile specimens used to assess the longitudinal-to-pipe-axis (LPA) properties of the X100 pipe as a function of clock position with the seam weld used to indicate the 12:00 position. The round bar tests showed that specimens from 12:30 and 1:30 positions displayed the lowest strengths, whereas those from near 4:30 exhibited the highest strengths. The stress-strain curves for the strap tensile specimens were more variable with specimens near 12:00 and one from near 8:00 giving lower strengths than those from other locations. Similar spread in stress strain

behavior of LPA strap tensile specimens is seen between different clock positions of Pipe B used in the validation welds, as shown in Figure 11. In contrast, Pipe A shows a tighter spread in stress strain behavior as a function of clock position, as shown in Figure 12. The clock positions in these results are the 5G girth welding clock positions, and not with respect to the seam weld. In general, both Pipe A and B exhibit stress strain behaviors that fall inside the band of variation observed with the X-100 pipe from the 1G rolled welds, with Pipe A having slightly higher longitudinal strength than Pipe B.

4.2 WELD METAL TENSILE PROPERTIES

Tensile property data from a large number of round and strip tensile specimens from the single- and dual-torch welds are summarized in Table 5, Table 6, and Table 7. Calculated values for the yield to tensile strength (Y/T) ratio and strength mismatch factors (based on upper-bound pipe tensile data) are also provided. This allows the consistency among the welds and the variation within a given weld to be established. In addition, from strip tensile results, all welds met or exceeded the targeted yield strength of 810 MPa. This targeted yield strength was established in early weld qualification research conducted by Hudson [3] and is based on overmatching the pipe specified minimum yield strength (SMYS) of 690 MPa by 120 MPa to cover a typical distribution of pipe strengths for X100 (grade 690) pipes.

The results for the single-torch welds follow the same trend as previously observed in that the yield strengths of the ID-biased specimens are consistently higher than those of the OD-biased specimens [5,21,22,26]. Hamada *et al.* [27] also found very high yield strength for a single-torch weld, by the use of small-diameter tensile specimens cut from near the mid-wall. Additionally, the strip tensile specimen provides an average between the round bars, as is evident in the Y/T ratios and the uniform strain values (Table 5).

There is a clear tendency for the weld metal uniform strain values to be greater than those of the pipe, irrespective of tensile specimen type. In the majority of cases, the OD-biased specimens exhibit higher uniform strain. The calculated strength mismatch factor M [28] provides a good indication of the relative differences in strength levels between AWM and LPA pipe properties. The differences in strength mismatch factors based on yield, flow (average of yield and ultimate stresses) and ultimate stresses for the round-bar specimens are consistent for all the single-torch welds. For the OD-biased specimens M_{UTS} is somewhat higher, whereas calculated strength mismatch factors decrease in the order M_{YS} , M_{FS} and M_{UTS} for ID-biased round-bar specimens. The strip tensile specimens provide consistent values for all three calculated factors (M_{YS} , M_{FS} , M_{UTS}), representing an average between the ID- and OD-biased round bar specimens.

The dual-torch welds also met the targeted yield strength with results ≥ 821 MPa being achieved. In this case the variations between the different tensile specimen geometries were small. It is worth pointing out that these yield strength values are greater than previously observed with a dual-torch variant with NiMo-1 wire and a closer torch spacing [21]. For similar types of welds, Hamada *et al.* [27] also reported yield strengths that are consistent with those obtained in this investigation. The calculated strength mismatch factors are quite consistent and reveal a small decrease in the order M_{YS} , M_{FS} and M_{UTS} for tensile specimens.

Comparison of representative stress-strain curves from the single- and dual-torch welds and a typical range of pipe (LPA) curves reveals clear differences, as shown in Figure 13. Continuous yielding and uniform strain close to 5 % for the pipe steel (dashed lines in Figure 13) contrast with the respective parameters for the weld metals (solid lines). For the single-torch weld, discontinuous yielding is observed for the ID-biased round bar and marginally discontinuous yielding for the OD-biased and strip tensile specimens, and uniform elongations are significantly greater than those of the pipe steel. The weld would be considered overmatched if based on the upper curves (ID-biased and strip specimens), and only evenly matched for the lower curve (OD-biased specimen), at least for strain values up to about 3 %. In contrast, all dual-torch welds yielded discontinuously. Overmatching is absent or marginal after the (discontinuous) yield strain.

The stress-strain curves for AWM round and strip tensile specimens from different clock positions for the 5G single- and dual-torch welds are shown in Figure 14 and Figure 15, respectively. The same general trends, as indicated above, are evident with respect to differences for OD- and ID-biased round bars and the strip tensile specimens, although it can be seen that the curve for the specimen near 6:30 was lower than those at 12:00 and 9:00 for the single-torch weld. The strip tensile results (Figure 14 (b)) are almost identical for all three clock positions. In the case of the dual-torch weld, the stress-strain curves are more discontinuous with yield points and Lüders extensions, as shown in Figure 15(a). The curves for round-bar specimens from near 12:00 follow the same trend as observed for the single-torch weld. The nearly identical curves for the round specimens from near 6:30 fall between those from near 9:30. Figure 15(b) shows the curves from AWM strip specimens. Higher strength is observed for the specimen from near 12:00, while those from 9:00 and 6:00 are virtually identical, which is consistent with the AWM strip specimen providing an average measure of WM strength. Comparisons of the 0.2 % offset yield and ultimate strengths in the bar charts presented in Figure 16 and Figure 17 further illustrates the variations in strength that can exist within a given weld, as well as the marked differences between the single- and dual-torch process variants. As seen for the single-torch welds, the results are very consistent with higher strength measured for ID-biased versus OD-biased round bar specimens, while almost identical curves are obtained for the AWM strip tensile specimens from the different clock positions. In contrast, the results for the dual-torch are more variable, with those near 12:00 and 9:30 exhibiting stress-strain curves that are similar to the single-torch with respect to OD versus ID. Noticeably smaller differences are seen for the curves of specimens from near 9:30 and 6:30. Again, the AWM strip provides a measure of the average properties. The major differences between the single- and dual-torch welds are highlighted by comparison to the AWM strip tensile data, where it can be seen that the yield strengths are 49 MPa - 89 MPa higher, while the ultimate strengths are 50 MPa - 77 MPa higher. It is worthwhile and interesting to compare these AWM strip tensile results with those of the respective rolled welds (Table 5 and Table 6). In general, the single-torch 5G weld exhibits slightly higher strengths, with yield strength mismatch factors of 1.08 to 1.12 and a constant ultimate strength mismatch factor of 1.08. The dual-torch 5G weld had slightly lower mismatch strength factors (1.01 to 1.04 for yield strength and 0.99 to 1.02 for ultimate strength).

In the validation 5G single- and dual-torch welds, in general, the strip tensile stress strain behavior of the weld metal was quite similar between the different clock positions with some minor variations as seen in the examples shown in Figure 18. The stress strain curves from the

corresponding clock positions from Pipe B are also included in these figures. In spite of the variation in the pipe stress strain behavior as a function of clock position, the stress strain curves for the weld metal still exceed the highest values exhibited by the pipe by 100-140 MPa. These figures also show that, in contrast to the results obtained with the ER62S-G consumable, selection of higher strength ER76S-G and ER83S-G consumables for single- and dual-torch welding respectively provide very high overmatch over the pipe properties.

Table 7 shows detailed comparisons between the strip tensile results from the welds and the corresponding clock positions in the pipe. The mismatch factor varies depending on the contractor and the type of pipe used in the welding. The yield strength mismatch factor varies quite a bit because of variation in the measurement of the yield strength which is discussed in the following section. For single-torch welds made by contractor A, the ultimate tensile strength mismatch factor (M_{TS}) is in the range of 1.01 to 1.16 with pipe A and 1.15 to 1.25 with pipe B. The corresponding values with contractor B are 1.04 to 1.14 with pipe A and 1.15 to 1.25 with pipe B. The low mismatch values, which were the exceptions, were usually in the 12:00 clock position, possibly caused by excessive softening of the as-deposited passes due to reheat from the top passes. For dual-torch welds made by contractor A, M_{TS} is in the range of 1.10 to 1.14 with pipe A and 1.16 to 1.25 with pipe B. The corresponding values with contractor B are 1.11 to 1.16 with pipe A and 1.20 to 1.28 with pipe B.

The bar charts in Figure 19 and Figure 20 illustrate the variation in yield and tensile strengths as a function of clock position for the 5G validation single- and dual-torch welds respectively. In general, the tensile strengths at the 12:00 and 3:00 clock positions are quite similar for the single-torch welds 952-F through Weld-4. The 6:00 clock position shows slightly higher strengths than the other clock positions in welds 952-D, Weld 3 and Weld 4. This is a result of the reduced penetration in the 6:00 clock position which leaves more as-deposited regions in the weld resulting in higher strength; details of which are provided elsewhere [19]. In general, the lower strengths at the 12:00 clock position in 952-D is possibly because of increased softening due to reheating of the weld metal from the top passes. Similar trends are exhibited in the dual-torch welds 952-G through Weld-2 illustrated in Figure 19. Also, the tensile strengths in the dual-torch welds are comparable to those in the single-torch welds, which is a result of the higher strength consumable used in the former welds as mentioned before.

There is some scatter associated with the reported 0.2 % offset yield strength in some of these welds. This could be an artefact of the process of testing the strip tensile specimens for the following reasons. The thinner gage cross section area (0.19 in x 0.31in) combined with asymmetrical geometry of the strip tensile specimen compared to a round specimen can render the test vulnerable to some variation in its early part in the linear elastic range. Since the 0.2 % yield strength calculation is based on the slope of the linear elastic portion of the stress strain curve, any testing related variation in this elastic portion can cause this slope to differ significantly from the elastic modulus. This can result in variations in the reported yield strength from similar stress strain curves. However, the flow stress measured at 1 % total strain from the stress strain curve is very consistent and mirrors the variation in tensile strength quite well. At 1 % total strain, the stress strain curve is out of the linear range, and in the steady state plastic portion, and the resulting flow stress is not vulnerable to testing related variation in the elastic range. As a result, for strip tensile specimens (< 5.08 mm (0.2 in.) wide) and possibly also

circular tensile specimens of (< 5.08 mm (0.2 in.) diameter) small cross sections, the 1 % flow stress may be a more consistent indicator of yield behavior in X-100 welds until the testing methodology is refined enough to eliminate the variations in the elastic range.

4.3 WELD METAL AND HAZ CHARPY IMPACT PROPERTIES

The Charpy impact transition curves (based on averages at each test temperature) for X100 pipe, HAZ and weld metal regions are presented in Figure 21, while the full data sets are listed in Table 8 and Table 9. The superior toughness of the pipe is clearly evident, with high absorbed energies recorded even at -60 °C. For the single-torch welds, the HAZ and WMC (biased towards the root) exhibit lower impact energies than those of the pipe steel to test temperatures down to nearly -80 °C. For the WMC (biased towards the cap), a much flatter transition is evident.

For the dual-torch welds, the transition temperature for the HAZ is shifted upwards from the curve of the pipe steel by ~35 °C. Despite this, the impact energies are still quite high. The WMC (biased towards the root) shows a flatter transition curve than for the single-torch case. The transition curve for the WMC (biased towards the cap) is also shifted downward, but not quite so much as the WMC (biased towards the root). It is interesting to note that in all cases, except for the HAZ region of the dual-torch weld, the impact energies are well above 100 J at -20 °C, and the transition temperatures are at or below -60 °C.

To establish the consistency within each series of the single- and dual-torch rolled welds, additional WM CVN tests were carried out at -60 °C and -20 °C (Table 10 and Figure 22). Fairly consistent WM CVN results were obtained for the series of single-torch welds, although the results from the first weld were higher than those from the remaining five single-torch welds. The three dual-torch welds exhibited very consistent CVN results similar to those of the single-torch welds.

The Charpy toughness values obtained from the validation 5G welds are shown in the bar charts in Figure 23 and Figure 24. The Charpy toughness in the single-torch welds 952-D and 952-F and dual-torch welds 952-G and 952-H are all higher than 140 J, in the range of about 140 J to 250 J at -20 °C, and represent mostly ductile behaviour as observed on the fracture surface. In contrast, the Charpy toughness values in single-torch welds Weld-3 and Weld-4 and dual-torch welds Weld-1 and Weld-2 are much lower and range from 90 J to 180 J. These lower values are because of the higher percentage oxygen values (> 0.040 %) in these welds (Table 4), caused by the use of 50 % Ar:50 % CO₂ shielding gas. In most of these cases except for Weld-1, in a given weld, the toughness at the 6:00 clock position is higher than at the 12:00 and 3:00 clock positions. This is likely a result of the as-deposited structure having a high degree of toughness as described in a related final report [20]. Except in a couple of instances such as 952-D at 12:00 clock and Weld 2 at 12:00 clock, the HAZ toughness values from the rest of the welds from both single- and dual-torch are quite high and in the range of 160 J to 300 J.

4.4 WELD METAL AND HAZ FRACTURE TOUGHNESS

4.4.1 CTOD SE(B) Tests

Fracture toughness results for through-thickness fatigue-precracked Bx2B WM and HAZ specimens tested at -40 °C, -20 °C and RT (~20 °C) are listed in Table 12 for the first two series

of welds and in Table 13 for the third series of welds (all tests at -20 °C, base material from pipe A included). The WM fracture toughness of the single- and dual-torch welds for all three rounds is very consistent, with δ_m/J_m performance exhibiting fully ductile behavior over the complete range of test temperatures. It is worth noting that the toughness is significantly higher for dual-torch than for single-torch welds.

The HAZ test results obtained for the single-torch welds are quite varied, with δ_m , δ_u , and δ_c values⁴ being recorded over the range of test temperatures. Note that relatively high δ_m values were obtained at room temperature. For the single-torch welds, δ_c and δ_u performance was observed at -20 °C and -40 °C for series 1 with values ranging from $\delta_c = 0.04$ mm to $\delta_u = 0.27$ mm (Table 12), but δ_m performance was observed at -20 °C for series 3 (Table 13) except for one δ_u result at relatively high toughness ($\delta_u = 0.21$ mm). In contrast, for the dual-torch HAZ (Table 12) the CTOD value (only one result was obtained) at RT is somewhat lower than for the single-torch weld (series 1), but at -20 °C and -40 °C δ_u performance was observed at relatively high toughness levels between 0.14 mm and 0.28 mm. The relatively good performance of the dual-torch HAZ at low temperatures is somewhat surprising, since for the dual-torch weld there was a shift in the CVN transition curve to higher temperatures, and lower HAZ fracture toughness was observed by other researchers for dual-torch welds made in high strength steel X80 pipe [29]. Note also that, while all HAZ tests at -20 °C for the first two series of welds terminated with unstable fracture (u or c), this occurred for only one specimen out of five⁵ for the third series of welds.

4.5 METALLOGRAPHIC ANALYSIS AND MICROHARDNESS SURVEYS

4.5.1 Weld Macrostructures

Figure 26 shows representative macrographs of the single- and dual-torch rolled X100 welds. These figures reveal several important features, including aspects related to the macrostructure, the relative distribution of as-deposited AD and reheated regions, the profile of the fusion line and the width of the HAZ regions within the pipe steel material. In the single-torch weld the overall columnar structure extends from the fusion line towards the weld centerline in the majority of fill passes and ends up being essentially vertical in the cap pass (Figure 26(a)). Reheated regions appear as slightly darker bands that are evident between the passes including beneath the cap pass. At this magnification the columnar structure appears to extend unaltered through the reheated bands. This observation is important because distinguishing between the AD and reheated regions becomes very difficult for high strength WM. Because the weld torch is oscillated during welding to improve fusion with the side wall, the fusion line tends to have a wavy profile, as does the visible HAZ. Note the light-etching and relatively narrow grain-coarsened HAZ regions immediately adjacent to the fusion line. The most obvious differences seen for the dual-torch weld (Figure 26(b)) relate to the bead shape and fusion line profile as well as the relative distribution of AD and reheated regions. Also important is the marginally wider

⁴ Note that subscripts “c” and “u” indicate brittle (cleavage) fracture before and after a small amount (0.2 mm) of ductile tearing crack growth, respectively, and “m” indicates maximum load during ductile tearing without cleavage (Figure 25).

⁵ Six HAZ specimens were tested for the third series of welds. However, one specimen (HAZ of pipe A, clock position 3:00) was accidentally overloaded before the test and the results had to be discarded.

coarse region next to the fusion line and overall extent of the visible HAZ. Again a WM columnar structure dominates, and there is only a faint demarcation between the leading and trailing beads of a given dual-torch run. Generally wider reheated bands are observed, especially beneath the cap pass, where a significant amount of reheated WM was found. Note also that some small regions of buried lack-of-fusion flaws are present slightly above the pipe mid-wall (Figure 26(b)).

4.5.2 Microstructure and Microhardness

Detailed characterization of the microstructural features of single- and dual-torch rolled X100 welds was carried out at CANMET to provide information on the consistency of the welding procedures and to identify the major variations in microstructure and microhardness among the welds. As expected, the WM and HAZ regions contain areas that experience single or multiple thermal cycles as a result of the multipass welding techniques employed. This can produce subtle to marked differences in the morphology of transformed microstructures as a result of small changes in the thermal cycle experienced at a given location. For example, obvious microstructural differences between the cap pass and underlying passes are often observed, as evidenced in Figure 27 for the single-torch weld. The as-deposited WM region of the cap pass has a columnar structure, with prior austenite grains delineated by continuous or discontinuous grain boundary ferrite (GF) and/or occasional aligned ferrite-with-second-phase (upper bainite) [FS(A)]. A comparatively fine martensite/bainite/acicular ferrite mixed microstructure formed within the grain interiors. The structure of the underlying pass consists of bainite/acicular ferrite with occasional GF.

The dual-torch weld procedure had a relatively large torch separation (distance between the leading and trailing wires of 121 mm (4.75 in)), and used two dual-torch runs with a single-torch F5 (Figure 3) fill pass (F5) that was followed by offset dual-torch cap passes to complete the weld. The subtle differences in microstructure revealed in the micrographs shown in Figure 28 illustrate the marginal coarsening of the dual-torch WM that is further complicated by the inherent complexity of the thermal cycles and cooling periods resulting from deposition of two passes in close succession. The grain interiors in the cap pass have a relatively fine lath structure with occasional polygonal ferrite, whereas the structure in the underlying fill pass has mixed fine and coarse laths with polygonal ferrite. Further detail regarding the complex microstructures is provided in a related topical report [17].

In the HAZ region of these multipass welds, major variations in microstructure were expected to exist and some examples are presented in Figure 29 and Figure 30. In the grain coarsened (GC) HAZ region, bainite and martensite structures were formed within the prior austenite grains. Although no quantitative assessment of the prior austenite grain size was made, it is apparent from these images that the dual-torch weld HAZ is much coarser. It is also important to point out that the relative proportion of the constituent phases is greatly affected by the weld thermal cycle, especially the cooling period through the transformation range. For the X100 pipe steel used in this work, small changes in cooling period can lead to significant differences in the fraction of bainite and low-carbon lath martensite that is formed [30]. In addition, because the welds were made with multiple passes, the influence of reheating and tempering cannot be dismissed. Examples of reheated HAZ structures, shown in Figure 29(b) and Figure 30(b), provide some indication of the degree of microstructural change. In single- and dual-torch welds, it is often

considered important to evaluate and assess regions that are reaustenitized into the intercritical region (temperatures between Ac1 and Ac3). For example, the intercritically reheated GHAZ microstructure near the fusion line, shown in Figure 29(b), has been retransformed more than the structure in Figure 30(b). In the latter case, the austenite grains are delineated by a second phase that is subsequently transformed to a dark-etching constituent on cooling.

To further characterize the degree of microstructural variation in the experimental welds, complete microhardness maps were created for both series of rolled pipe welds (see reference [17] for further details). For the single-torch pipe welds, there was a relatively consistent pattern of hardness that corresponds well with the distribution of AD and reheated regions within the welds (Figure 31 and Figure 32). The alternating pattern of high-hardness AD regions and softer reheated regions is clearly evident. There is a tendency for more slivers of AD to be retained in the hot and first few fill passes compared to the last fill passes beneath the high-hardness cap pass. It is also clear that the HAZ region is considerably softer than the WM. In the dual-torch welds there was some inconsistency with respect to the microhardness maps. In some instances, they were very similar to the single-torch welds, while in other cases more uniform hardness was observed along with a wider HAZ region. This alternating pattern of AD and reheated regions of higher and lower hardness respectively was also evident in the single- and dual-torch welds of the validation 5G welds. This is shown in Figure 33 where the 6:00 clock weld shows more AD regions of higher hardness which results in higher strengths compared to the other clock positions. The strip tensile specimen provides a good measure of strength of the composite specimen and corresponds well to the trends in microhardness map of the weld.

The supplementary microhardness testing completed at CANMET revealed some interesting trends, as seen in the through-thickness traverses in Figure 34 to Figure 37. For both the single- and dual-torch welds, cyclic saw-tooth-type hardness profiles were observed. The through-thickness WM and HAZ hardness profiles in Figure 34 and Figure 35 show the periodic nature of the hardness profiles, which correspond with the periodic variation in thermal cycle that occurs throughout the entire weld. In both cases (single- and dual-torch), relatively high hardness exists in the vicinity of the cap passes. Reheating of the underlying material produces significant softening that is more pronounced in the HAZ regions. The periodic or saw-tooth profiles are observed throughout the pipe wall thickness. Profiles for the dual-torch welds tend to have wider peaks and valleys. Superimposing the through-thickness WM and HAZ hardness profiles (Figure 36 and Figure 37) for each process variant illustrates the differences and similarities between the pipe welds.

5 DISCUSSION

The primary emphasis of the research reported in this paper has been on development and application of the AWM tensile protocol and toughness testing for assessment of mechanized GMAW-P single- and dual-torch pipeline girth welds, particularly for high-strain applications where strength overmatching and good low-temperature toughness are required. Another objective of the research is to establish a better understanding of the factors that control weld metal and HAZ structure and properties of pipeline girth welds produced in high strength X100 (grade 690) pipes.

Two series of narrow-gap single- and dual-torch rolled welds, made under ideal shop/laboratory conditions, have provided very consistent welds for testing and evaluation. The AWM tensile testing protocol was further developed through evaluation of two 5G fixed-position single- and dual-torch girth welds. This allowed the test protocols for strength and toughness evaluations to be further developed and refined for demanding strain-based-design pipeline applications. This approach was eventually applied in the evaluation of tensile properties of the validation 5G girth welds.

5.1 AWM TENSILE PROPERTIES

To measure AWM tensile properties consistently and reliably and to assure overall weld strength overmatch for qualification of pipeline girth welds, it is essential to have a good understanding of the factors that influence pipe and weld metal properties [28,31]. The results obtained in this investigation support adoption of a strip tensile specimen that allows a greater proportion of weld metal to be sampled. The through-thickness variation in strength observed in the single-torch welds is now well understood and can be accounted for based on the different distribution of as-deposited and reheated weld metal (and tempering). In the area above the hot pass and the first few fill passes, slivers of high-hardness (high-strength), as-deposited weld metal have been shown to exist, whereas toward the pipe OD there is an increase in the amount of reheated weld metal, which lowers strength (see Figure 31). In the case of the dual-torch welds, much less through-thickness variation and yield strengths above the target (810 MPa) were observed and can be explained in part on the basis of weld pass sequence and torch spacing that was used with the specific welding consumable employed. That the two dual-torch runs (D1-D2 and D3-D4) are sampled in both the round-bar and strip tensile specimens supports the similar tensile properties observed. However, as evident in Figure 32, some differences in the microhardness maps were found, and this suggests that larger differences in tensile properties may at times be measured. For the dual-torch rolled welds the torch spacing (121 mm or 4.75 in) plays a role in achieving relatively high weld metal yield strengths. This relates to the effective energy input and actual thermal cycle that the weld experiences. With this relatively-large torch spacing, shorter cooling periods (faster cooling rates) will be experienced by the weld bead deposited by the trailing wire, and therefore favor lower-temperature transformation products (higher hardness) than would be observed with closer spacing [3,18]. For assessing strength mismatch, full WM stress-strain curves are required to obtain a better indication of initial and post-yield behavior in relation to pipe properties (

Figure 13). From the stress-strain data the strength mismatch factors at yield, flow and ultimate tensile strength can be determined. Based on the results listed in Table 5, Table 6, and Table 7, it is recommended that all three factors be used to characterize strength mismatch and ultimately provide sufficient information for design strains of several percent. In the validation welds, there was some scatter in the measurement of the 0.2 % offset yield strength from the thin strip tensile specimens. As an alternative, the flow stress at 1 % total strain can be utilized to investigate the yield behavior, until variations in the 0.2 % offset yield stress are sorted out.

The AWM tensile test protocol was used to evaluate two 5G single- and dual-torch welds produced with the nominal welding procedures of the rolled welds. This revealed some interesting trends and differences that warrant discussion. First, the same consistent trend of higher strength for ID-biased versus OD-biased round-bar tensile specimens and average strip tensile results was observed for the single-torch weld. Near-identical stress-strain curves were

obtained with the AWM strip tensile specimen irrespective of clock position. This is helpful in determining which regions should be tested during weld qualification testing and for identifying data to be used for defect assessments. It is also important that the strengths of the 5G weld are slightly higher than those for the corresponding single-torch rolled weld. In the case of the dual-torch weld, the results were more variable, with comparatively higher values in the 11:00 to 12:00 position compared with 9:00 and 6:00. The strength levels measured for the 5G dual-torch weld are considerably lower than those for the single-torch and marginally less than those for the corresponding dual-torch rolled weld. However, in the validation 5G welds, by the choice of appropriate higher strength consumables, the strengths in the dual-torch weld were comparable to that obtained in the single-torch welds. After comparing both sets of data, it is recommended that multiple clock positions continue to be tested to determine AWM tensile properties of mechanized pipe girth welds. Such an approach allows gauging the effectiveness of the control methodology of the welding variables in minimizing strength variations around the pipe.

5.2 CVN TRANSITION CURVES

Charpy impact tests of the single- and dual-torch welds revealed some interesting trends for both WM and HAZ regions. First, they confirm that the series of welds exhibited similar impact properties, especially in the case of the dual-torch welds (Table 10 and Figure 22). The impact transition curves in Figure 21 show that the pipe steel exhibited high impact energies (notch toughness) with fully ductile behavior down to temperatures well below $-40\text{ }^{\circ}\text{C}$ and a transition temperature around $-70\text{ }^{\circ}\text{C}$. For the single-torch weld, the HAZ exhibited a decrease in upper shelf and transition-region impact energies without a significant shift in transition temperature. In contrast, for the dual-torch weld the HAZ curve was shifted to higher temperatures by $\sim 35\text{ }^{\circ}\text{C}$. This is generally attributed to the wider and coarser HAZ of the dual-torch weld.

For the weld metal there were marked differences in toughness for specimens biased towards the cap or root regions, especially in the case of the single-torch weld. In this case the root-biased CVN toughness was superior, maintaining high energies down to nearly $-80\text{ }^{\circ}\text{C}$. Much lower upper-shelf energies were found in the case of the cap-biased CVN toughness, although the transition was not steep; therefore reasonably high energies were achieved down to almost $-60\text{ }^{\circ}\text{C}$. The root-biased CVN transition curve was very similar in shape, but consistently above the cap-biased curve for the dual-torch weld.

The Charpy toughness behavior in the validation 5G welds at $-20\text{ }^{\circ}\text{C}$ of both WM and HAZ corresponded to mostly ductile behavior in both single- and dual-torch welds, in spite of some variation in the actual values. The lower values were mostly observed with welds made with contractor B, where the 50 % Ar:50 % CO_2 shielding gas resulted in higher oxygen values in the weld metal.

5.3 FRACTURE TOUGHNESS OF WM AND HAZ

Standard fracture toughness results for standard SE(B) specimens with through-thickness fatigue precracks (Table 12 and Table 13) show some interesting trends. For both the single- and dual-torch welds, comparatively high WM fracture toughness (fully ductile behavior with J_m/δ_m values) occurred over the complete range of test temperatures. The dual-torch weld exhibited marginally higher toughness values at both $-20\text{ }^{\circ}\text{C}$ and $-40\text{ }^{\circ}\text{C}$. However, the fracture toughness of the HAZ of the single-torch variant was quite scattered and generated $J_{m/w/c}/\delta_{m/w/c}$ values. In

contrast, the HAZ of the dual-torch weld exhibited J_{II}/δ_{II} values that ranged from 216 kJ/m² to 434 kJ/m² (0.14 mm to 0.28 mm). Although this is consistent with the results from other fracture toughness tests conducted in this program [13,14], it is somewhat unexpected because other researchers [29] have reported low HAZ fracture toughness results for other dual-torch girth welds. This was believed to be related to the higher effective energy input during welding that resulted in a wider HAZ along with a potential for coarser grains and a tendency to form more-brittle microstructures. In the present study, there was a shift in the dual-torch HAZ CVN transition curve to higher temperatures (Figure 21). Also, it was confirmed that simulated HAZ regions of the same X100 pipe steel showed low CVN notch toughness [30]. Further post-test evaluations of the HAZ Bx2B test specimens are required to help explain these observations.

6 CONCLUSIONS

This investigation focused on evaluation of three series of baseline experimental single- and dual-torch rolled pipeline girth welds with small-scale conventional tests to assess AWM tensile properties, CVN transition behavior, and standard fracture toughness. This was supplemented by characterization of WM and HAZ microstructures with optical microscopy, microhardness surveys, and full-section hardness maps. Some of the observations and conclusions drawn from this evaluation are:

1. AWM tensile properties of single-torch rolled welds exhibited high yield and ultimate strengths and a consistent trend of ID-biased round bars exhibiting higher strength compared with OD-biased specimens. AWM strip tensile specimens provided an average measure of WM strength. This behavior correlated with the variation in AD and RH WM observed in the weld, confirmed by microhardness maps which showed more high-hardness AD WM towards the hot pass (ID side), and more low-hardness (reheated) WM toward the OD side. The same trend was observed for the single-torch 5G weld, although the overall strength was marginally higher than for the rolled welds. For the dual-torch rolled welds, the tensile properties were generally very consistent for all test specimens and yield strengths in excess of the targeted value of 810 MPa were achieved. In contrast, the tensile properties of the 5G dual-torch weld were more variable and the yield strengths (based on AWM strip tensile results) were marginally below the targeted value. In the validation 5G welds, with higher strength consumables and control of welding variables in a tight range, consistent tensile properties with significant overmatch with respect to the pipe properties were obtained.
2. The WM CVN impact energy results (at -60 °C and -20 °C) for the complete series of single-torch welds showed some variation, with the first-produced weld exhibiting slightly higher toughness than the remaining five welds. The three dual-torch welds had very good and reasonably consistent notch toughness. The notch toughness performance of all welds was deemed good, with high upper-shelf energies and nearly identical transition temperatures close to -70 °C except for the HAZ region of the dual-torch weld which exhibited a transition temperature of -35 °C. In the validation 5G single- and dual-torch welds, the WM CVN impact energy at -20 °C showed some variation around the pipe, but the average values were all higher than 140 J and showed mostly ductile behavior with welds made by contractor A, and were significantly lower (90 J and above) with welds made by contractor B.
3. The WM $J/CTOD$ results were very consistent with fully ductile J_m/δ_m values of about 200

kJ/m^2 to $350 \text{ kJ/m}^2 / 0.15 \text{ mm}$ to 0.23 mm at all temperatures. On the other hand, most of the HAZ results from the first two series of welds exhibited brittle cleavage ($\delta_{w/c}/J_{w/c}$), although only one very low value occurred (for the single-torch weld HAZ) while all others were preceded by ductile crack growth. In contrast, for the third series of welds (all single-torch), only one HAZ specimen out of five exhibited unstable crack propagation - and only after significant ductile crack growth - whereas the remaining tests provided fully ductile behavior and, in most cases, high toughness values ($J_m > 550 \text{ kJ/m}^2$, $\delta_m > 0.36 \text{ mm}$)

4. The complex WM microstructures formed in the single-torch pipe welds consisted of mixed bainite/martensite, with higher hardness in AD compared to RH regions. Periodic through-thickness hardness profiles reflect the reheating and tempering of the WM deposited sequentially. In the dual-torch pipe welds, high hardness of the leading-wire deposit is significantly altered by deposition of the trailing wire.
5. Three HAZ structures/regions formed in the multipass pipe welds include the GHAZ, SCR-GHAZ and ICR-GHAZ. The microstructures formed within these regions are consistent with the periodic through-thickness variation in constituent phases and hardness.
6. Microhardness maps give a good visual indication of the hardness and microstructure distribution, especially in the WM region where reheated zones are difficult to distinguish by conventional metallographic examination.
7. Through-thickness microhardness traverses provide a good indication of the relative changes in hardness as a function of local thermal cycle and allow specific regions such as the GHAZ to be better quantified. For example, the lower through-thickness hardness of the HAZ compared to the WM provides a good indication of the relative tensile properties.

7 ACKNOWLEDGMENTS

This research was funded, in part, by NIST, CANMET-MTL and the Federal Interdepartmental Program for Energy Research and Development (PERD). The authors would like to thank Mr. M. Kerry for precision machining, Mr. R. Eagleson for mechanical testing, Dr. Mark Richards for fractography and Ms. P. Liu for metallographic analysis and microhardness testing. The research is part of a larger consolidated program jointly funded by the Pipeline and Hazardous Materials Safety Administration of the U.S. Department of Transportation (DOT), and the Pipeline Research Council International, Inc. (PRCI). The technical guidance and support provided Mr. D. Taylor, TransCanada PipeLines Ltd., and Mr. D. Horsley, BP Exploration is also gratefully acknowledged.

8 REFERENCES

1. Seo, D-H., Yoo, J-Y., Song, W-H. and Kang, K-B., "Development of X100 Linepipe Steel with High Deformation Capacity," Proc. of 7th Int. Pipeline Conf., ASME, IPC2008-64220, pp. 1-8, 2008.
2. Hara, T., Shinohara, Y., Terada, Y., Hitoshi, A. and Doi, N., "Metallurgical Design and Development of High Deformable X100 Line Pipe Steels Suitable for Strain Based Design," Proc. of 19th Int. Offshore and Polar Eng. Conf., ISOPE, Osaka, Japan, pp. 73-79, 2009.
3. Hudson, M.G., "Welding of X100 Linepipe," Ph.D. Thesis, Welding Engineering Research Centre, Cranfield University, 2004.
4. Gianetto, J.A., Bowker, J.T., Dorling, D.V. and Horsley, D., "Structure and Properties of X80 and X100 Pipeline Girth Welds," 5th Int. Pipeline Conf., ASME, IPC04-0316, pp. 1-13, 2004.
5. Fiore, S. R., Gianetto, J.A., Hudson, M. G., Vase, S., Khurana, S., Bowker, J.T. and Dorling, D.V., "Development of Optimized Weld Metal Chemistries for Pipeline Girth Welding of High Strength Line Pipe," 7th Int. Pipeline Conf., ASME, IPC2008-64593, pp. 1-12, 2008.
6. Hukle, M.V., Horn, A.M, Hoyt, D.S. and LeBleu, Jr., J.B., "Girth Weld Qualification for High Strain Pipeline Applications", ASME, Int. Conf. on OMAE, Paper-67573, pp. 1-6, 2005.
7. Hukle, M.V., Hoyt, D.S. and LeBleu, Jr., J.B., Dwyer, J.P. and Horn, A.M., Qualification of Welding Procedures for ExxonMobil High Strain Pipelines", ASME, Int. Conf. on OMAE, Paper-92503, pp. 1-6, 2006.
8. Newbury, B.D., Hukle, M.V., Crawford, M.D. and Lillig, D.B., "Welding Engineering for High Strain Pipelines", Proc. of 17th Int. Offshore and Polar Eng. Conf., ISOPE, Lisbon, Portugal, pp. 2996-3000, 2007.
9. Fairchild, D.P., Crawford, M.D, Cheng, W., Marcia, M.L., Nissley, N.E., Ford, S.J., Lillig, D.B. and Sleight, J., "Girth Welds for Strain-Based Design Pipelines," Proc. of 18th Int. Offshore and Polar Eng. Conf., ISOPE, Vancouver, BC, Canada, pp. 48-56, 2008.
10. Wang, Y-Y., Liu, M., Stephens, M., Petersen, R. and Horsley, H., "Recent Development in Strain Based Design in North America," Proc. of 19th Int. Offshore and Polar Eng. Conf., ISOPE, Osaka, Japan, pp. 11-19, 2009.

11. DOT-PRCI, 2007 “Update of Weld Design, Testing, and Assessment Procedures for High Strength Pipelines,” <http://primis.phmsa.dot.gov/matrix/PrjHome.rdm?prj=225>.
12. DOT-PRCI, 2007 “Development of Optimized Welding Solutions for X100 Linepipe Steel,” <http://primis.phmsa.dot.gov/matrix/PrjHome.rdm?prj=226>.
13. Park, D.Y., Tyson, W.R., Gianetto, J.A., Shen, G. and Eagelson, R., “Small-scale Low Constraint Fracture Toughness Test Results”, Final Report 277-T-06 to PHMSA per Agreement # DTPH56-07-T-000005, 277-T-06, September 2011.
14. Park, D.Y., Tyson, W.R., Gianetto, J.A., Shen, G. and Eagelson, R., “Small-scale Low Constraint Fracture Toughness Test Discussion and Analysis”, Final Report 277-T-07 to PHMSA per Agreement # DTPH56-07-T-000005, September 2011.
15. Tyson, W.R., Park, D.Y., Gianetto, J.A. and G. Shen, “Summary of Mechanical Properties, Final Report 277-T-08, to PHMSA per Agreement # DTPH56-07-T-000005, September 2011.
16. Panday, R. and Daniel, J., “ Materials Selection, Welding and Weld Monitoring”, Final Report 278-T-02, to PHMSA per Agreement # DTPH56-07-T-000005, September 2011.
17. Gianetto, J.A., Tyson, W.R., Goodall, G.R, Rajan, V.B., Quintana, M.A. and Chen, Y. “Microstructural Characterization of High Strength Steel Pipeline Girth Welds”, Final Report 278-T-03, to PHMSA per Agreement # DTPH56-07-T-000005, September 2011.
18. Chen, Y., Wang, Y-Y., Quintana, M.A., Rajan, V.B. and Gianetto, J.A., “Thermal Model for Welding Simulations”, Final Report 278-T-07, to PHMSA per Agreement # DTPH56-07-T-000005, September 2011.
19. Rajan V. B., “Essential Welding Variables”, Final Report 278-T-06, to PHMSA per Agreement # DTPH56-07-T-000005, September 2011.
20. Rajan V. B., “Application to Other Welding Processes”, Final Report 278-T-09, to PHMSA per Agreement # DTPH56-07-T-000005, September 2011.
21. Gianetto, J.A., Bowker, J.T. and Dorling, D.V. “Assessment of Properties and Microstructure of X100 Pipeline Girth Welds,” *Welding in the World*, Vol. 49, No. 11/12, pp. 71-89, 2005.
22. Gianetto, J.A., Bowker, J.T., Bouchard, R., Dorling, D.V. and Horsley, D., “Tensile and Toughness Properties of Pipeline Girth Welds,” *Welding in the World*, Vol. 51, No. 5/6, pp. 64-75, 2007.
23. ASTM E 1290–08: Standard Test Method for Crack-Tip Opening Displacement (CTOD) Fracture Toughness Measurement, ASTM International, West Conshohocken, PA, United States, 2008.
24. ASTM E 1820-08: Standard Test Method for Measurement of Fracture Toughness, ASTM International, West Conshohocken, PA, United States, 2008.
25. British Standard BS 7448: Fracture Mechanics Toughness Tests, British Standards Institution, London, England, 1997.
26. Gianetto, J.A., Bowker, J.T., Dorling, D.V., Taylor, D., Horsley, D. and Fiore, S.R., “Overview of Tensile and Toughness Testing Protocols for Assessment of X100 Pipeline Girth Welds”, 7th Int. Pipeline Conf., ASME, IPC2008-64668, pp. 1-10, 2008.

27. Hamada, M., Shitamoto, H. and Hirata, H., "Tensile Properties and Microstructure of Girth Welds for High Strength Linepipe," Proc. of 19th Int. Offshore and Polar Eng. Conf., ISOPE, Osaka, Japan, pp. 50-55, 2009.
28. Denys, R.M. and Lefevre, A.A., "Material Test Requirements for Strain Based Pipeline Design" Proceedings of Int. Symp. on Microalloyed Steels for the Oil and Gas Industry, Eds. W.J. Fazackerley, P. Bordignon, K. Hulka and F. Siciliano, TMS, pp. 513-531, 2007.
29. Hamad, F., Collins, L. and Volkers, R., "Effects of GMAW Procedure on the Heat-Affected Zone (HAZ) Toughness of X80 (Grade 550) Line Pipe," 7th Int. Pipeline Conf., ASME, IPC2008-64097, pp. 1-17, 2008.
30. Gianetto, J.A., Goodall, G.R., Tyson, W.R., Quintana, M.A., and Chen, Y., "Microstructure and Properties of Simulated Heat Affected Zones", Final Report 278-T-04 to PHMSA per Agreement # DTPH56-07-T-000005, September 2011.
31. Wang, Y-Y., Liu, M., Gianetto, J. and Tyson, B. "Considerations of Line Pipe and Girth Weld Tensile Properties for Strain-Based Design of Pipelines," 8th Int. Pipeline Conf., ASME, IPC2010-31376, pp. 1-10, 2010.

Table 1: Welding parameters for Rolled 1G Welds

Single-Torch Variant				
Pass	Hot	Fill 1-4	F5	Cap
Current (A)	198-223	196-219	197-205	146-192
Voltage (V)	18-25	19-24	22-24	18-25
Travel Speed (mm/min)	11.9	8.43	7.58-7.83	6.3-7.83
Preheat/Interpass T (°C)	101-108	102-120	100-109	100-119
Energy Input (kJ/mm)	0.17-0.19	0.44-0.56	0.52-0.61	0.38-0.52
Dual-Torch Variant				
Pass	Hot	Fill D1-D4	F5	Cap
Current (A)	221-252	194-215	193-226	133-148
Voltage (V)	19-24	20-24	22-24	20-26
Travel Speed (mm/min)	11.9	9.32	8.0-11.0	9.32-9.74
Preheat/Interpass T (°C)	102-125	107-125	109-118	107-120
Heat Input (kJ/mm)	0.47-0.55	0.48-0.55	0.39-0.55	0.31-0.39

Note: Root pass used ER70S-G wire/75 % Ar:25 % CO₂ shielding gas. Fill and cap passes used ER90S-G wire/85 % Ar:15 % CO₂ shielding gas. Dual-torch spacing was set at 121 mm (4.75 in).

Table 2: Welding parameters for validation 5G welds

Single-Torch Variant using ER76S-G electrode – Contractor A				
Power Source Mode & Shielding Gas	Pulse with 85 % Ar:15 % CO ₂			
Pass	Hot	Fill 1-3	Cap1	Cap2
Preheat/Interpass T (°C)	100-125	100-125	100-125	100-125
Heat Input (kJ/mm)	0.30-0.31	0.60-0.84	0.50-0.71	0.49-0.70
Single-Torch Variant using ER76S-G electrode – Contractor B				
Power Source Mode & Shielding Gas	Constant Voltage with 50 % Ar:50 % CO ₂			
Pass	Hot	Fill 1- 4	Cap1	Cap2
Preheat/Interpass T (°C)	100-130	100-145	110-135	105-120
Heat Input (kJ/mm)	0.49-0.61	0.46-0.61	0.39-0.68	0.40-0.68
Dual-Torch Variant with 121 mm (4.75 in) torch spacing using ER83S-G electrode–Contractor A				
Power Source Mode & Shielding Gas	Pulse with 85 % Ar:15 % CO ₂			
Pass	Hot	Fill D1-D3	Cap1	Cap2
Preheat/Interpass T (°C)	100-125	100-125	100-125	100-125
Heat Input (kJ/mm)	0.29-0.31	0.61-0.82	0.47-0.61	0.48-0.63
Dual-Torch Variant with 51 mm (2 in) torch spacing using ER83S-G electrode–Contractor B				
Power Source Mode & Shielding Gas	Constant Voltage with 50 % Ar:50 % CO ₂			
Pass	Hot	Fill D1-D4	Cap1	Cap2
Preheat/Interpass T (°C)	110-120	120-195	155-190	155-190
Heat Input (kJ/mm)	0.28-0.39	0.43-0.60	0.38-0.54	0.48-0.62

Table 3: Chemical composition of weld metals and pipe steels from 1G rolled welds

Element Wt %	Single-Torch				Dual-Torch			
	807F	807H	807J	Pipe	883D	883E	883F	Pipe
C	0.11	0.10	0.10	0.061	0.11	0.11	0.11	0.067
Mn	1.38	1.38	1.39	1.76	1.48	1.44	1.43	1.76
Si	0.54	0.56	0.58	0.10	0.56	0.55	0.57	0.10
S	0.010	0.009	0.011	0.002	0.011	0.011	0.011	0.001
P	0.013	0.013	0.013	0.006	0.014	0.014	0.014	0.006
Ni	0.95	0.95	0.96	0.50	0.99	0.96	0.98	0.50
Cr	0.05	0.05	0.05	0.025	0.07	0.06	0.06	0.025
Mo	0.35	0.35	0.35	0.27	0.36	0.35	0.35	0.35
Cu	0.13	0.14	0.13	0.28	0.14	0.14	0.13	0.27
Al	0.006	0.006	0.005	0.038	0.005	0.006	0.006	0.038
Ti	0.032	0.035	0.038	0.012	0.038	0.037	0.036	0.012
O	0.023	0.029	0.027	-	0.032	0.031	0.025	-
N	0.008	0.008	0.005	0.0025	0.004	0.004	0.004	0.0028
B	0.0002	0.0002	0.0001	0.0004	0.0005	0.0003	0.0003	0.0004
V	0.003	0.003	0.003	-	0.004	0.004	0.004	-
Nb	0.003	0.003	0.003	0.029	0.006	0.005	0.004	0.029
CE _{IW}	0.50	0.49	0.48	0.47	0.52	0.51	0.51	0.47
P _{cm}	0.25	0.24	0.24	0.20	0.26	0.25	0.26	0.20
M _s (°C)	437	441	445	459	433	435	435	457
B _s (°C)	607	609	611	612	595	601	601	611

Notes:

$$CE_{IW} = C + Mn/6 + (Cr+Mo+V)/5 + (Ni + Cu)/15$$

$$P_{cm} = C + Si/30 + (Mn+Cu+Cr)/20 + Ni/60 + Mo/15 + V/10 + 5B$$

$$B_s = 830-270(C)-90(Mn)-37(Ni)-70(Cr)-83(Mo)$$

$$M_s = 561-474(C)-33(Mn)-17(Ni)-17(Cr)-21(Mo)$$

Table 4: Chemical composition of weld metal and pipe from validation 5G welds

Element Wt %	Pipe		Single-Torch				Dual-Torch			
	Pipe A	Pipe B	952-D in Pipe A	952-F in Pipe B	Weld 3 in Pipe A	Weld 4 in Pipe B	952-G in Pipe A	952-H in Pipe B	Weld 1 in Pipe A	Weld 2 in Pipe B
C	0.06	0.05	0.08	0.08	0.08	0.09	0.09	0.09	0.10	0.09
Mn	1.90	1.97	1.63	1.63	1.48	1.56	1.57	1.70	1.58	1.62
Si	0.32	0.18	0.49	0.44	0.45	0.43	0.53	0.58	0.60	0.66
S	0.003	<0.003	0.008	0.008	0.006	0.006	0.009	0.009	0.010	0.011
P	0.012	0.008	0.015	0.014	0.015	0.013	0.015	0.009	0.008	0.009
Ni	0.23	0.45	1.24	1.24	1.36	1.31	1.50	1.77	1.88	1.98
Cr	0.04	0.56	0.17	0.29	0.19	0.28	0.21	0.41	0.41	0.32
Mo	0.23	0.10	0.42	0.37	0.44	0.39	0.46	0.44	0.48	0.51
Cu	0.24	0.48	0.18	0.25	0.19	0.24	0.19	0.27	0.24	0.18
Al	0.038	0.016	0.02	0.002	0.002	0.002	0.001	0.002	0.003	0.003
Ti	0.017	0.012	0.034	0.032	0.027	0.027	0.035	0.024	0.022	0.027
O	-	-	0.037	0.028	0.051	0.040	0.032	0.032	0.048	0.047
N	-	-	0.004	0.007	0.005	0.004	0.004	0.004	0.005	0.004
B	0.0002	0.0002	0.0002	0.0002	0.0003	0.0003	0.0003	0.0002	0.0003	0.0002
V	0.003	0.003	0.003	0.003	0.003	0.003	0.003	0.004	0.005	0.004
Nb	0.040	0.021	0.010	0.006	0.007	0.006	0.005	0.008	0.007	0.008
CE _{IW}	0.46	0.57	0.57	0.58	0.56	0.59	0.63	0.68	0.68	0.67
Pcm	0.20	0.22	0.25	0.25	0.24	0.26	0.28	0.29	0.29	0.28
M _s (°C)	460	453	433	433	437	431	427	415	415	416
B _s (°C)	612	575	565	564	574	564	555	521	524	522

Notes:

$$CE_{IW} = C + Mn/6 + (Cr+Mo+V)/5 + (Ni + Cu)/15$$

$$Pcm = C + Si/30 + (Mn+Cu+Cr)/20 + Ni/60 + Mo/15 + V/10 + 5B$$

$$Bs = 830-270(C)-90(Mn)-37(Ni)-70(Cr)-83(Mo)$$

$$Ms = 561-474(C)-33(Mn)-17(Ni)-17(Cr)-21(Mo)$$

Table 5: AWM tensile properties of single-torch 1G rolled welds

Weld ID	Tensile Type	YS 0.2 % (MPa)	UTS (MPa)	EL (%)	RA (%)	Flow Stress (MPa)	Y/T Ratio	uEl (%)	Strength Mismatch		
									M_{YS}	M_{FS}	M_{UTS}
807F	R1-OD	786	939	21	58	863	0.84	6.9	1.01	1.05	1.09
	R1-ID	911	952	21	65	932	0.96	7.0	1.17	1.14	1.11
	S1	845	928	21	52	887	0.91	6.9	1.08	1.08	1.08
807G	R1-OD	808	906	23	61	857	0.89	8.7	1.03	1.04	1.05
	R1-ID	882	934	19	56	908	0.94	7.4	1.13	1.11	1.09
	S1	838	919	23	51	879	0.91	7.8	1.07	1.07	1.07
807H	R1-OD	781	917	16	61	849	0.85	-	1.00	1.03	1.07
	R1-ID	895	936	21	66	916	0.96	8.6	1.15	1.12	1.09
	S1	830	913	22	52	872	0.91	7.5	1.06	1.06	1.06
	R2-OD	813	902	23	64	858	0.90	7.1	1.04	1.05	1.05
	R2-ID	874	920	20	63	897	0.95	7.3	1.12	1.09	1.07
	S2	835	911	23	56	873	0.92	7.8	1.07	1.06	1.06
	R3-OD	796	902	23	64	849	0.88	7.2	1.02	1.03	1.05
	R3-ID	871	917	20	60	894	0.95	6.0	1.12	1.09	1.07
S3	828	907	21	54	868	0.91	7.9	1.06	1.06	1.05	
807I	R1-OD	838	898	23	64	868	0.93	8.4	1.07	1.06	1.04
	R1-ID	874	930	21	61	902	0.94	6.1	1.12	1.10	1.08
	S1	841	916	22	49	879	0.92	7.8	1.08	1.07	1.07
807J	R1-OD	780	909	23	61	845	0.86	7.6	1.00	1.03	1.06
	R1-ID	879	924	21	65	902	0.95	7.9	1.13	1.10	1.07
	S1	831	913	21	47	872	0.91	7.0	1.06	1.06	1.06
807K	R1-OD	782	911	22	61	847	0.86	6.9	1.00	1.03	1.06
	R1-ID	885	931	21	61	908	0.95	7.7	1.13	1.11	1.08
	S1	834	915	22	51	875	0.91	7.5	1.07	1.07	1.06
LPA	X100-Pipe	781	860	30	70	821	0.91	4.9	1.00	1.00	1.00

Notes:

YS-yield strength, UTS-ultimate tensile strength, uEl-uniform strain, R-round tensile, S-strip tensile (Gauge Length: R = 20 mm; S = 25 mm); LPA-Longitudinal to pipe axis X100 pipe (Strap tensile test, Gauge Length = 50.8 mm)

M_{YS} is based on yield strengths, M_{FS} on flow stresses, and M_{UTS} on ultimate tensile strengths [26]

Table 6: AWM tensile properties of dual-torch welds

Weld ID	Tensile Type	YS 0.2 % (MPa)	UTS (MPa)	EL (%)	RA (%)	Flow Stress (MPa)	Y/T Ratio	uEl (%)	Strength Mismatch		
									M_{YS}	M_{FS}	M_{UTS}
883D	R1-OD	822	880	21	68	851	0.93	7.6	1.05	1.04	1.02
	R1-ID	828	874	21	66	851	0.95	6.4	1.06	1.04	1.02
	R2-OD	840	893	22	68	867	0.94	7.9	1.08	1.06	1.04
	R2-ID	835	876	22	63	856	0.95	7.1	1.07	1.04	1.02
	S1	821	878	24	50	850	0.93	7.4	1.05	1.03	1.02
	S2	831	881	23	50	856	0.94	7.0	1.06	1.04	1.02
	S3	828	892	23	50	860	0.93	7.4	1.06	1.05	1.04
	S4	835	901	23	50	868	0.93	7.8	1.07	1.06	1.05
883E	R1-OD	833	900	24	71	867	0.93	8.5	1.07	1.06	1.05
	R1-ID	830	886	19	57	858	0.94	7.1	1.06	1.05	1.03
	S1	824	894	22	49	859	0.92	7.5	1.06	1.05	1.04
	S2	824	892	23	51	858	0.92	7.4	1.05	1.05	1.04
883F	R1-OD	826	896	23	68	861	0.92	8.2	1.06	1.05	1.04
	R1-ID	823	871	22	70	847	0.94	7.1	1.05	1.03	1.01
	S1	829	883	23	52	856	0.94	6.9	1.06	1.04	1.03
	S2	826	888	23	55	857	0.93	7.5	1.06	1.04	1.03

Notes:

YS-yield strength, UTS-ultimate tensile strength, uEl-uniform strain, R-round tensile, S-strip tensile (Gauge Length: R = 20 mm; S = 25 mm)

M_{YS} is based on yield strengths, M_{FS} on flow stresses, and M_{UTS} on ultimate tensile strengths [26]

Table 7: AWM strip tensile properties of validation 5G welds

Weld ID	Pipe ID	Clock Pos.	Mean True Heat Input Fill Passes (kJ/mm)	0.2% Offset Yield Stress (MPa)	Flow Stress @ 1% Total Strain (MPa)	UTS (MPa)	Y/T Ratio	1% Flow Stress/T Ratio	Strength Mismatch		
									M _{YS}	*M _{FS}	M _{UTS}
Single Torch - Contractor A											
952-D	A	12	0.72	738	789	840	0.88	0.94	1.09	1.06	1.01
952-D	A	3	0.66	893	906	944	0.95	0.96	1.29	1.21	1.14
952-D	A	6	0.77	897	923	960	0.93	0.96	1.27	1.21	1.16
952-F	B	12	0.77	672	834	909	0.74	0.92	1.16	1.19	1.16
952-F	B	3	0.66	818	874	917	0.89	0.95	1.39	1.29	1.25
952-F	B	6	0.80	785	832	897	0.87	0.93	1.18	1.13	1.15
Single Torch - Contractor B											
Weld 3	A	12	0.58	805	820	865	0.93	0.95	1.19	1.10	1.04
Weld 3	A	3	0.48	831	850	885	0.94	0.96	1.20	1.14	1.06
Weld 3	A	6	0.56	867	893	943	0.92	0.95	1.23	1.17	1.14
Weld 4	B	12	0.59	776	855	901	0.86	0.95	1.34	1.22	1.15
Weld 4	B	3	0.47	839	861	897	0.94	0.96	1.42	1.27	1.23
Weld 4	B	6	0.55	803	925	965	0.83	0.96	1.20	1.26	1.24
Dual Torch - Contractor A											
952-G	A	12	0.73	809	843	914	0.88	0.92	1.20	1.13	1.10
952-G	A	3	0.65	915	920	945	0.97	0.97	1.33	1.23	1.14
952-G	A	6	0.79	752	859	928	0.81	0.93	1.07	1.13	1.12
952-H	B	12	0.78	720	824	912	0.79	0.90	1.25	1.18	1.16
952-H	B	3	0.67	775	827	916	0.85	0.90	1.31	1.22	1.25
952-H	B	6	0.81	752	855	944	0.80	0.00	1.13	1.16	1.21
Dual Torch - Contractor B											
Weld 1	A	12	0.53	789	837	931	0.85	0.90	1.17	1.13	1.12
Weld 1	A	3	0.45	811	856	922	0.88	0.93	1.17	1.14	1.11
Weld 1	A	6	0.51	726	816	958	0.76	0.85	1.03	1.07	1.16
Weld 2	B	12	0.54	809	845	943	0.86	0.90	1.40	1.20	1.20
Weld 2	B	3	0.45	828	871	938	0.88	0.93	1.40	1.28	1.28
Weld 2	B	6	0.55	811	854	991	0.82	0.86	1.21	1.16	1.27
LPA Pipe Properties											
Pipe A	A	12		675	744	828	0.82	0.90			
Pipe A	A	3		690	748	831	0.83	0.90			
Pipe A	A	6		705	763	827	0.85	0.92			
Pipe B	B	12		578	701	784	0.74	0.89			
Pipe B	B	3		590	679	732	0.81	0.93			
Pipe B	B	6		667	734	780	0.86	0.00			

Notes:

LPA-Longitudinal to pipe axis

UTS-ultimate tensile strength,

M_{YS} is based on yield strengths, *M_{FS} on 1% flow stresses, and M_{UTS} on ultimate tensile strengths

Table 8: CVN results for X100 pipe steel and single-torch welds (807F)

Region ID	Test Temperature (°C)	Charpy Impact Energy (J)	Average Charpy Impact Energy (J)
Pipe Steel BM	-20	300, 282, 278	287
	-60	243, 246, 223	237
	-80	26, 40, 162	76
	-100	115, 29, 97	80
	-120	17, 18, 12	16
807F –WMC Sub-Cap	22	181, 147, 159	162
	-20	146, 134, 168	149
	-40	144, 111, 118	124
	-60	139, 115, 98	117
	-80	57, 73, 85	72
	-100	53, 32, 50	45
	-120	25, 28, 18	24
807F –HAZ Sub-Cap	-20	224, 232, 247	234
	-40	224, 205, 220	216
	-60	187, 125, 211	174
	-80	127, 37, 26	63
	-100	68, 22, 43	44
	-120	21, 10, 8	13
807F –WMC Towards Root	-20	241, 237, 202	227
	-60	141, 140, 177	153
	-80	127, 58, 115	100
	-120	35, 24, 32	30

Table 9: CVN results for X100 pipe steel and dual-torch weld (883D)

Region ID	Test Temperature °C	Charpy Impact Energy (J)	Average Charpy Impact Energy (J)
Pipe Steel BM	-20	300, 282, 278	287
	-60	243, 246, 223	237
	-80	26, 40, 162	76
	-100	115, 29, 97	80
	-120	17, 18, 12	16
883D –WMC Sub-Cap	-5	139, 145, 140	141
	-20	145, 128, 132	135
	-40	119, 127, 109	118
	-60	101, 107, 94	101
	-80	78, 75, 58	70
	-100	42, 46, 28	39
883D –HAZ Sub-Cap	-5	229, 232, 232	231
	-20	248, 233, 224	235
	-30	240, 88, 100	143
	-40	221, 36, 38	98
	-60	37, 86, 30	51
	-80	37, 19, 36	31
883D –WMC Towards Root	-20	180, 162, 184	175
	-60	106, 112, 78	99
	-80	62, 141, 60	88
	-100	50, 72, 50	57

Table 10: Comparison of WM CVN results for tests conducted at -60 and -20 °C

Material Identification	Region ID	Test Temperature (°C)	Charpy Impact Energy Measurements (J)	Average Charpy Impact Energy (J)	
Single-Torch X100 Rolled Welds	807F	-20	146, 134, 168	149	
		-60	139, 115, 98	117	
	807G	-20	120, 118, 117	118	
		-60	91, 83, 68	81	
	807H	-20	124, 125, 128	126	
		-60	92, 86, 89	89	
	807I	-20	127, 133, 143	134	
		-60	113, 109, 106	109	
	807J	-20	125, 110, 140	125	
		-60	92, 82, 87	87	
	807K	-20	131, 134, 131	132	
		-60	100, 92, 98	97	
	Dual-Torch X100 Rolled Welds	883D	-20	145, 128, 132	135
			-60	101, 107, 94	101
883E		-20	132, 142, 121	132	
		-60	91, 96, 82	90	
883F		-20	122, 133, 136	130	
		-60	104, 99, 102	102	

Table 11: CVN results of WM and HAZ for validation 5G welds

Weld ID	Clock Position	Weld Charpy Impact Energy @ -20 C J	Average Charpy Impact Energy J	HAZ Charpy Impact Energy @ -20 C J	Average Charpy Impact Energy J
Single Torch - Contractor A					
952-D	12	202, 178, 171	184	240, 89, 61	130
952-D	3	145, 142, 145	144	248, 245, 264	252
952-D	6	229, 296, 217	247	281, 278, 293	284
952-F	12	159, 172, 163	165	254, 282, 271	269
952-F	3	171, 169	170	218, 279, 260	252
952-F	6	199, 240, 233	224	264, 251, 279	265
Single Torch - Contractor B					
Weld 3	12	102, 108, 104	105	242, 249, 251	247
Weld 3	3	95, 95, 85	92	168, 194, 172	178
Weld 3	6	127, 123, 117	122	223, 239, 240	237
Weld 4	12	91, 100, 98	96	267, 271, 274	271
Weld 4	3	113, 107, 94	105	236, 228, 275	246
Weld 4	6	226, 171, 157	185	249, 224, 251	241
Dual Torch - Contractor A					
952-G	12	232, 207, 172	204	247, 229, 256	244
952-G	3	182, 163, 133	159	245, 249, 256	250
952-G	6	228, 260, 214	234	246, 249, 248	248
952-H	12	165, 175, 184	175	280, 307, 311	299
952-H	3	203, 195, 199	199	99, 148, 247	165
952-H	6	220, 271, 180	224	279, 301, 300	293
Dual Torch - Contractor B					
Weld 1	12	91, 100, 104	98	138, 293, 289	240
Weld 1	3	113, 156, 216	162	286, 291, 289	289
Weld 1	6	113, 100, 114	109	226, 235, 125	195
Weld 2	12	99, 102, 98	100	58, 165, 159	127
Weld 2	3	77, 83, 104	88	174, 104, 209	162
Weld 2	6	103, 111, 104	106	233, 258, 271	254

Table 12: J-CTOD SE(B) results for Bx2B specimens from single and dual-torch rolled welds (Series 1 & 2)

Weld	Single-Torch				Dual-Torch			
Position	WMC		HAZ		WMC		HAZ	
Temperature °C	<i>J</i> (kJ/m ²)	<i>CTOD</i> (mm)						
RT	*239	0.16 (m)	*533	0.35 (m)	287	0.18 (m)	408	0.25 (m)
	*271	0.18 (m)	*526	0.35 (m)	314	0.20 (m)		
	*209	0.14 (m)						
-20	303	0.19 (m)	*176	0.12 (c)	353	0.23 (m)	216	0.14 (u)
	286	0.18 (m)	419	0.27 (u)	355	0.23 (m)	290	0.18 (u)
	*211	0.14 (m)	69	0.04 (c)			434	0.28 (u)
			222	0.14 (u)				
-40	258	0.16 (m)	271	0.17 (u)	335	0.22 (m)	232	0.15 (u)
			317	0.20 (u)	338	0.22 (m)	251	0.16 (u)

* From J-R curve using ASTM E1820. Other values from E1290-08, which entails calculation of *CTOD* from *J* rather than specimen rotation.

Subscripts “c” and “u” indicate brittle (cleavage) fracture before and after a small amount (0.2 mm) of ductile crack growth, respectively, and “m” results indicate maximum load during ductile tearing.

Table 13: J-CTOD SE(B) results at -20 °C for B x 2B specimens from single torch 5G pipe welds (952-D and 952-F, Series 3) and Pipe A

Notch Position						
BM		Clock Position	WMC		HAZ	
<i>J</i> (kJ/m ²)	<i>CTOD</i> (mm)		<i>J</i> (kJ/m ²)	<i>CTOD</i> (mm)	<i>J</i> (kJ/m ²)	<i>CTOD</i> (mm)
Pipe A		Clock Position	Pipe A		Pipe A	
683 (m)	0.49 (m)		12:00	296 (m)	0.20 (m)	310 (u)
624 (m)	0.45 (m)	3:00	247 (m)	0.15 (m)	*	*
496 (m)	0.36 (m)	6:00	320 (m)	0.20 (m)	663 (m)	0.40 (m)
			Pipe B		Pipe B	
		12:00	306 (m)	0.20 (m)	555 (m)	0.36 (m)
		3:00	248 (m)	0.16 (m)	622 (m)	0.39 (m)
		6:00	303 (m)	0.20 (m)	576 (m) [#]	0.37 (m) [#]

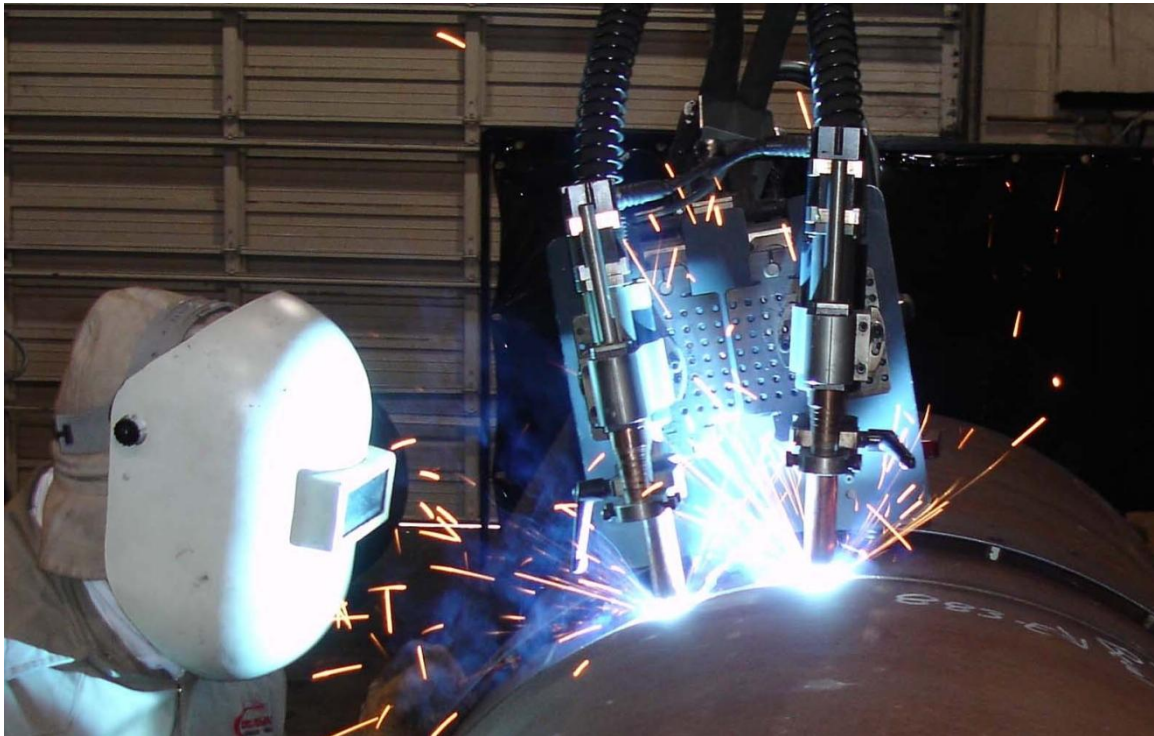
* The HAZ specimen from Pipe A, 3:00 position, was accidentally overloaded before the test, and therefore its results were unusable.

[#] The HAZ specimen from Pipe B, 6:00 position, exhibited a small pop-in event at $J = 295 \text{ kJ/m}^2$ and $CTOD = 0.18 \text{ mm}$, with $\Delta a = 0.12 \text{ mm}$. This event, however, was deemed not significant according to ASTM E1820.

Subscripts “c” and “u” indicate brittle (cleavage) fracture before and after a small amount (0.2 mm) of ductile crack growth, respectively, and “m” results indicate maximum load during ductile tearing.



(a)



(b)

Figure 1: (a) Single- and (b) dual-torch roll welding.

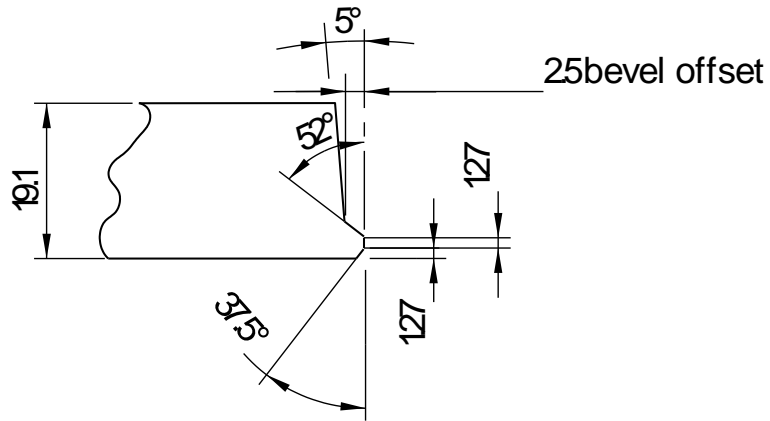


Figure 2: Narrow gap joint design for single- and dual-torch X100 rolled welds (dimensions in mm).

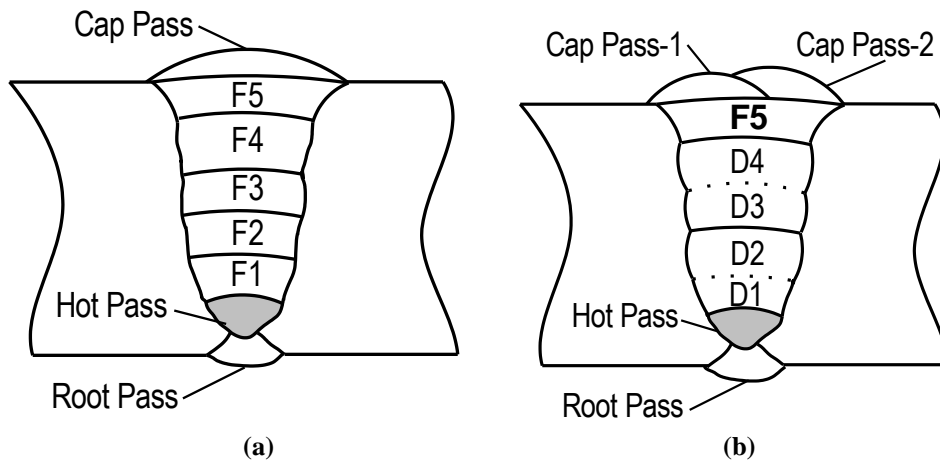
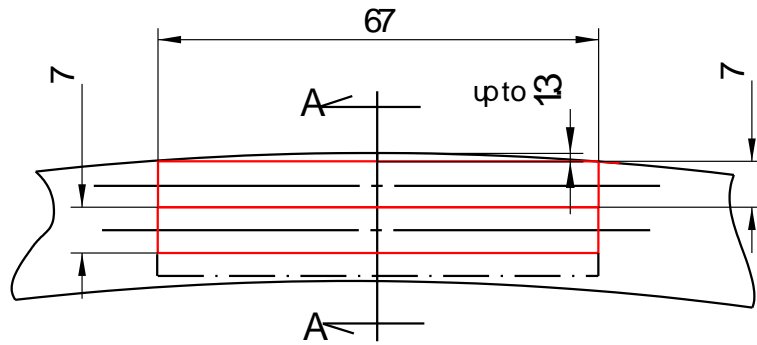
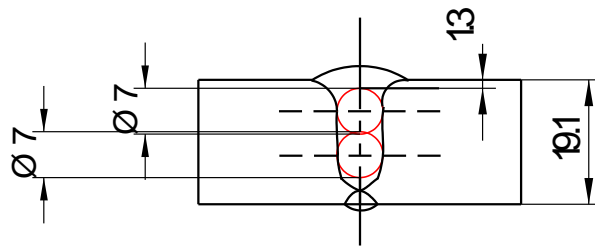


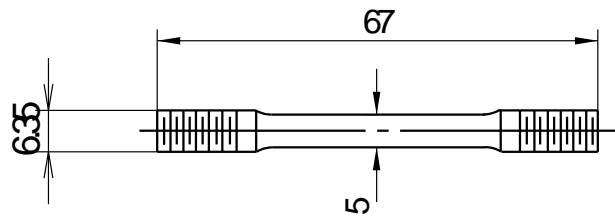
Figure 3: Pass sequences for (a) single- and (b) dual-torch X100 rolled welds.



Location of tensile specimen blanks

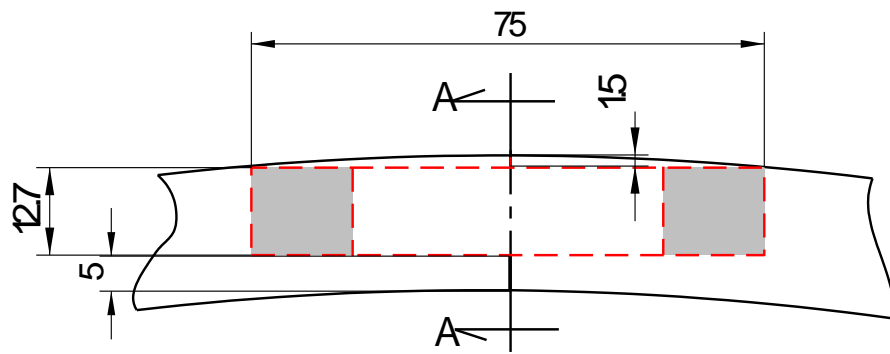


**Section A-A
Mid-Length with weld cap and root passes**

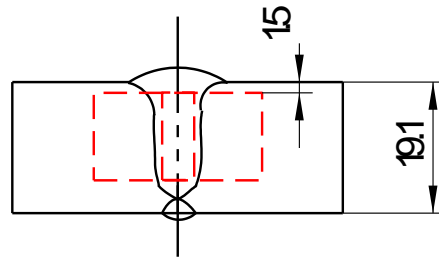


All-weld metal round bar tensile specimen

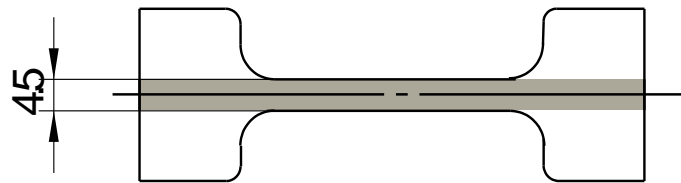
Figure 4: Details of round bar tensile specimens from weld in 19 mm thick pipe (dimensions in mm).



Location of strip tensile specimen blank

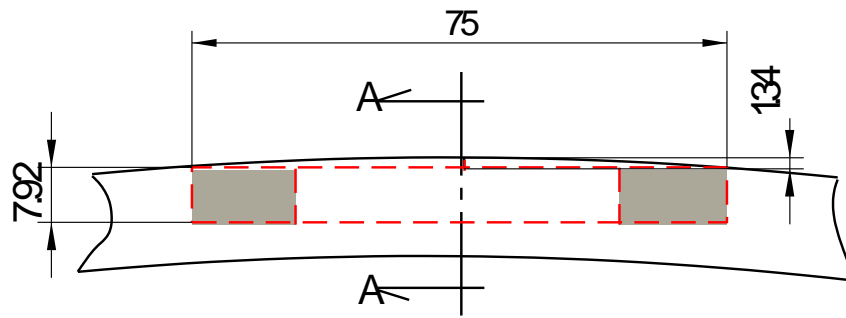


**Section A-A
Mid-Length with weld cap and root passes**

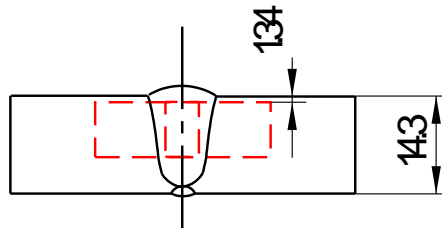


Top view of all-weld metal strip tensile specimen

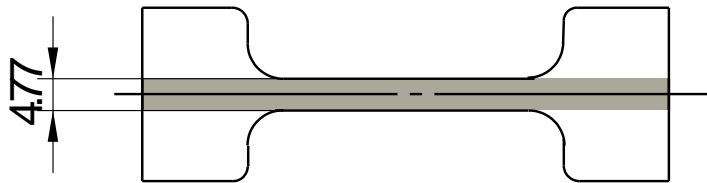
Figure 5: Details of strip tensile specimen from weld in 19 mm thick pipe (dimensions in mm).



Location of strip tensile specimen blank

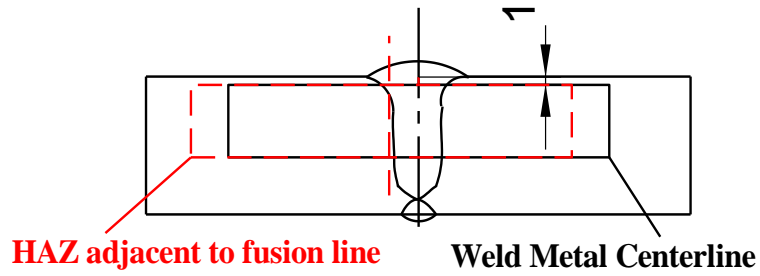


**Section A-A
Mid-Length with weld cap and root passes**

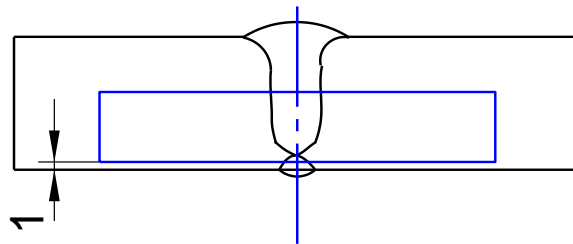


Top view of all-weld metal strip tensile specimen

Figure 6: Details of strip tensile specimen from weld in 14.3 mm thick pipe (dimensions in mm).



(a) WMC and HAZ biased towards the cap pass (OD)



(b) WMC biased towards hot/root pass (ID)

Figure 7: Orientation and position of WMC and HAZ CVN specimens (dimensions in mm).

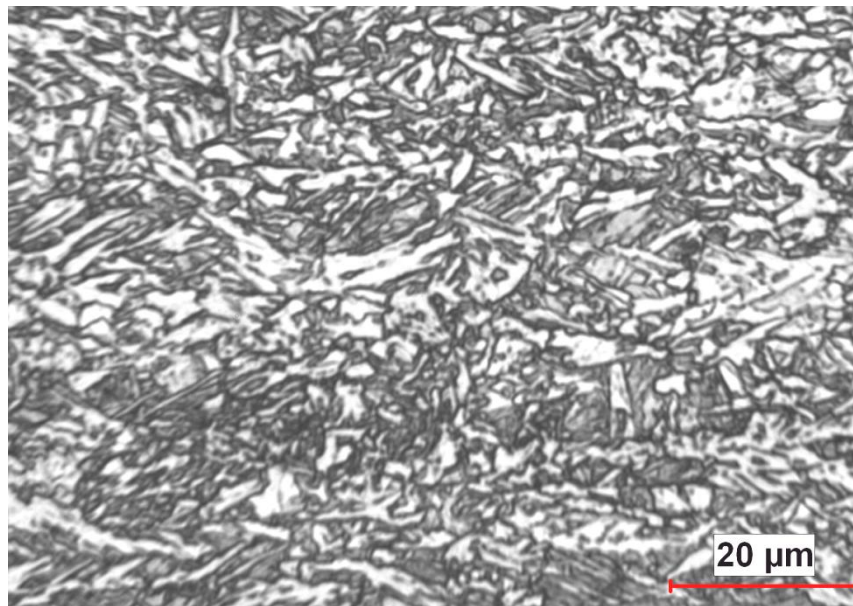


Figure 8: Optical micrograph of the X100 pipe steel near mid-wall. Etched with 2 % Nital.

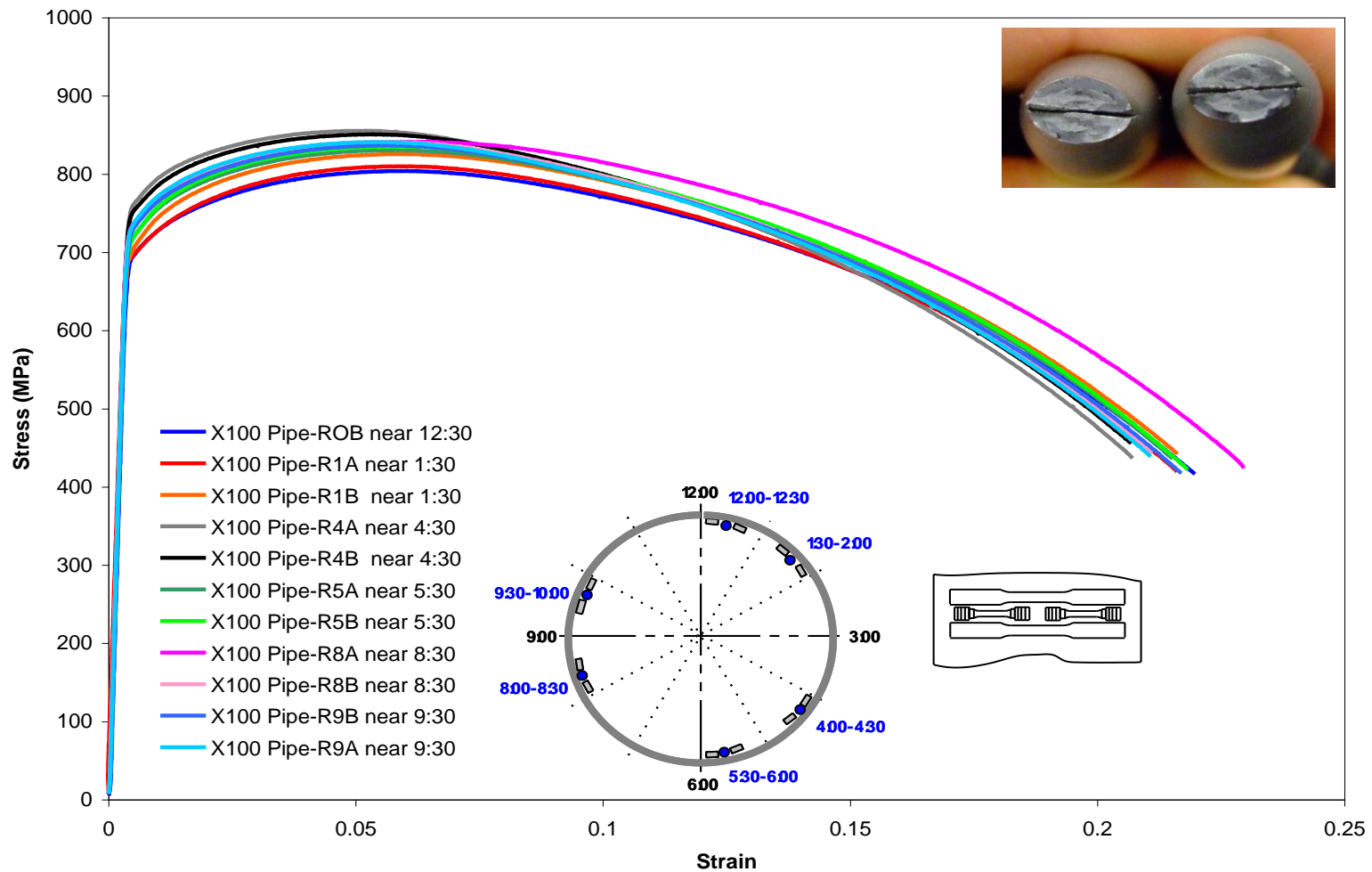


Figure 9: Stress-strain curves for round bar tensile specimens from X100 pipe as a function of clock position (12:00 to 2:00, 4:00 to 6:00 and 8:00 to 10:00). Duplicate round bar tensile specimens are indicated by solid blue circles. Insert photograph (upper right corner) shows fracture surface of broken tensile specimen with an elliptical shape and split near the mid wall.

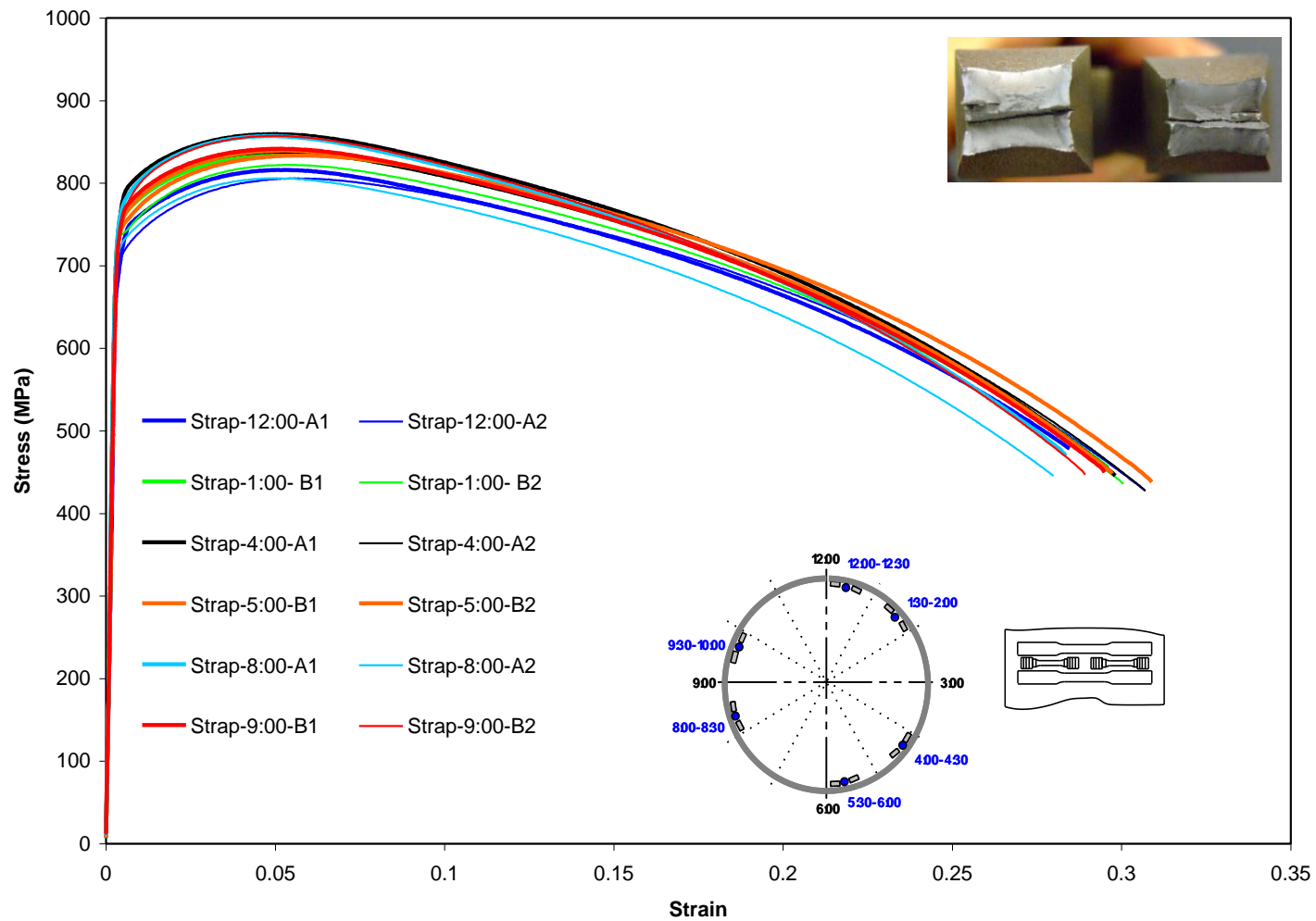


Figure 10: Stress-strain curves for strap tensile specimens from X100 pipe as a function of clock position (12:00 to 2:00, 4:00 to 6:00 and 8:00 to 10:00). Strap tensile specimens represented by small-solid grey rectangles. Insert photograph (upper right corner) shows fracture surface of broken tensile specimen with shear failure. Notice split that occurred at the mid wall.

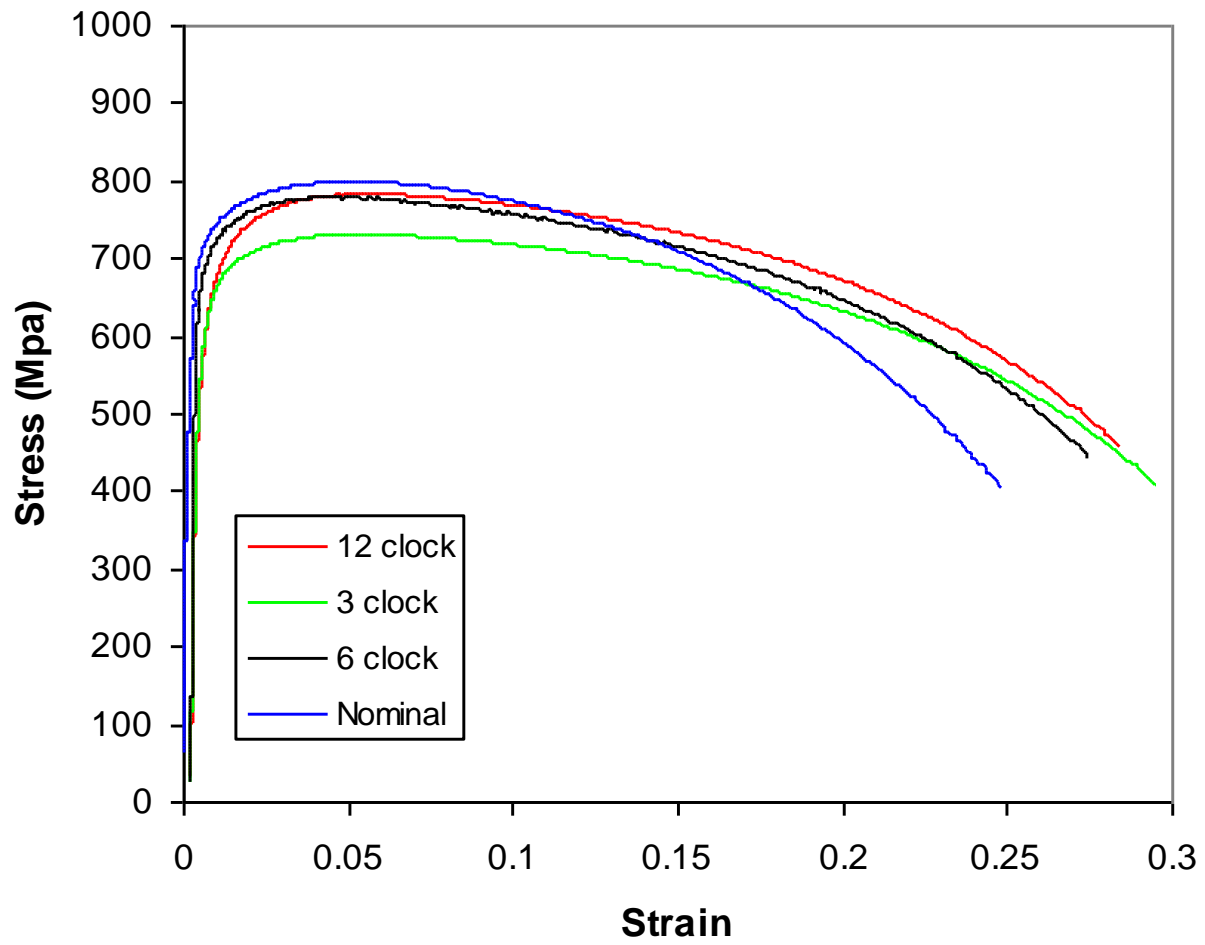


Figure 11: Stress-strain curves for strap tensile specimens from X100 Pipe B as a function of clock position (12:00, 3:00 and 6:00).

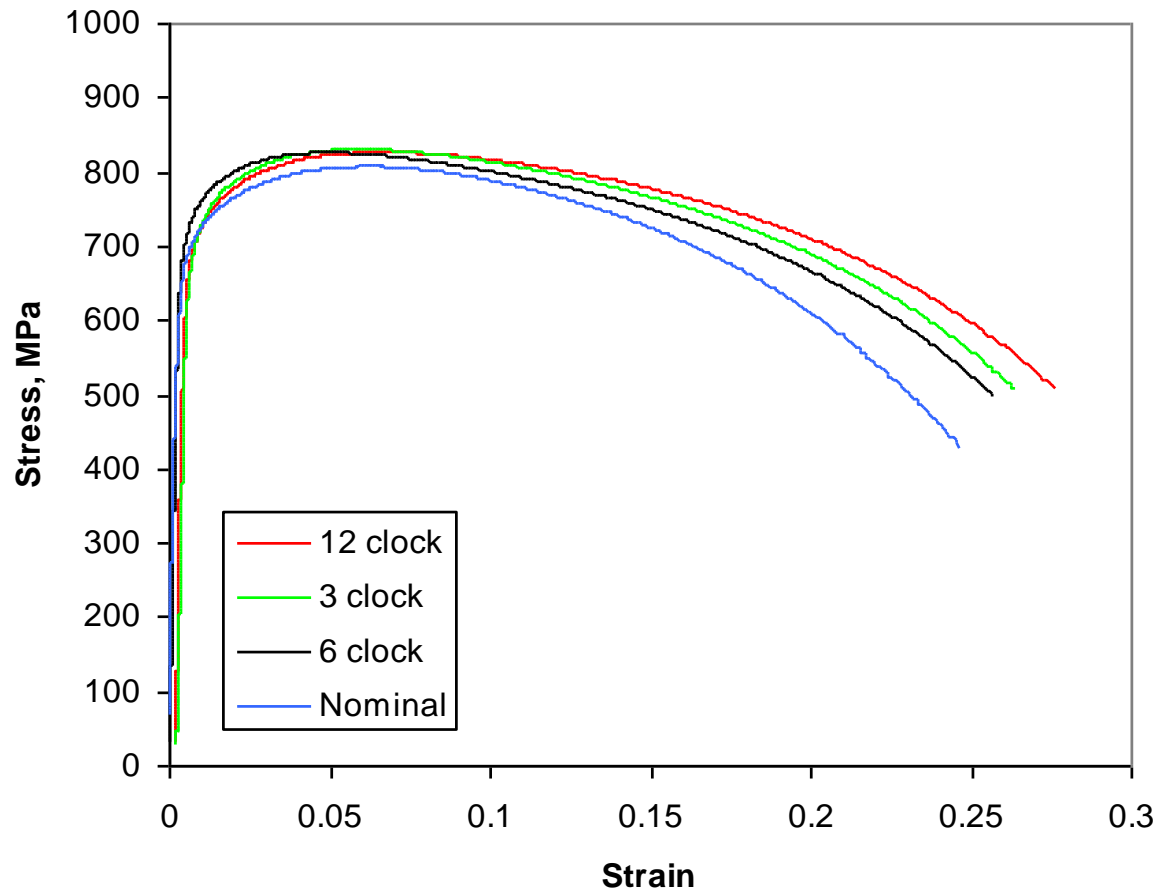
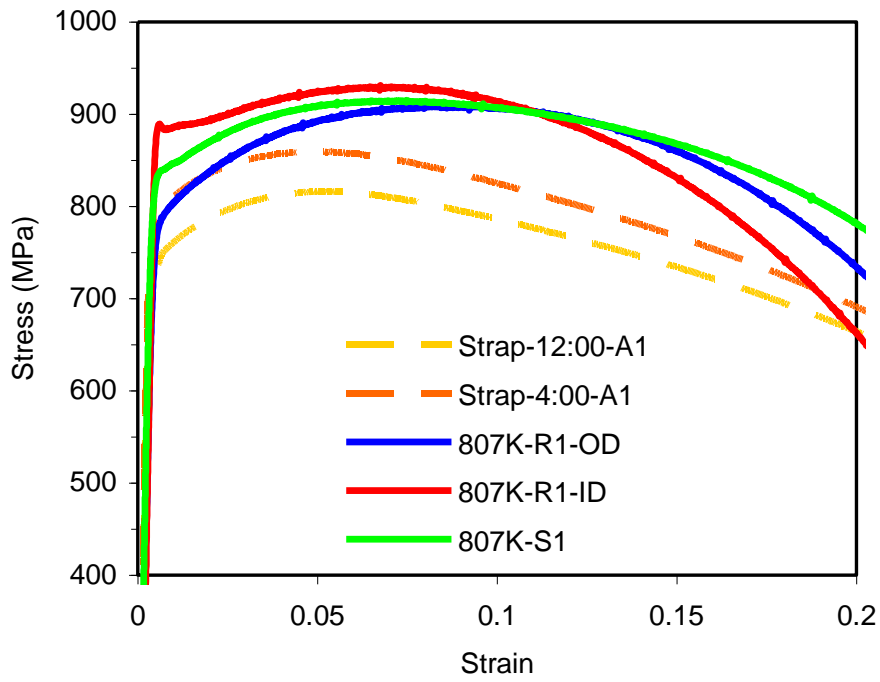
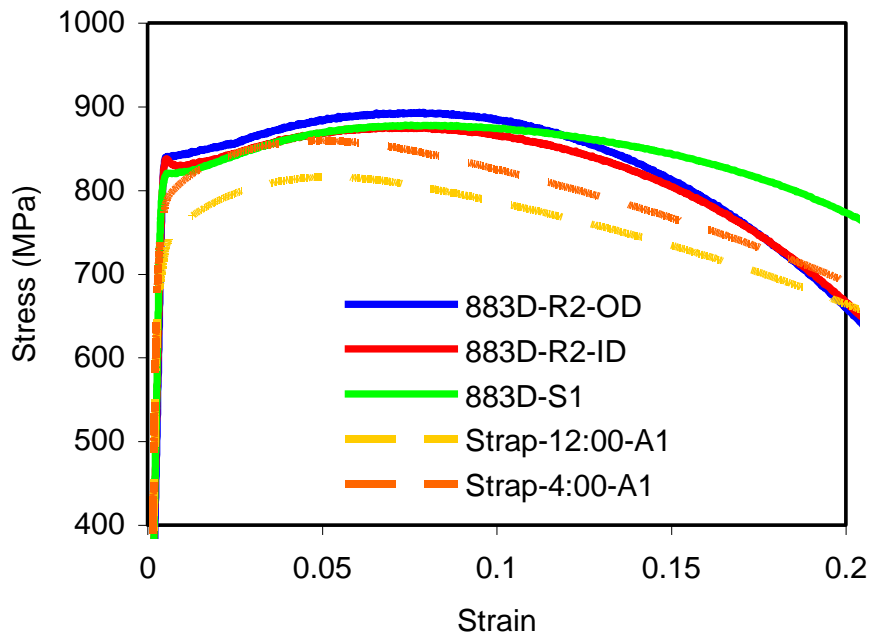


Figure 12: Stress-strain curves for strap tensile specimens from X100 Pipe A as a function of clock position (12:00, 3:00 and 6:00).

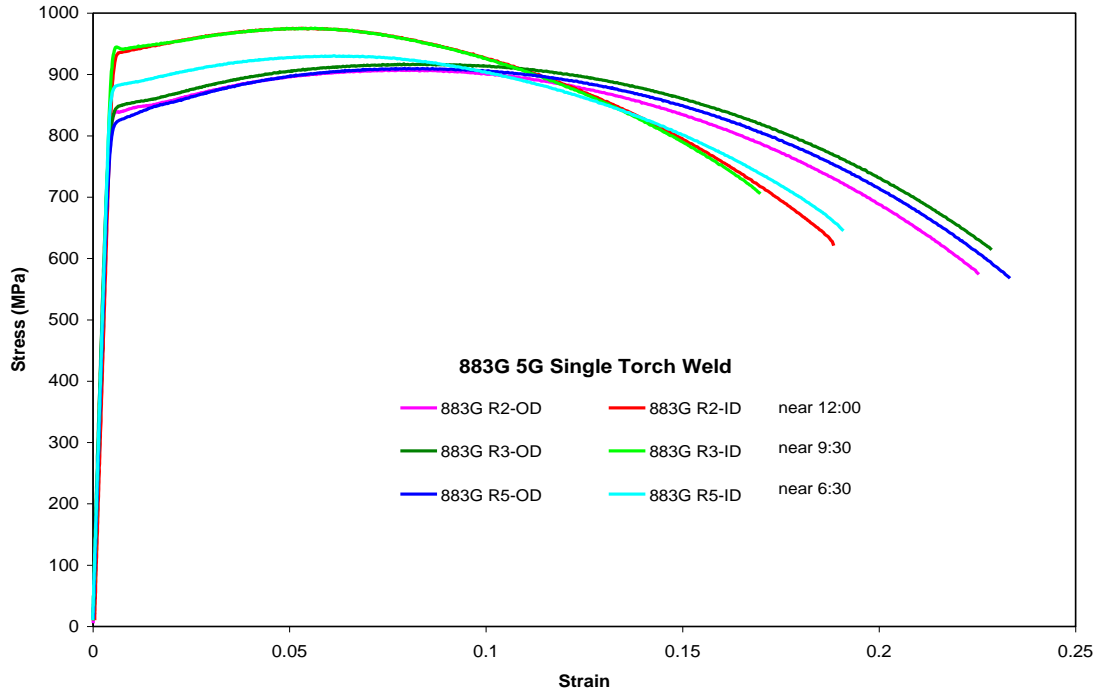


(a) Single-torch welds

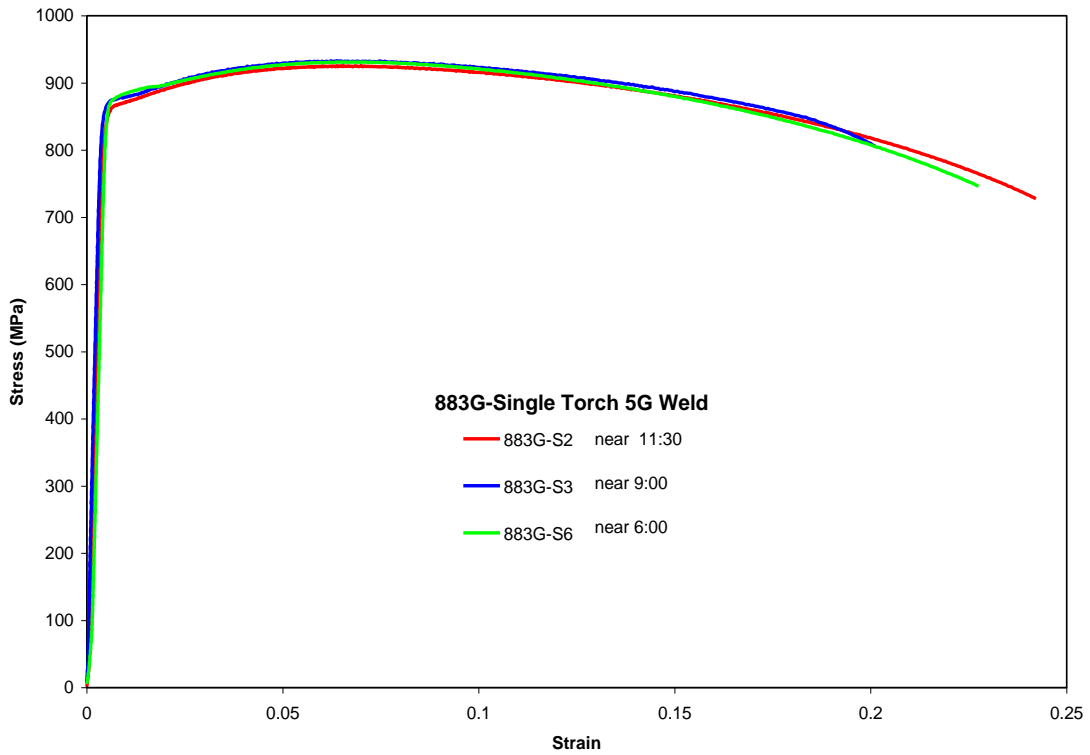


(b) Dual-torch welds

Figure 13: Stress-strain curves for single- and dual-torch welds versus X100 pipe data (Strap).

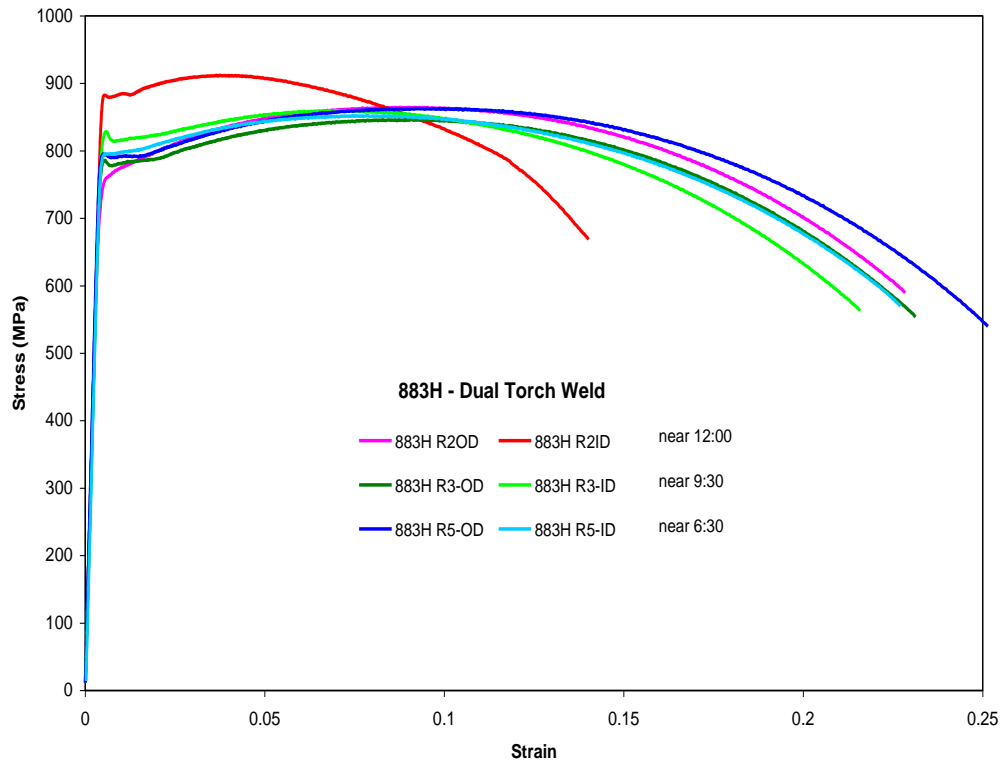


(a) Round bar tensile specimens

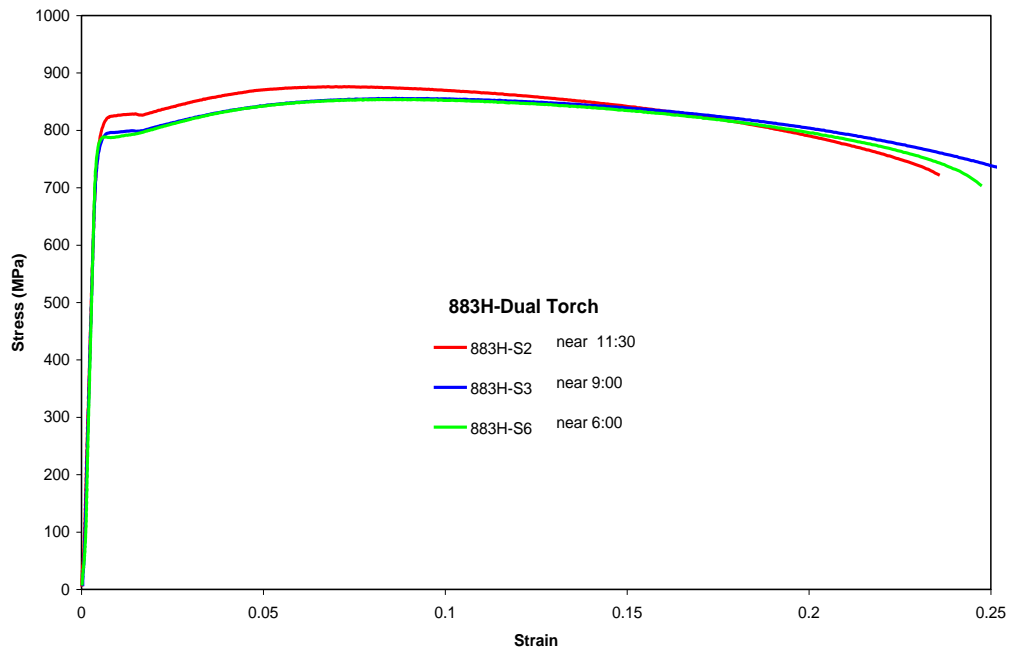


(b) Strip bar tensile specimens

Figure 14: Stress-strain curves for 5G single-torch weld, 883G.



(a) Round bar tensile specimens



(b) Strip tensile specimens

Figure 15: Stress-strain curves for 5G dual-torch weld, 883-H.

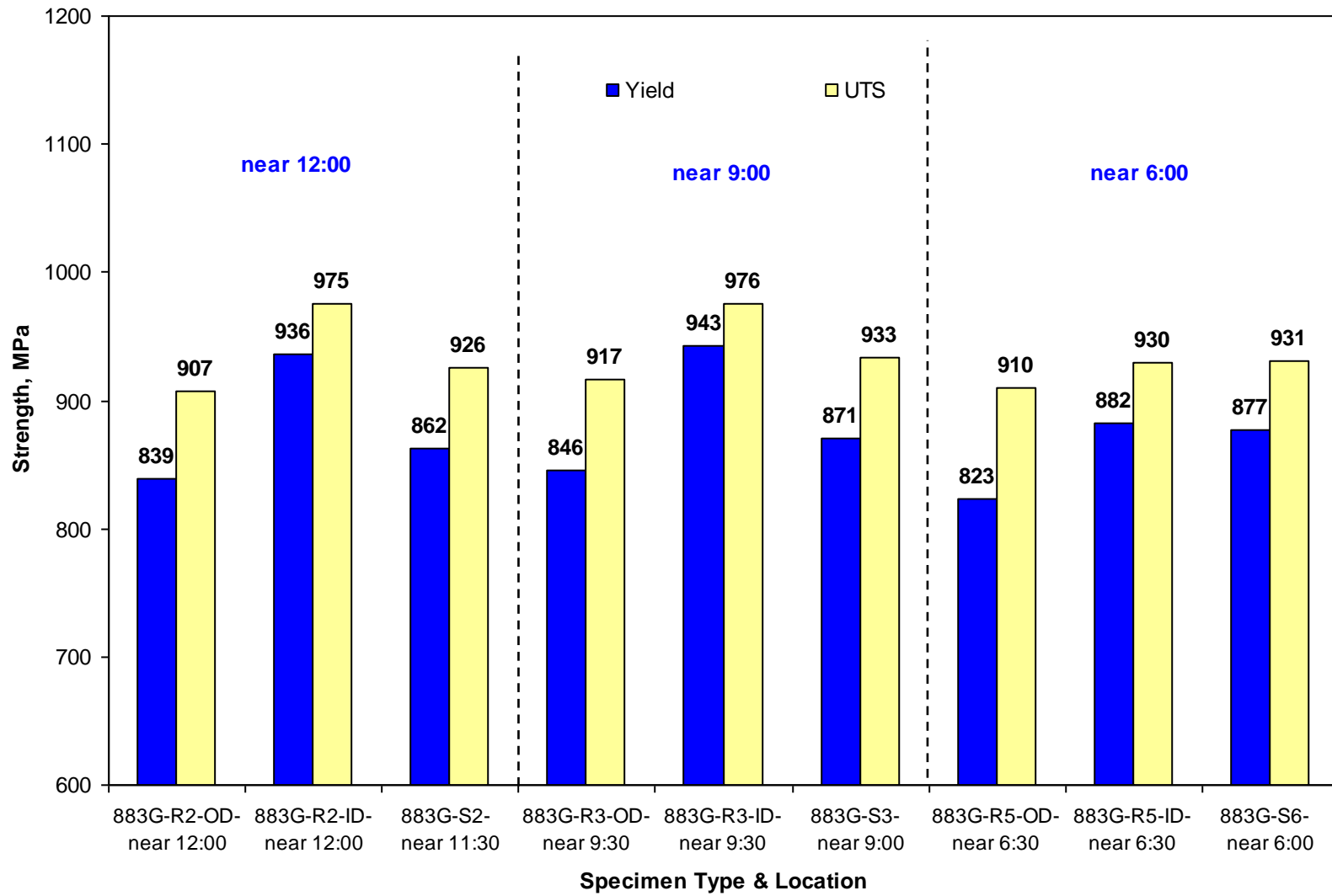


Figure 16: Yield (0.2 % offset) and ultimate tensile strengths versus clock position for the 5G single-torch weld.

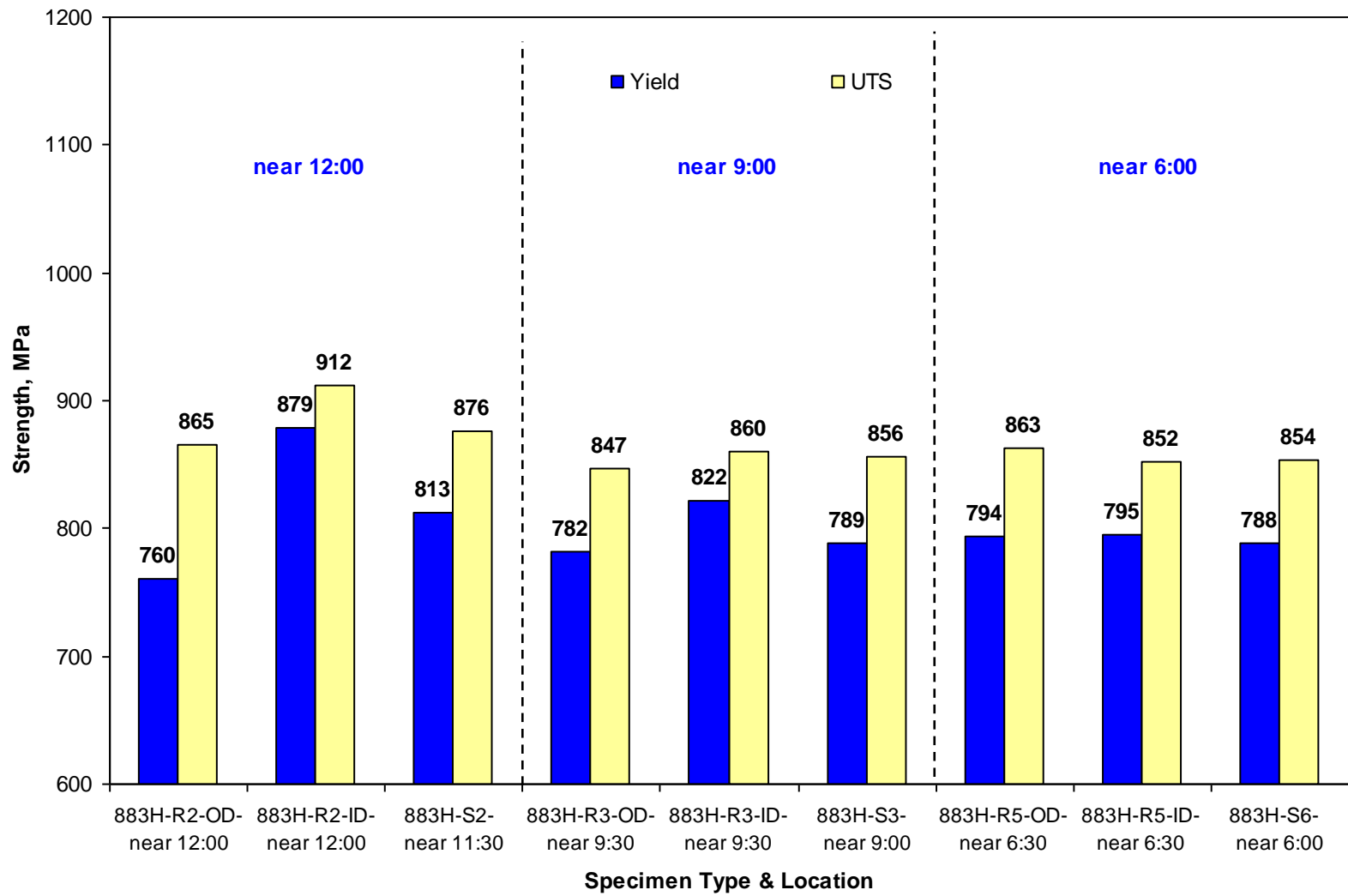
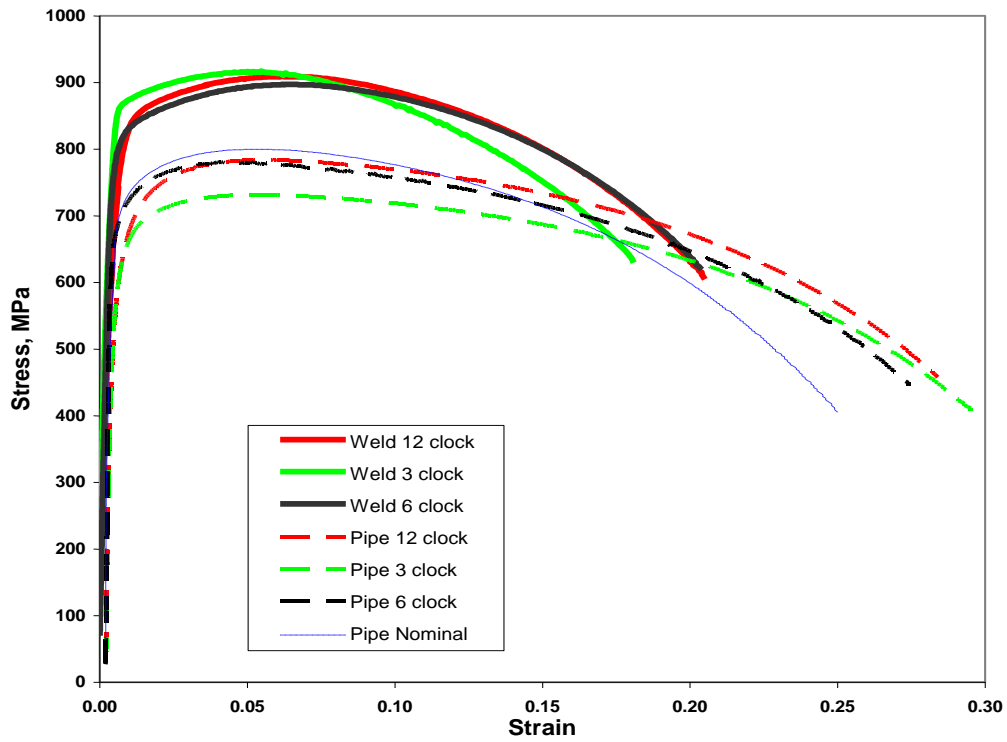
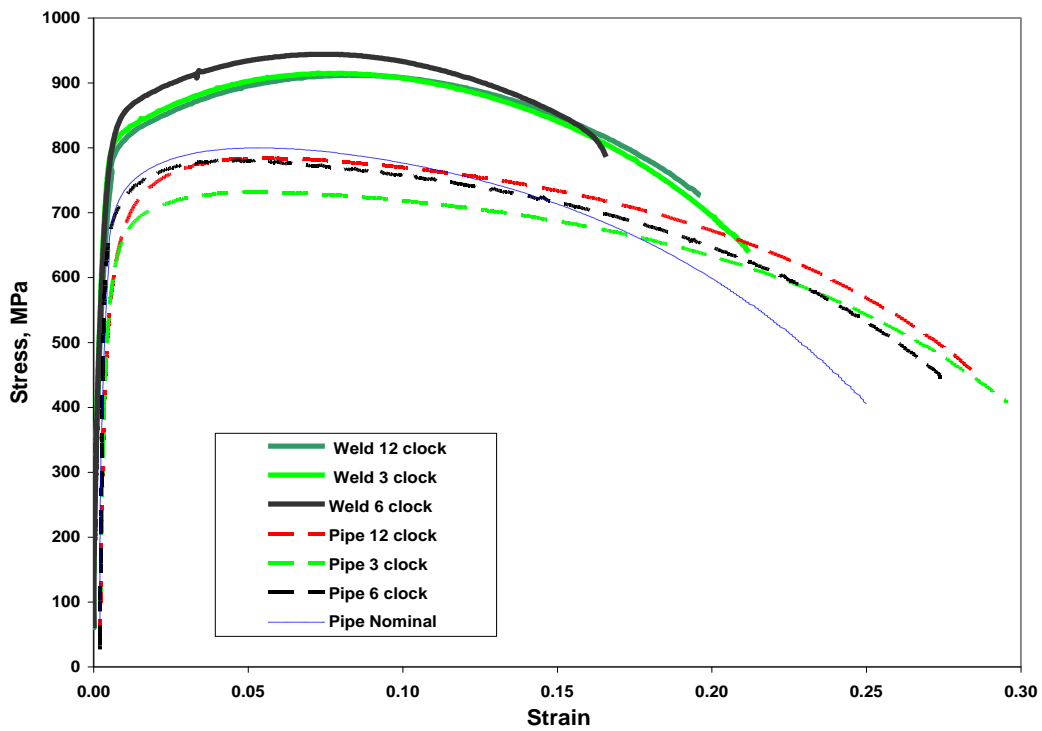


Figure 17: Yield (0.2 % offset) and ultimate tensile strengths versus clock position for the 5G dual-torch weld.



(a) 5G single-torch validation weld, 952-F and Pipe B



(b) 5G dual-torch validation weld, 952-H and Pipe B

Figure 18: Stress-strain curves for 5G single- and dual-torch validation welds.

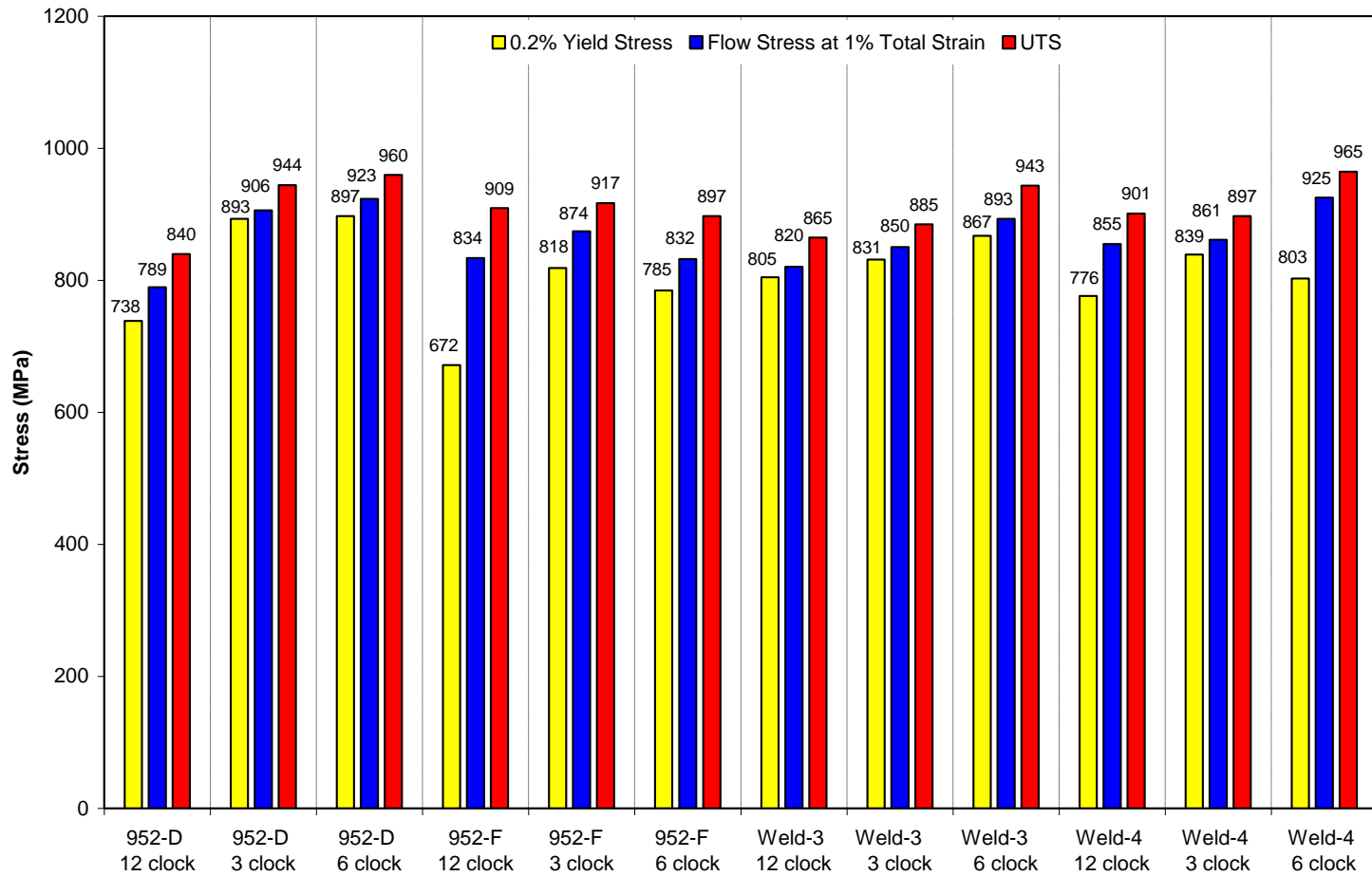


Figure 19: Yield (0.2% offset), flow stress and ultimate tensile strengths versus clock position for the validation 5G single-torch welds.

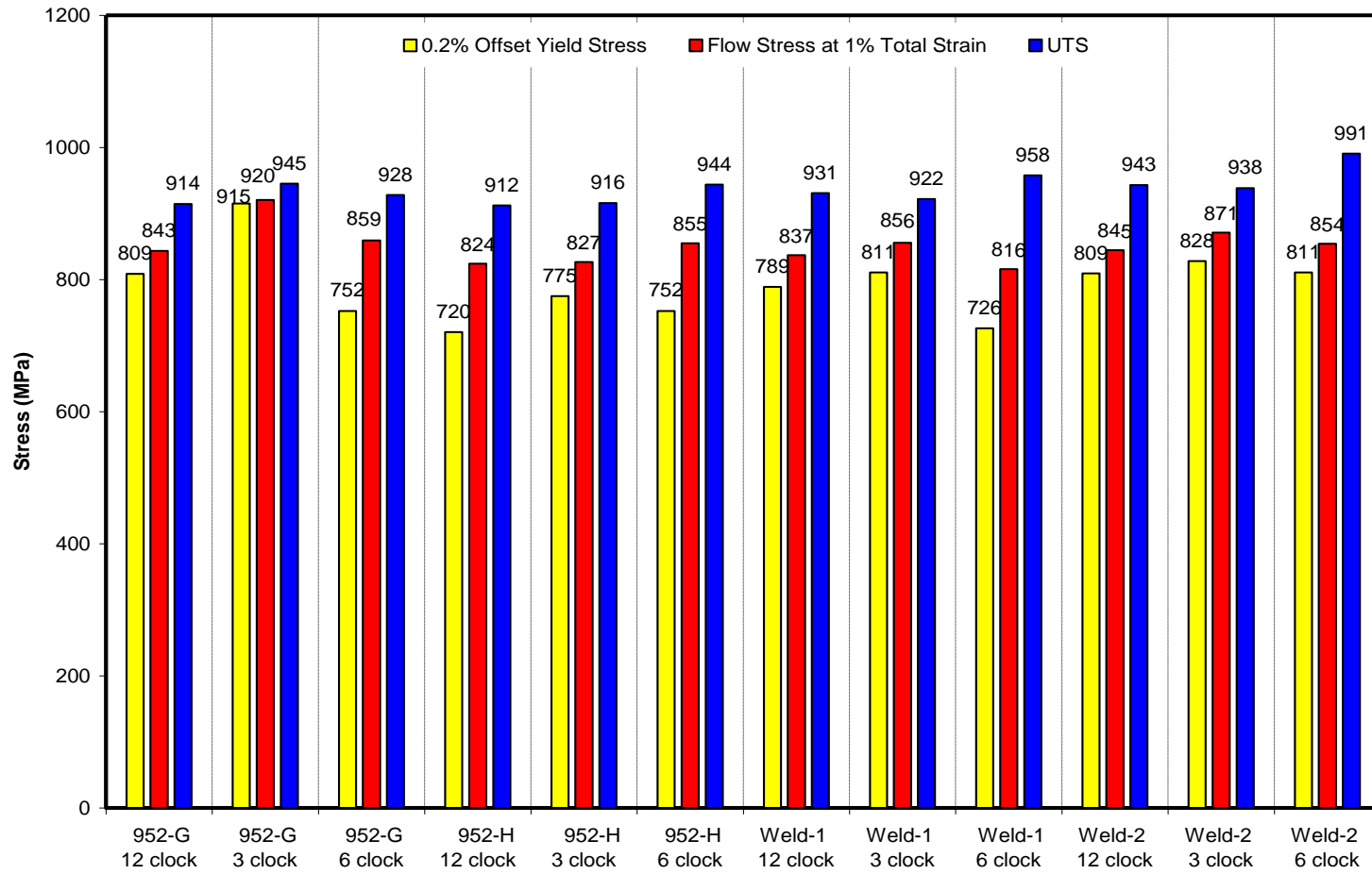
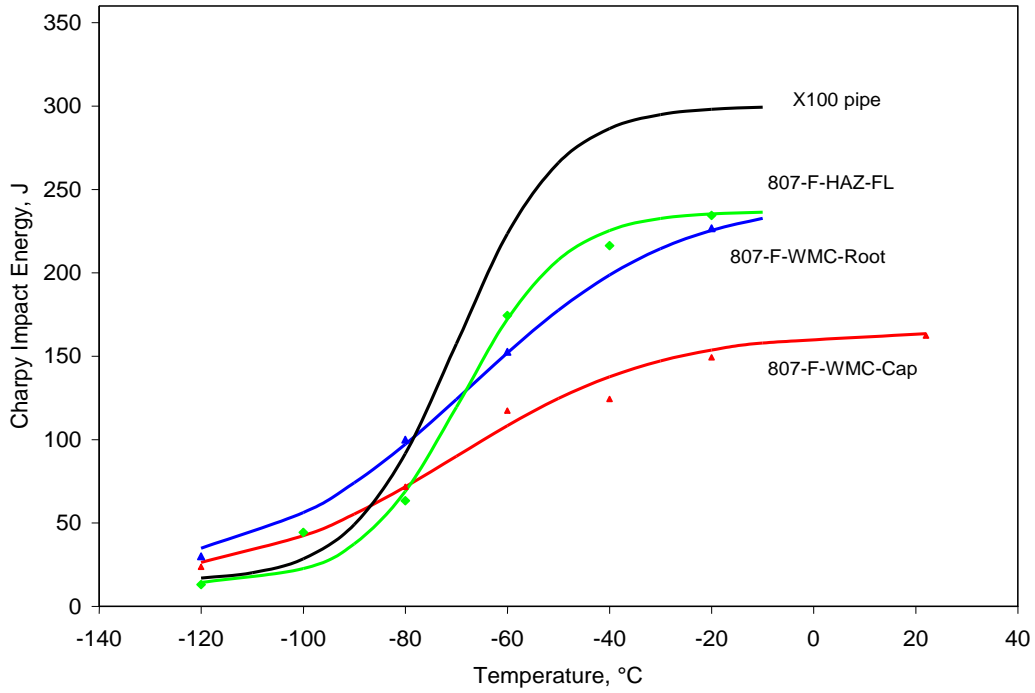
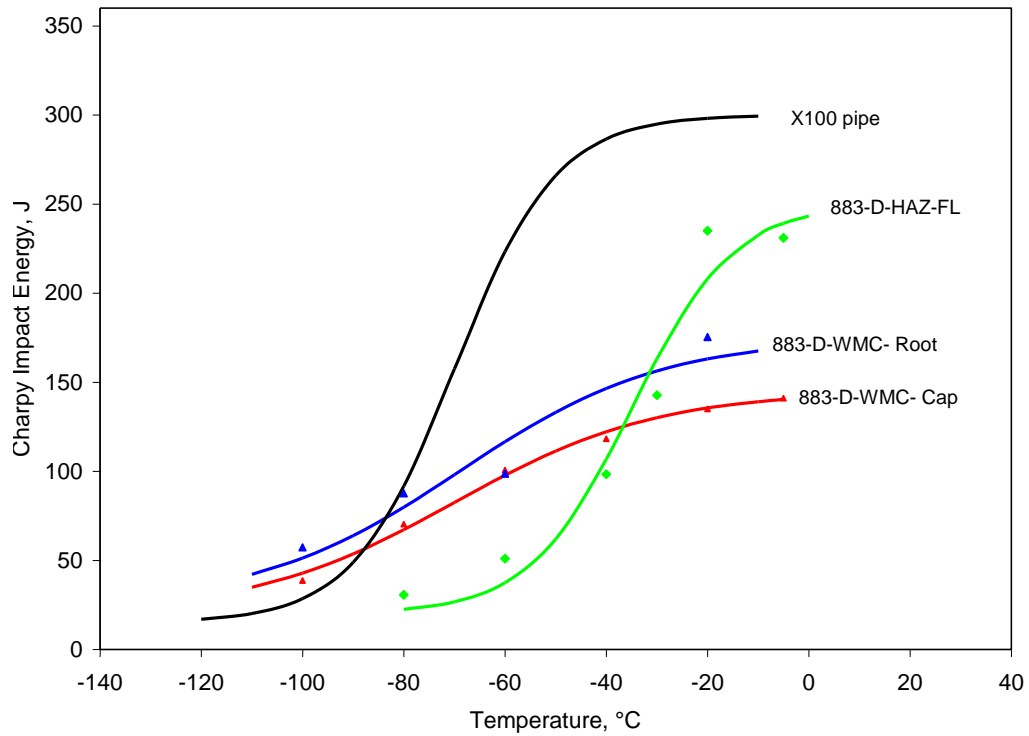


Figure 20: Yield (0.2% offset), flow stress and ultimate tensile strengths versus clock position for the validation 5G dual-torch welds.



(a) Single-torch weld, 807-F



(b) Dual-torch weld, 883-D

Figure 21: CVN transition curves for single- and dual-torch welds.

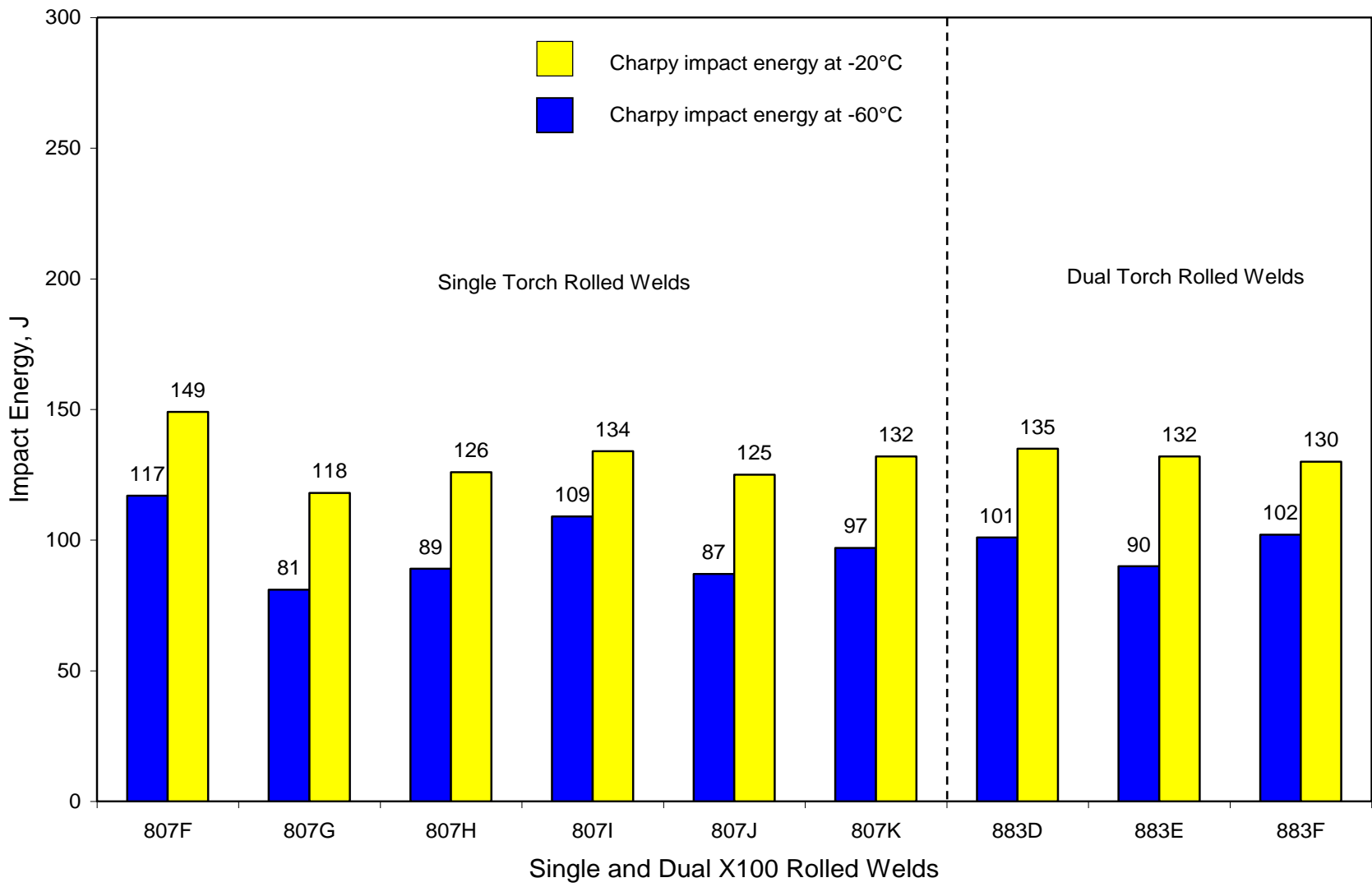


Figure 22: CVN impact energies at -60 and -20°C

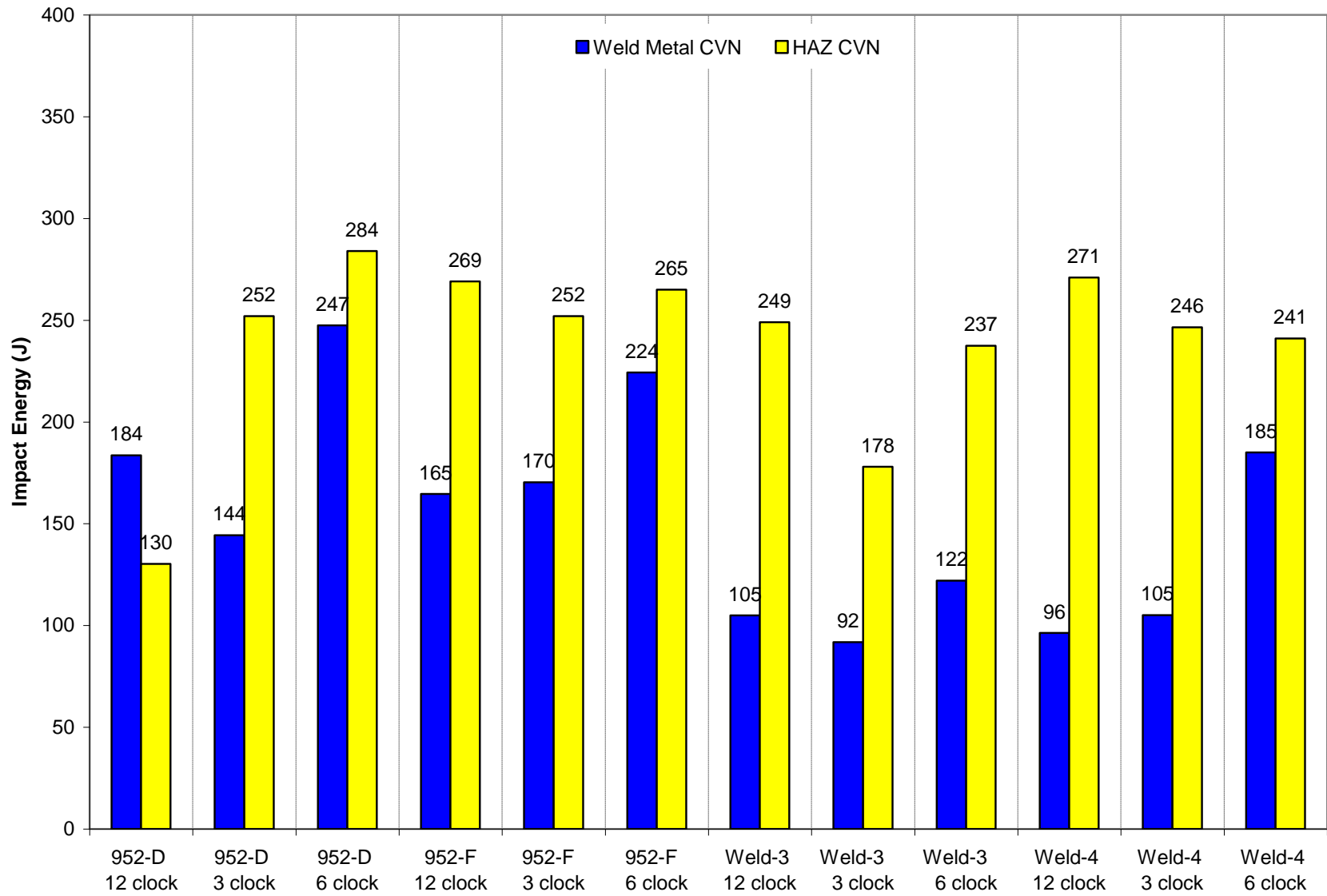


Figure 23: CVN impact energies at -20°C of the validation 5G single-torch welds.

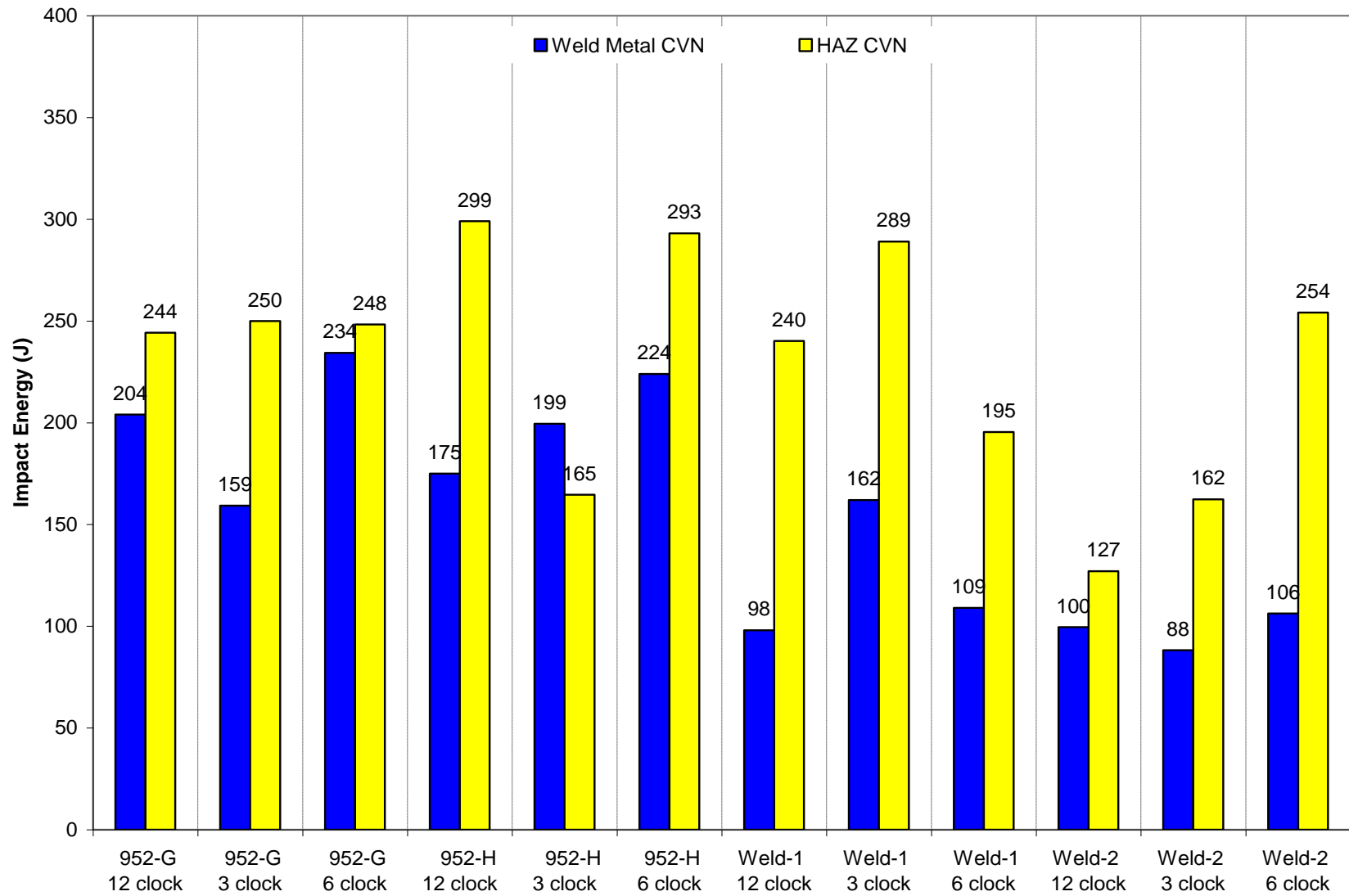
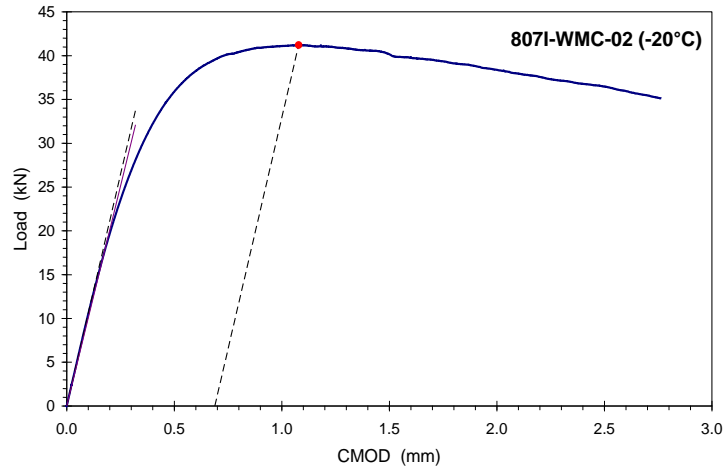
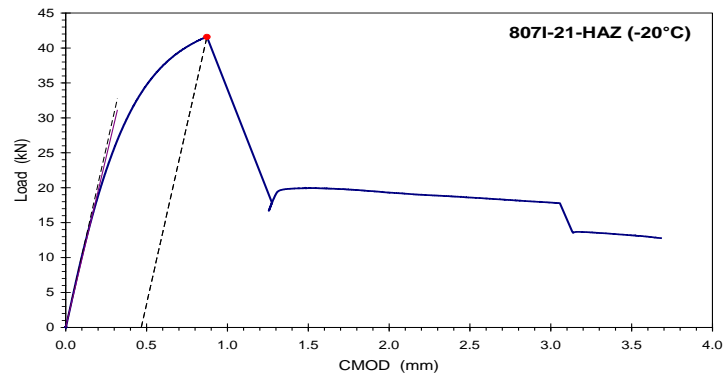


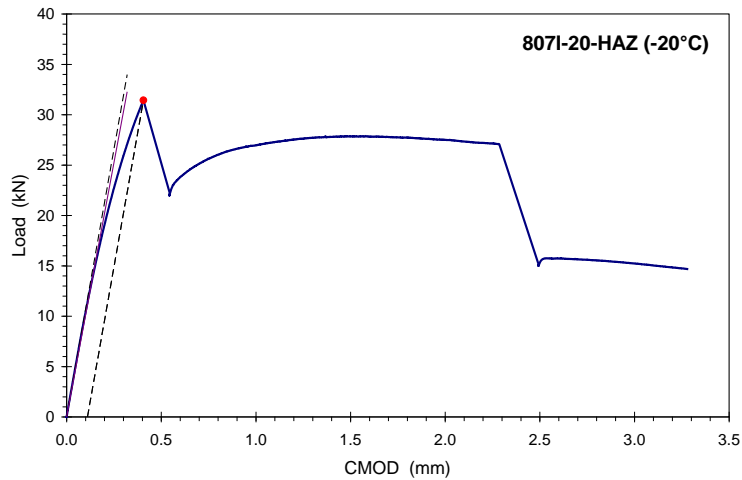
Figure 24: CVN impact energies at -20°C of the validation 5G dual-torch welds



(a) J_m or δ_m

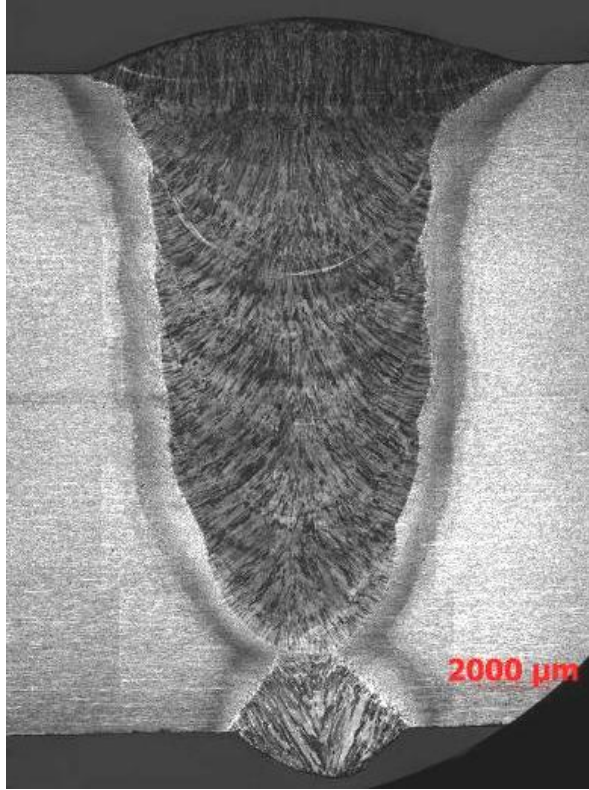


(b) J_u or δ_u

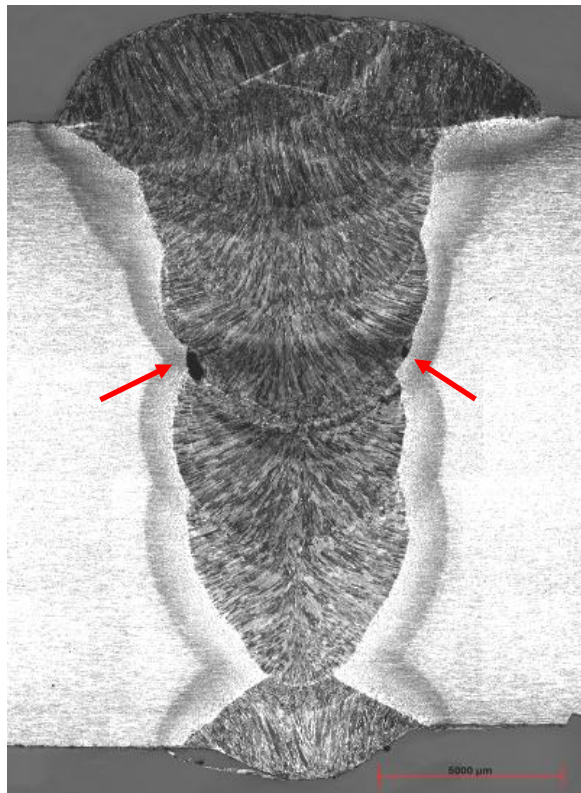


(c) J_c or δ_c

Figure 25: Load vs. CMOD curves for single-torch WM- and HAZ-notched B x 2B J/CTOD specimens. Dotted line from peak load enables measurement of plastic component of CMOD. Figure represents the J or δ determined at (a) maximum load, (b) after 0.2 mm of ductile tearing, and (c) before 0.2 mm of ductile tearing.

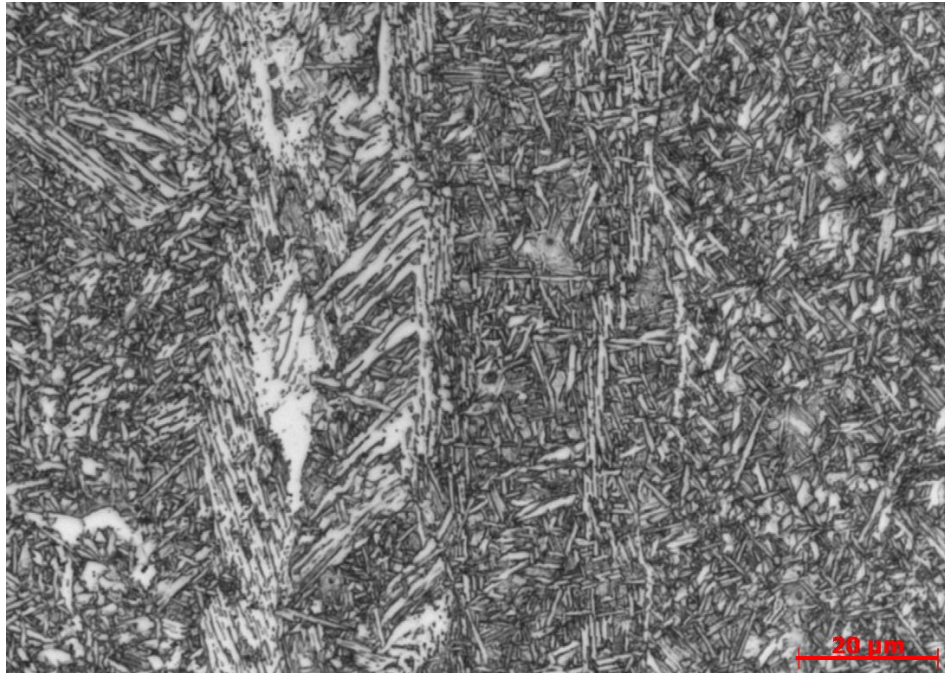


(a)

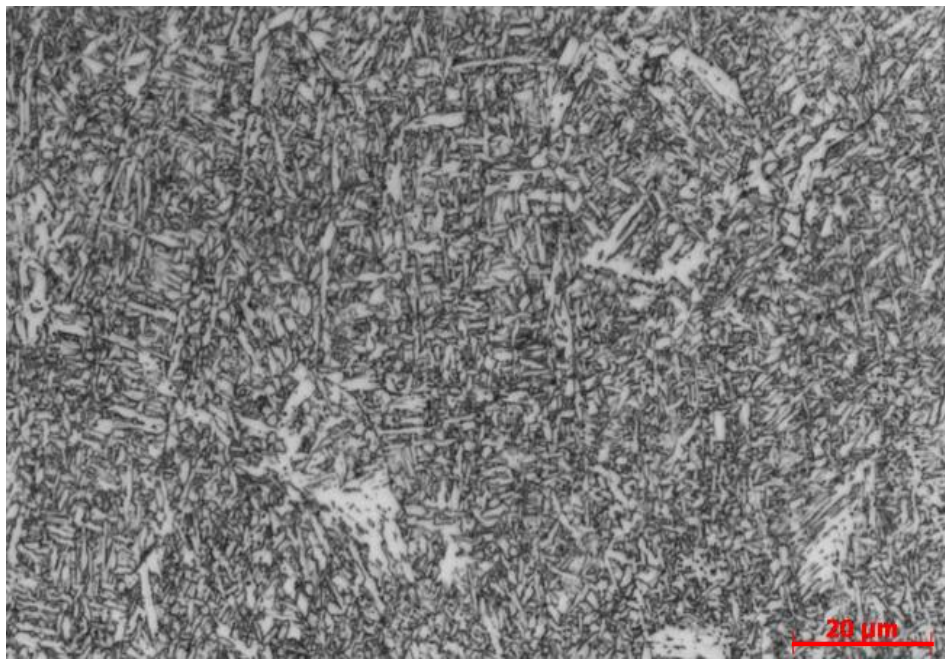


(b)

Figure 26: Macrographs of X100 rolled welds: (a) single-torch, 807-J and (b) dual-torch, 883-D. Arrows indicate small areas of lack of fusion.

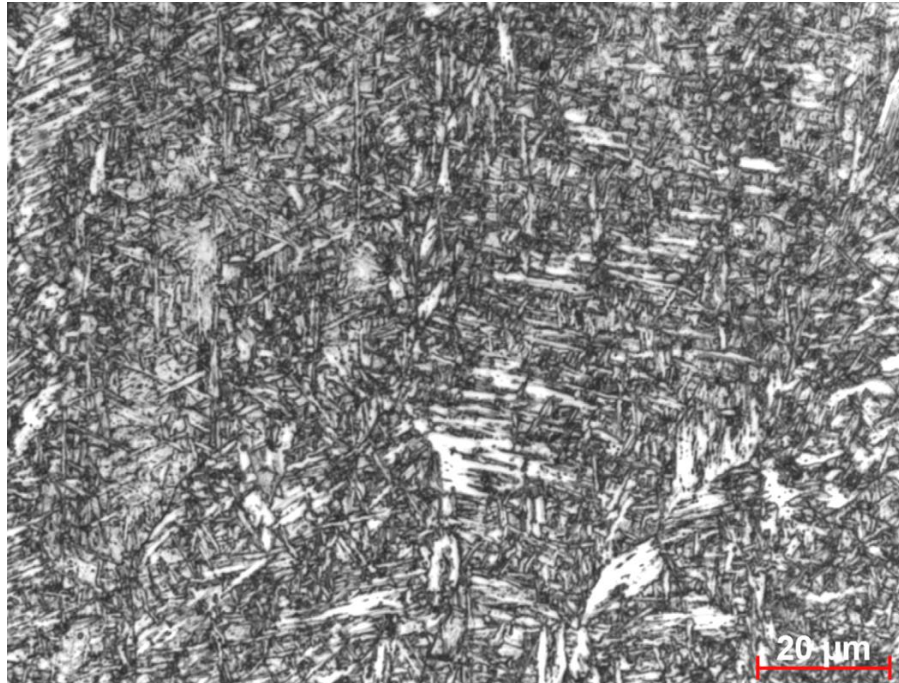


(a) Cap pass as-deposited region

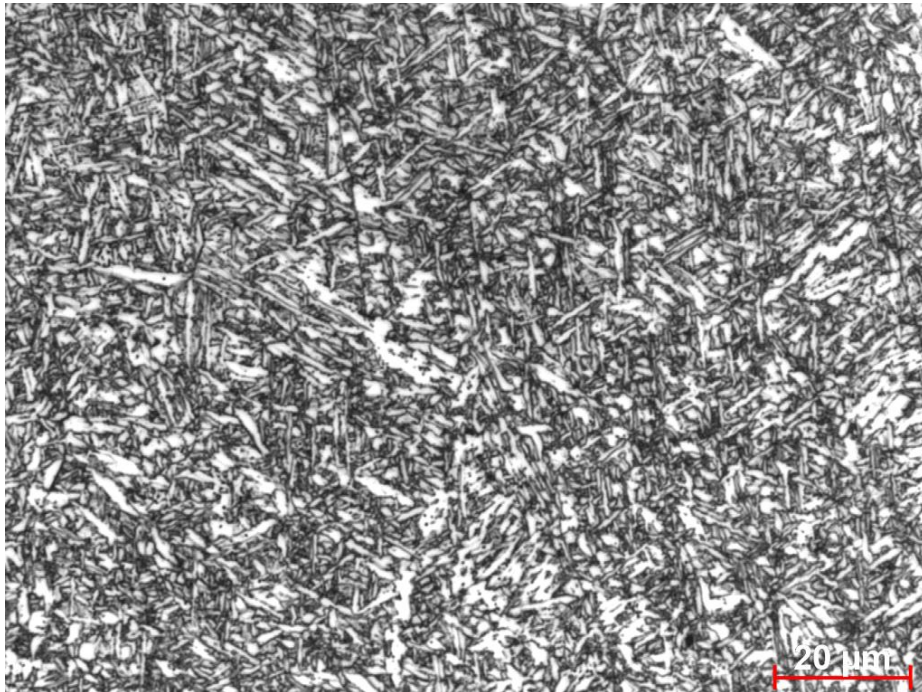


(b) Fill pass-2 weld metal region

Figure 27: Weld metal microstructure of single-torch weld.



(a) Cap pass as-deposited region



(b) Fill D4 weld metal region

Figure 28: Weld metal microstructure of dual-torch weld.



(a) Grain coarsened HAZ region

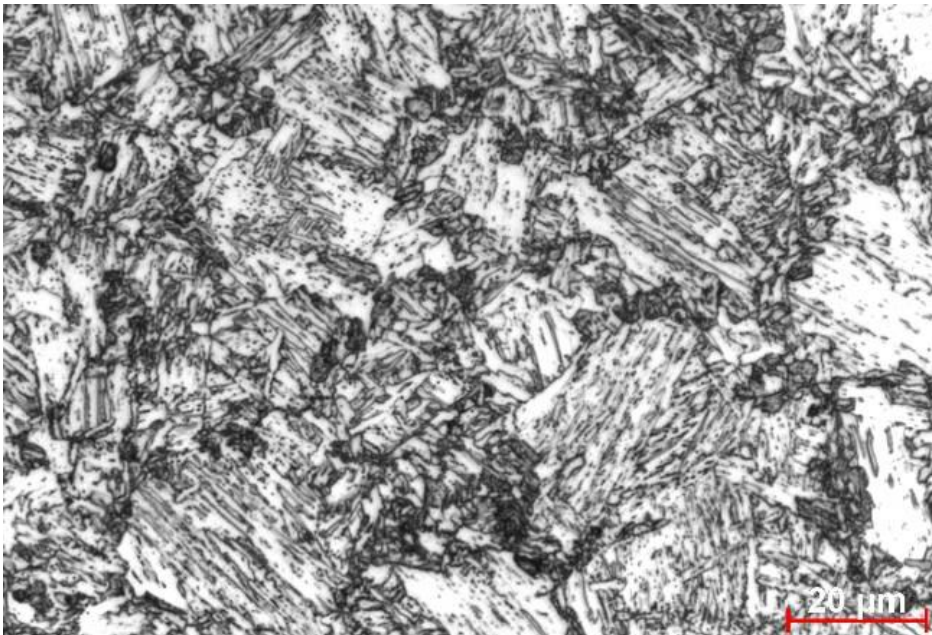


(b) Reheated HAZ region

Figure 29: HAZ microstructures of single-torch weld.

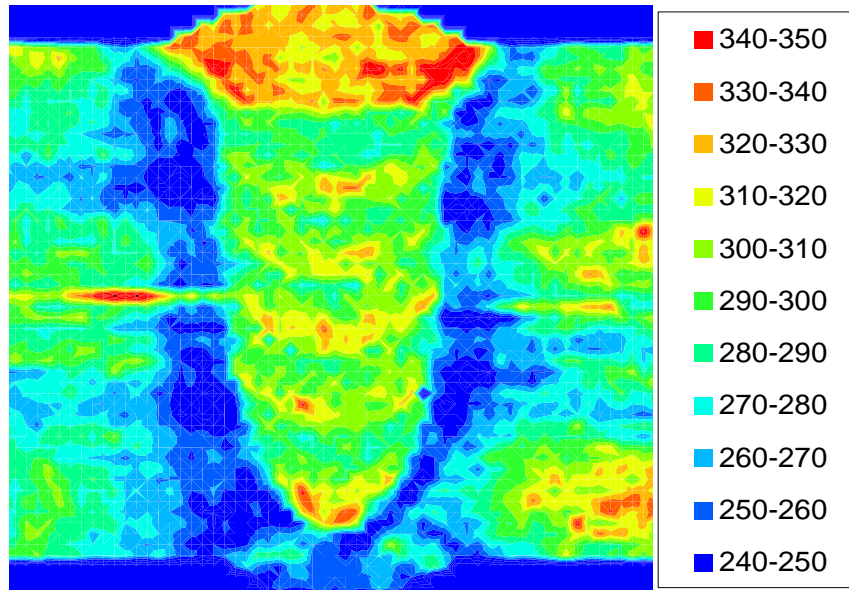


(a) Grain coarsened HAZ region

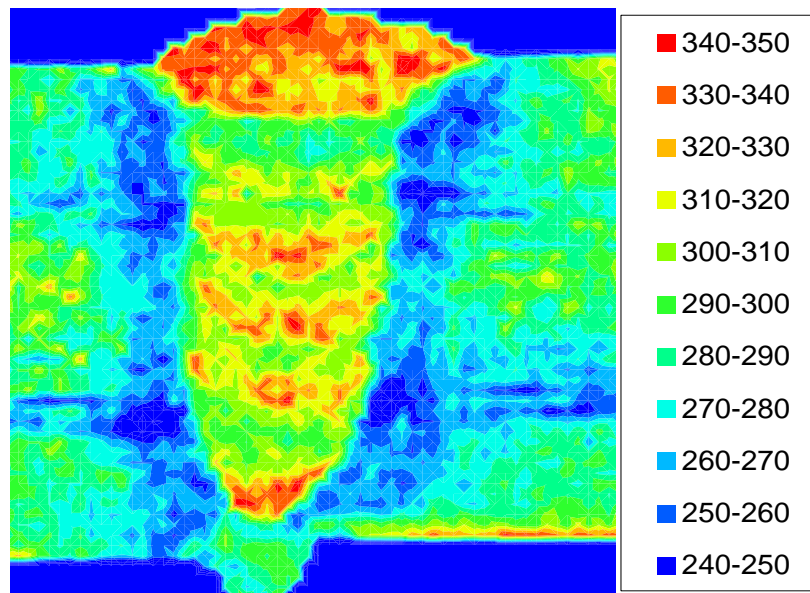


(b) Intercritically reheated grain coarsened HAZ region

Figure 30: HAZ microstructures of dual-torch weld.

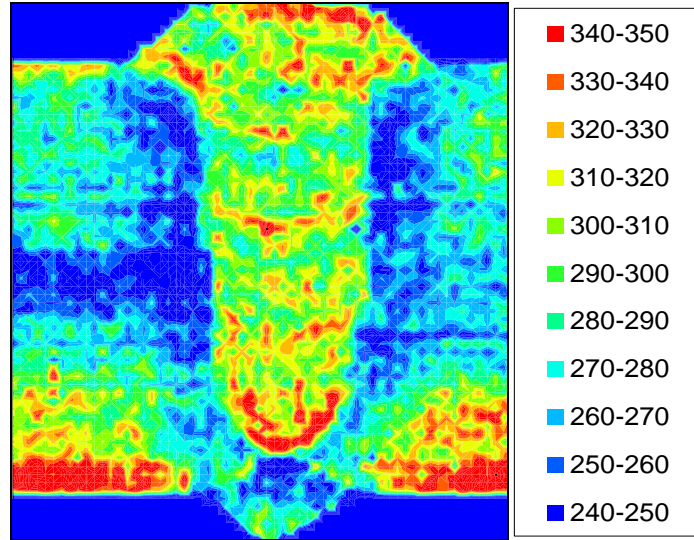


(a) 807-J

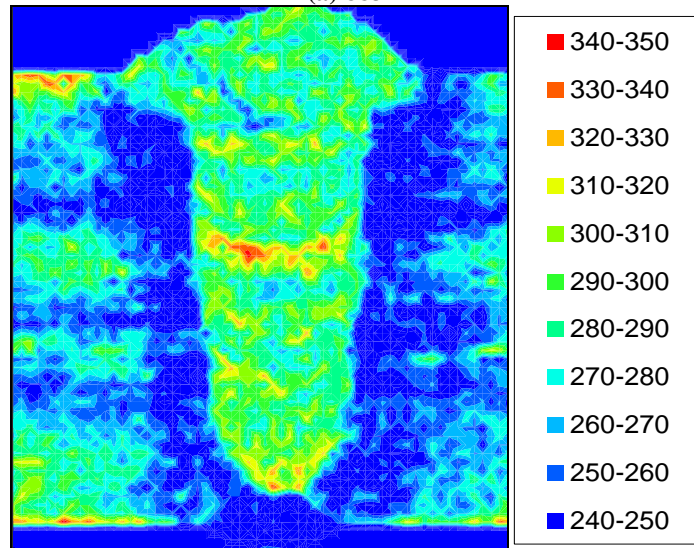


(b) 807-K

Figure 31: Microhardness maps for single-torch pipe welds. (Units of VHN 300 g)

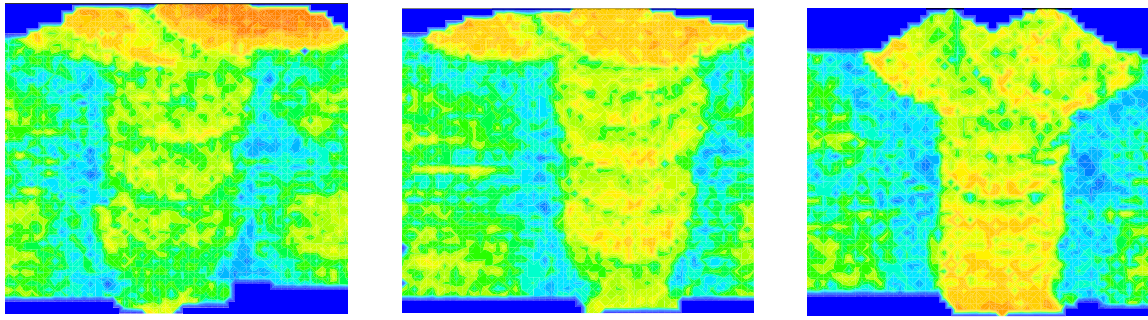


(a) 883-D



(b) 883-F

Figure 32: Microhardness maps for dual-torch pipe welds. (Units of VHN 300 g)



(a) 12:00

(b) 3:00

(c) 6:00

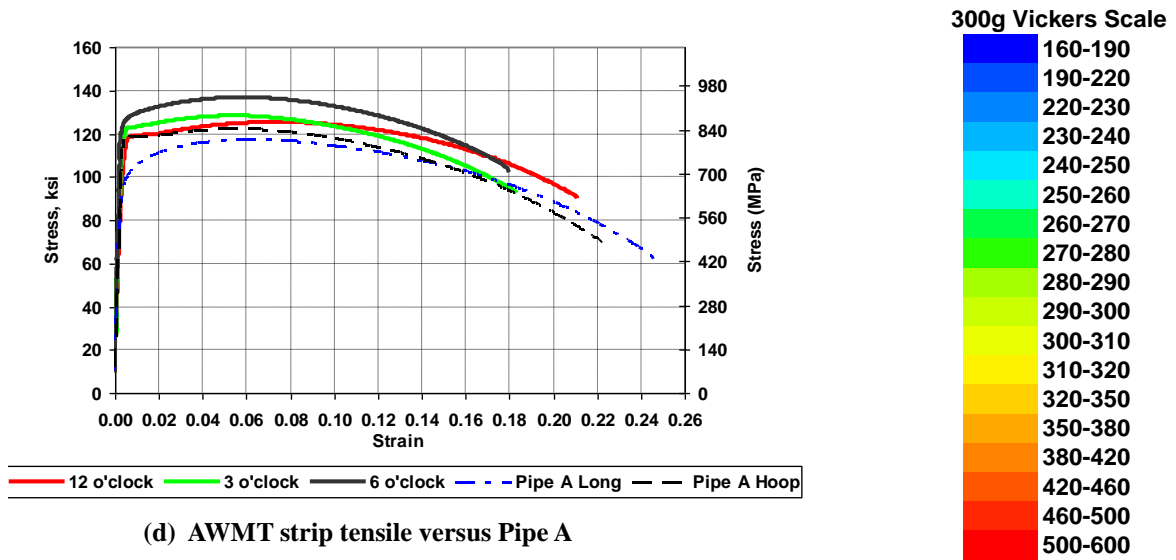


Figure 33: Weld 3 microhardness maps and stress-strain curves (single-torch). (Units of VHN 300 g)

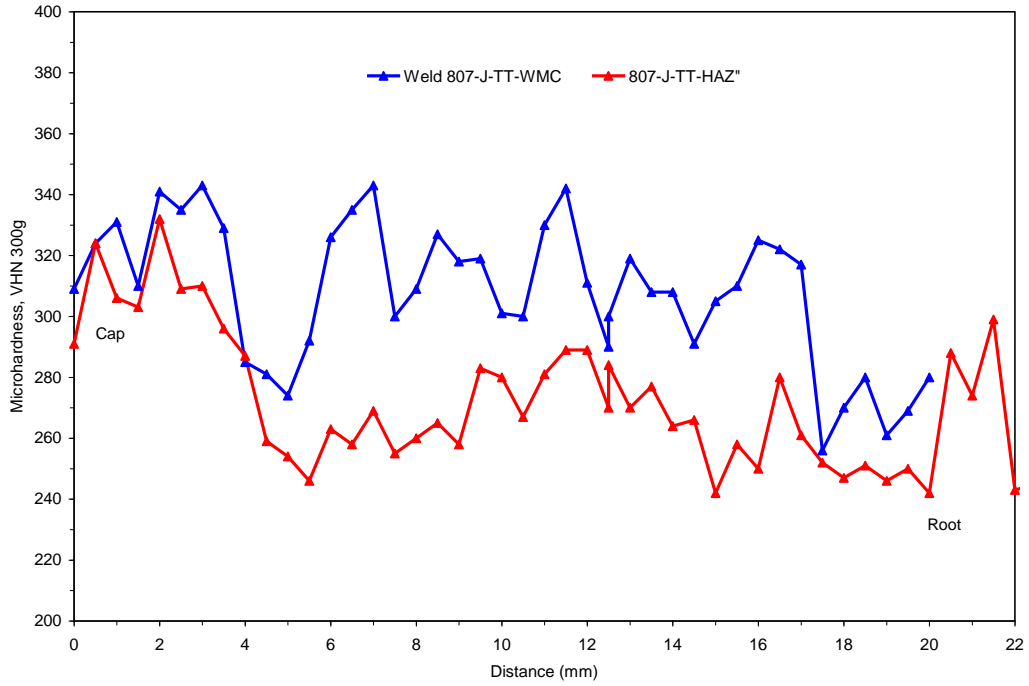


Figure 34: Through-thickness microhardness line map for single-torch pipe weld, 807-J.

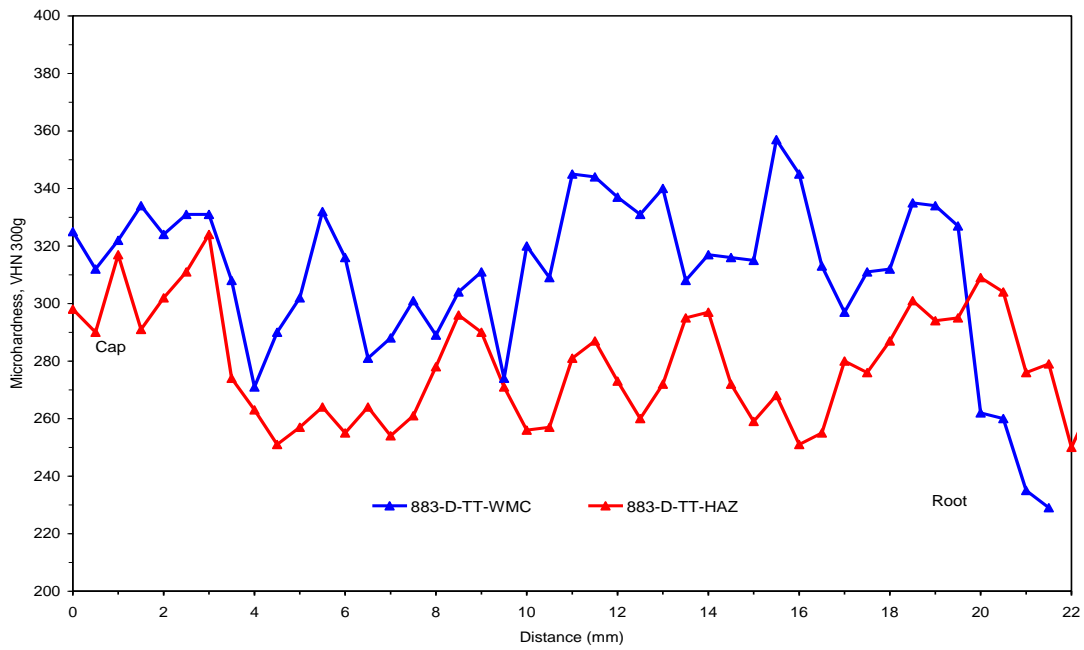


Figure 35: Through-thickness microhardness line map for single-torch pipe weld, 883-D.

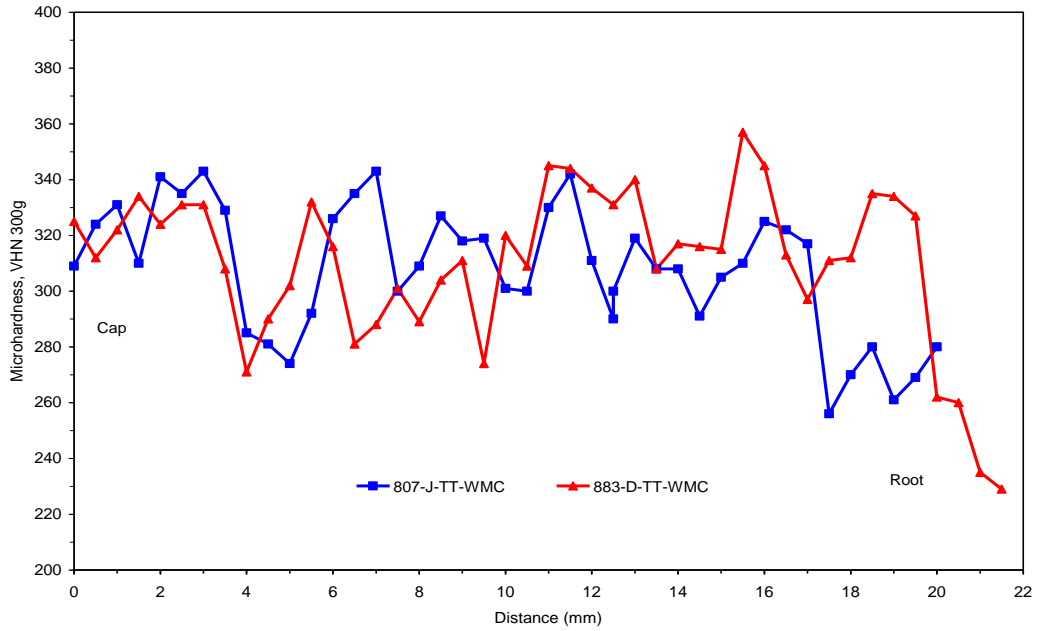


Figure 36: Comparison of through-thickness WMC microhardness line map.

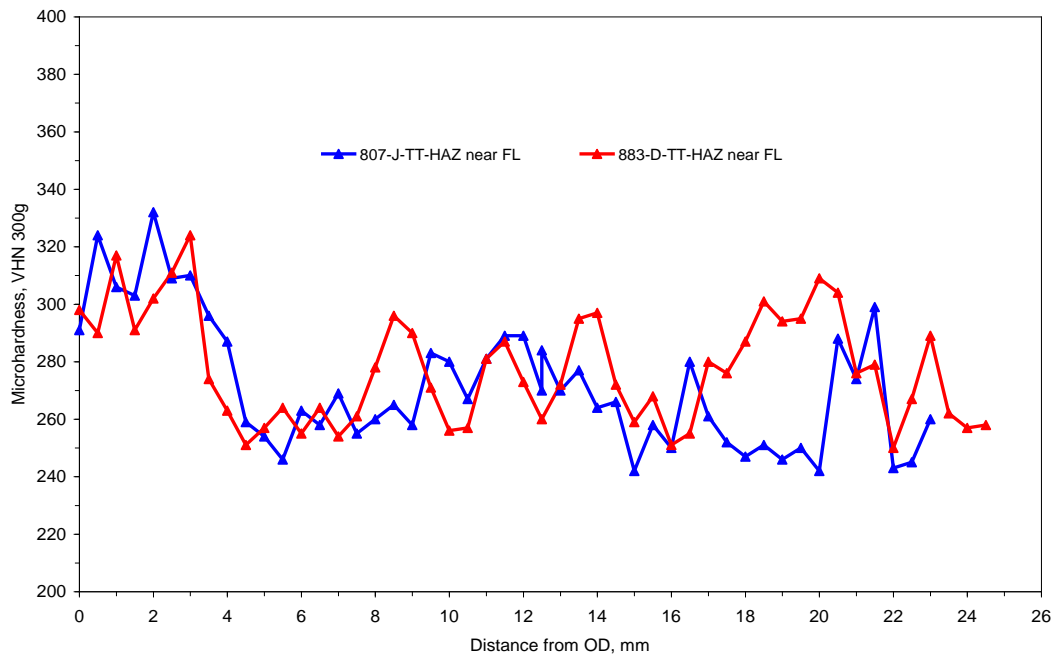


Figure 37: Comparison of through-thickness HAZ microhardness line map.